University of Trento
Department of Physics

Thesis submitted for the degree of
Doctor of Philosophy in Physics

Sound propagation in dilute Bose gases

Miki Ota

Under the supervision of Prof. Sandro Stringari

January 2020

Ph.D. Supervisor:
Sandro Stringari

Members of the Comittee:
Gabriele Ferrari (Univesity of Trento)
Michele Modugno (Ikerbasque)
Sylvain Nascimbène (École Normale Supérieure)

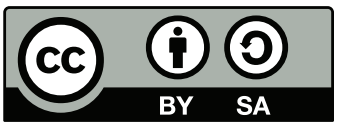

Abstract

In this doctoral thesis, we theoretically investigate the propagation of sound waves in dilute Bose gases, in both the collisionless and hydrodynamic regimes. The study of sound wave is a topic of high relevance for the understanding of dynamical properties of any fluid, classical or quantum, and further provides insightful information about the equation of state of the system.

In our work, we focus in particular on the two-dimensional (2D) Bose gas, in which the sound wave is predicted to give useful information about the nature of the superfluid phase transition. Recently, experimental measurement of sound wave in a uniform 2D Bose gas has become available, and we show that the measured data are quantitatively well explained by our collisionless theory.

Finally, we study the mixtures of weakly interacting Bose gases, by developing a beyond mean-field theory, which includes the effects of thermal and quantum fluctuations in both the density and spin channels. Our new theory allows for the investigation of sound dynamics, as well as the fundamental problem of phase-separation.

Contents

Abstract **iii**

Introduction **1**

1 Sound propagation in ultracold quantum gases **5**
1.1 Sound propagation in classical fluids 5
1.1.1 Boltzmann transport equation 5
1.1.2 Hydrodynamic sound in classical fluids 7
1.1.3 Collisionless sound in classical fluids 9
1.2 Bose-Einstein condensation and superfluidity 10
1.2.1 Long-range order and density matrices 11
1.2.2 The ideal Bose gas 12
1.2.3 Weakly interacting Bose gas 13
1.2.4 Superfluidity 18
1.3 Sound propagation in quantum fluids 21
1.3.1 Two-fluid hydrodynamics 21
1.3.2 Linear response theory 24
1.3.3 Quantum Boltzmann equation 26
1.3.4 From the hydrodynamic to the collisionless regime 28
1.4 Overview of sound experiments in ultracold quantum gases 29

2 Sound propagation in three-dimensional Bose gases **33**
2.1 Weakly interacting Bose gas at finite temperature 33
2.1.1 Hartree-Fock theory 33
2.1.2 Results 35
2.2 Hydrodynamic sounds in a 3D Bose gas 37
2.3 Collisionless sound in a 3D Bose gas 41
2.3.1 Random Phase Approximation 42
2.3.2 Sum rules 44
2.3.3 Results 47
2.4 Comparative study of hydrodynamic and collisionless sounds 50

3 Sound propagation in two-dimensional Bose gases 53
3.1 The BKT phase transition . . . 53
3.1.1 The ideal Bose gas in 2D . . . 53
3.1.2 Weakly interacting Bose gas in 2D . . . 54
3.1.3 The role of vortices . . . 56
3.1.4 Universal description of the fluctuating region . . . 57
3.2 Thermodynamics of 2D Bose gases . . . 58
3.2.1 Theoretical framework . . . 58
3.2.2 Validity domain study . . . 60
3.3 Hydrodynamic sounds in a 2D Bose gas . . . 62
3.4 Collisionless sound in a 2D Bose gas . . . 66
3.4.1 Motivation . . . 66
3.4.2 Collisionless theory of the 2D Bose gas . . . 67
3.4.3 Comparison with the experiments . . . 73
3.5 Probing the BKT jump in the second sound . . . 79

4 Mixtures of 3D Bose gases at finite temperature 81
4.1 Theory of Binary Bose-Einstein condensates . . . 81
4.1.1 Binary BECs at zero temperature . . . 81
4.1.2 Binary BECs at finite temperature . . . 83
4.2 Magnetic phase transition in binary BECs . . . 85
4.2.1 Dynamical instability . . . 85
4.2.2 Energetic instability . . . 88
4.2.3 Effects of spatial inhomogeneity in trapped BECs . . . 92
4.3 Sound propagation in binary BECs . . . 94

Conclusion 97

A Popov theory for 3D dilute Bose gases 101
A.1 Single-component Bose gas . . . 101
A.1.1 Formalism . . . 101
A.1.2 Discussion . . . 105
A.1.3 Results . . . 108
A.2 Binary Bose mixtures . . . 109
A.2.1 General case . . . 109
A.2.2 Equal mass case . . . 114

B Interaction in two-dimensional Bose gases 117
B.1 Interaction in 2D . . . 117
B.1.1 2D system . . . 117
B.1.2 Confined 3D system . . . 118

B.2 Collisional time in 2D 119

C Quasi-condensate Popov theory for 2D dilute Bose gases 121
C.1 Bogoliubov theory revisited 121
C.1.1 Formalism 121
C.1.2 Effects of fluctuations 123
C.1.3 Algebraic decay of one-body density matrix 124
C.2 Quasi-condensate Popov theory 126
C.2.1 Formalism 126
C.2.2 Comparative study of different theories 129

D Study of the 2D RPA response function 131
D.1 Response of a harmonic oscillator 131
D.2 Poles study 135

Introduction

From our voice to musical instruments, sound is ubiquitous in nature. In classical fluids, sound corresponds to an adiabatic oscillation in pressure traveling in space, for which the propagation is mediated by the collisions between the particles in the medium, such as air or water [1]. The need for collisions between particles implies that, different from electromagnetic waves, sound can not propagate in vacuum. On the other hand in solids, the periodic arrangement of atoms allow for the existence of vibrational modes, which correspond to the collective excitations of the system in the quantum mechanical description. In contrast to the sounds in classical fluids (referred to hydrodynamic sounds), these *phonons* do not arise from the incoherent collisions between the atoms, but rather from the presence of a lattice. Finally the most exciting, yet not fully explored field concerns the sound propagation in quantum gases.

Quantum gases have been intensively investigated since their first experimental realization more than twenty years ago [2, 3], and are often referred to as *quantum simulators*, owing to their cleanness and high tunability [4–6]. The use of optical and magnetic traps allows for trapping millions of atoms of the same species without bringing any impurities, and for cooling them to a few micro-Kelvins, a temperature regime in which quantum effects become dominant. As for the high controllability of the system, it is achieved from the control of several external parameters at will, including the temperature, the atomic species, the shape of the trapping potential, and most importantly, the interaction strength between atoms, using Feshbach resonance. Consequently, playing on these available "knobs", one can conveniently sweep from a regime where there are enough collisions to sustain a hydrodynamic picture, to a collisionless regime where many-bodies interactions play a lead role.

The aim of my thesis is to study the propagation of sound in dilute Bose gases, in both the hydrodynamic and collisionless regimes. In particular, we focus on the sound properties of three-dimensional and two-dimensional Bose gases. We further develop the finite-temperature theory for three-dimensional Bose-Bose mixtures, in view of a future study of sound dynamics.

One of the most extraordinary manifestation of quantum behavior at the

macroscopic scale is the phenomenon of superfluidity [7]. Below a certain temperature, the quantum fluid is well described by the two-fluid picture introduced by Landau [8], where one may consider the gas to be a mixture of normal viscous component and a non-dissipative superfluid. This leads to the emergence of a new sound mode, which in the hydrodynamic regime is referred to as second sound, in contrast to the first sound known in normal fluids [9]. In a weakly interacting Bose gas, the second sound corresponds to an oscillation of the superfluid density. Instead, for a strongly interacting system such as the unitary Fermi gas, the second sound corresponds to an out-of-phase oscillation of the superfluid and normal components [10]. Therefore the second sound is closely related to the superfluid property of the gas. Recently, this connection has been used to achieve the first measurement of the superfluid density of an interacting Fermi gas [11], from an experimental probe of the second sound. Indeed, while in a weakly interacting Bose gas the superfluid density is practically the same as the Bose-Einstein condensate (BEC) fraction and therefore can be easily measured, this is no longer true in a Fermi gas, where the macroscopic occupation of a single state is prohibited from Fermi statistics. Another system where second sound is expected to provide useful information about the superfluid property is the two-dimensional (2D) quantum gas [12].

In two dimensions, Bose-Einstein condensation is ruled out at finite temperature, due to the presence of strong thermal fluctuations [13]. However, a superfluid can still exist, known as the Berezinskii-Kosterlitz-Thouless (BKT) superfluid phase [14,15]. One of the main characteristic of this phase is to be an infinite order phase transition, implying that any thermodynamic quantities evolve smoothly as one crosses the transition point, without showing any singular behavior. Instead, the superfluid density is predicted to exhibit a sudden jump at the phase transition, by taking abruptly a finite value as one enters in the superfluid regime. While 2D Bose and Fermi gases have been realized experimentally, this BKT jump of the superfluid density has never been observed explicitly in a quantum gas, also due to the difficulty in probing directly the superfluid density. The situation is therefore very similar to the aforementioned interacting Fermi gas, and one may expect the second sound to shed light on the BKT transition. This is indeed what was found in a preliminary theoretical work [16], in which the authors have predicted the occurrence of a BKT jump in the second sound speed too, for a weakly interacting 2D Bose gas.

In our work, we have extended this prior study to investigate the effects of inter-atomic interaction on the sound velocities, from the weak-coupling regime to the strong-coupling regime. In experimental systems, the two limits correspond to the weakly interacting 2D Bose gas on one side, and the BEC regime of a 2D Fermi gas on the other side. Our calculations based on Landau's two-fluid equation

and universal thermodynamics have revealed that the BKT jump of the second sound remains for any values of interaction, whereas the nature of the sound itself exhibits a great change, by evolving from a density wave to an entropic wave as one increases the interaction strength.

Besides the hydrodynamic regime in which the sound propagates through the individual atomic collisions, it is known that sound in interacting quantum gases can also propagate as an effect of the average interaction force. This is for instance the case of the Bogoliubov phonon at zero temperature in weakly interacting BEC, which corresponds to the collective mode of the superfluid system. Strongly motivated by the measurement of the sound velocity in a weakly interacting 2D Bose gas carried by the experimental group of Paris [17], where they did *not* observe the BKT jump but rather a finite sound velocity also in the absence of a superfluid, we have developed a theory to investigate the collisionless regime. Our theoretical framework is based on the collisionless Boltzmann equation, where one considers the atoms to freely evolve in a mean-field created by the other atoms. Consistent with the experimental observations, we found that sound can indeed propagate without collisions, both in the superfluid and normal phase of the system, sustained by the interaction between particles.

Finally, another system where the problem of sound remains practically unexplored, concerns the mixtures of quantum gases. Mixtures of atomic gases have been realized since the early age of Bose-Einstein condensates [18, 19]. Nowadays, it is possible to trap simultaneously atoms of same species lying in different hyperfine states, but also atoms of different species and different statistics (Bose-Fermi mixtures). A crucial question concerning mixtures, regardless of its quantum or classical nature, is the miscibility. One can indeed expect the sound to propagate in a different way as the mixture is homogeneous or phase-separated. For the two-component Bose gas at zero temperature, the simplest mean-field analysis predicts that the mixture is miscible if the interaction between the same atomic species is stronger than the interaction between unlike particles, and phase separates if not. On the other hand, the effects of temperature on the miscibility of mixtures are less known, and even less the interplay between thermal and quantum fluctuations. Intuitively, one may think that temperature favors mixing, as it is the case in classical fluids because of the entropy of mixing. However, our theoretical study based on the finite-temperature many-body theory demonstrates the opposite: the miscibility of a BEC mixture decreases as one increases the temperature, eventually leading to a phase-separation.

Thesis summary

The first chapter of the manuscript aims to give a comprehensive introduction to the theoretical concepts used in the thesis for the investigation of sound propa-

gation in ultracold quantum gases. After briefly discussing the sound dynamics in classical fluids, we will introduce the phenomena of Bose-Einstein condensation and superfluidity. This will bring us to the concept of two-fluid hydrodynamics developed by Landau. We then turn to the opposite collisionless regime, and set the general theoretical framework, based on linear response theory. Finally we summarize the existing and on-going experimental works on sound propagation in quantum gases, so as to formulate the main motivation of this work. The second chapter is devoted to the sound properties of single-component Bose gas. We start from reviewing the three-dimensional Bose gas, which has been the subject of several papers in the literature. This will provide us some insight into the thermodynamics of the weakly interacting Bose gas, as well as the theoretical tools introduced in the previous chapter. The main part of this thesis concerns the Chap. 3, devoted to the study of 2D Bose gas. After an introduction to the BKT physics of 2D quantum gases, we investigate the hydrodynamic regime of the 2D Bose gas. This part of the manuscript is mainly based on our work published in Physical Review A [20]. We then move to the collisionless regime, and compare our theoretical results for the sound speed with the recent experiment carried by the Paris group. This part of the work was published together with the experimental paper in Physical Review Letters [21]. In the final chapter, we study the finite-temperature properties of binary Bose mixtures. After a review of existing theories for the Bose mixtures at zero and finite temperatures, we develop the Popov theory for the mixtures. Different from the other chapters, the emphasis in this section is put on the study of the phase-separation. In particular, we discuss the effects of thermal and quantum fluctuations on the thermodynamic properties of the mixture. This part of the thesis is based on our work published in Physical Review Letters [22].

Chapter 1

Sound propagation in ultracold quantum gases

The aim of this first chapter is to introduce the theoretical tool needed for studying the propagation of sound in quantum gases. We will first calculate the speed of sound for the ideal classical fluids, by starting from the Boltzmann transport equation. Although this derivation is not the most straightforward, nor the most general one, it will provide us all the basic theoretical concept for the understanding of sound physics. After introducing the phenomenon of Bose-Einstein condensation and superfluidity, we will derive the equations for the sound waves in quantum gases, in both the hydrodynamic and collisionless regimes.

1.1 Sound propagation in classical fluids

1.1.1 Boltzmann transport equation

The general idea of physical kinetics for the description of transport phenomena, is to follow the motion of the fluid as a whole instead of looking at the motion of each individual atom [23, 24]. This is achieved by writing down the equation of motion for the distribution function of the system, $f(\mathbf{r}, \mathbf{p}, t)$, which corresponds to the number of particles per unit volume of phase space $\{\mathbf{r}, \mathbf{p}\}$ at time t, where $\mathbf{r}$ and $\mathbf{p}$ are, respectively, the spatial and momentum coordinates. Let us consider a monoatomic gas, with atoms initially occupying a region A of the phase space, of volume $d^3\mathbf{r}d^3\mathbf{p}$ at $(\mathbf{r}, \mathbf{p})$. In the absence of collisions and under an external force $\mathbf{F}$, the atoms will be found after an interval of time δt in a region B of volume $d^3\mathbf{r}'d^3\mathbf{p}'$ at coordinates $(\mathbf{r}', \mathbf{p}')$, where $\mathbf{r}' = \mathbf{r}+\mathbf{v}\delta t$ and $\mathbf{p}' = \mathbf{p}+\mathbf{F}\delta t$, with $\mathbf{v} = \mathbf{p}/m$. This statement is equivalent to the following equality:

$$f(\mathbf{r} + \mathbf{v}\delta t, \mathbf{p} + \mathbf{F}\delta t, t + \delta t)d^3\mathbf{r}'d^3\mathbf{p}' = f(\mathbf{r}, \mathbf{p}, t)d^3\mathbf{r}d^3\mathbf{p}\,. \tag{1.1}$$

From geometric construction, one can show that $d^3\mathbf{r}'d^3\mathbf{p}' = d^3\mathbf{r}d^3\mathbf{p}$, and expanding the left-hand side of Eq. (1.1) up to linear order, one obtains the Boltzmann transport equation,

$$\left(\frac{\partial}{\partial t} + \frac{\mathbf{p}}{m}\nabla - \nabla U(\mathbf{r},t)\nabla_{\mathbf{p}}\right) f(\mathbf{p},\mathbf{r},t) = \left.\frac{\partial f}{\partial t}\right|_{\text{coll}}, \tag{1.2}$$

where we have assumed a conservative force $F = -\nabla U$ and introduced the collisional term, $\partial f/\partial t|_{\text{coll}}$.

For a sufficiently small volume $d^3\mathbf{r}d^3\mathbf{p}$, and time δt, one may consider that any collisions occurring inside A will drift atoms away from B. Equivalently, there might be atoms reaching the elemental volume B from collisions occurring outside the region A. For the dilute system which we are interested in, one can restrict to binary collisions, and the collision integral takes the general form [25]:

$$\left.\frac{\partial f}{\partial t}\right|_{\text{coll}}(\mathbf{p},\mathbf{r},t) = \int d^3\mathbf{p}_2 d^3\mathbf{p'}_1 d^3\mathbf{p'}_2 [w(\mathbf{p'}_1,\mathbf{p'}_2|\mathbf{p},\mathbf{p}_2) f_2(\mathbf{r},\mathbf{p'}_1,\mathbf{r},\mathbf{p'}_2,t) - w(\mathbf{p}_1,\mathbf{p}_2|\mathbf{p'}_1,\mathbf{p'}_2) f_2(\mathbf{r},\mathbf{p},\mathbf{r},\mathbf{p}_2,t)], \tag{1.3}$$

where we have introduced the scattering function $w(\mathbf{p}_1,\mathbf{p}_2|\mathbf{p'}_1,\mathbf{p'}_2)$ containing all the information about the nature of the collisions, and the two-body correlation function $f_2(\mathbf{r}_1,\mathbf{p}_1,\mathbf{r}_2,\mathbf{p}_2)$, corresponding to the probability to find simultaneously atoms in $(\mathbf{r}_1,\mathbf{p}_1)$ and $(\mathbf{r}_2,\mathbf{p}_2)$. Therefore, the first term in the right-hand side of Eq. (1.3) describes the process in which the colliding atoms reach the state $\mathbf{p}$, whereas the second one corresponds to the scattering out term. In general, the scattering function depends on the inter-atomic interaction and has to be defined in the quantum mechanical context. The study of the two-body problem will be done in Sec. 1.2.4 and here we only discuss some general features of $w(1,2|1',2')$. In what follows we consider the collisions to be elastic, implying that the momentum and the energy are conserved. Under these considerations, the scattering amplitude has to be invariant under time reversal and parity transformation, $w(\mathbf{p'}_1,\mathbf{p'}_2|\mathbf{p},\mathbf{p}_2) = w(\mathbf{p}_1,\mathbf{p}_2|\mathbf{p'}_1,\mathbf{p'}_2)$, and Eq. (1.3) can be rewritten as:

$$\left.\frac{\partial f}{\partial t}\right|_{\text{coll}} = \int d^3\mathbf{p}_2 d^3\mathbf{p'}_1 d^3\mathbf{p'}_2 w(\mathbf{p'}_1,\mathbf{p'}_2|\mathbf{p}_1,\mathbf{p}_2) \times \left[f(\mathbf{r},\mathbf{p'}_1,t) f(\mathbf{r},\mathbf{p'}_2,t) - f(\mathbf{r},\mathbf{p}_1,t) f(\mathbf{r},\mathbf{p}_2,t)\right]. \tag{1.4}$$

In the above equation, we have further assumed the molecular chaos hypothesis to hold, by neglecting the correlations between the colliding atoms: $f_2(1,2) \simeq f(1)f(2)$. Equation (1.2) together with Eq. (1.4) constitute the Boltzmann transport equations for the classical fluids. It is worth noticing that, beside the diffusion terms, the Boltzmann equation (1.2) possesses two distinct contributions for the

restoring force to the equilibrium: the collisional integral (1.4) on one hand, and the conservative force $\nabla U \nabla_{\mathbf{p}} f$ on the other hand. As one shall see in more details in Sec. 1.3.4, the transport regime in which the former contribution plays a major role is referred to the *hydrodynamic* regime, whereas one speaks about the *collisionless* regime when the later contribution becomes dominant.

For a homogeneous gas ($\nabla = 0$) in the absence of an external potential ($U = 0$), an equilibrium solution of the Boltzmann equation is obtained by noticing that the left-hand side of Eq. (1.2) is equal to zero for any distribution function $f(\mathbf{p})$ which does not depend on time and position. As for the collisional term Eq. (1.4), it vanishes when the detailed-balance condition is satisfied:

$$f\left(\mathbf{r}, \mathbf{p'}_1, t\right) f\left(\mathbf{r}, \mathbf{p'}_2, t\right) = f\left(\mathbf{r}, \mathbf{p}_1, t\right) f\left(\mathbf{r}, \mathbf{p}_2, t\right) . \tag{1.5}$$

Recalling the conservation of energy, the above condition is found to be satisfied for the Maxwell-Boltzmann distribution function:

$$f(\mathbf{p}) = e^{-\beta(\frac{p^2}{2m} - \mu)} , \tag{1.6}$$

where $\beta = 1/(k_B T)$ is the inverse thermal energy, and the chemical potential μ is found from the normalization condition

$$n(\mathbf{r}) = \left(\frac{k_B T}{2m}\right)^{3/2} \int d^3\mathbf{p} f(\mathbf{r}, \mathbf{p}) , \tag{1.7}$$

with $n(\mathbf{r})$ the number density of particles.

1.1.2 Hydrodynamic sound in classical fluids

We start from the hydrodynamic solution of the Boltzmann equations [24, §4]. As one shall see below, the solution of Boltzmann equation correctly retrieves the adiabatic sound speed of a classical fluid. First, it is important to notice that the collisional term (1.4) vanishes not only for the special choice of the distribution function (1.6), but for a more general class of solutions:

$$f(\mathbf{r}, \mathbf{p}, t) = \exp\left[-\beta(\mathbf{r}, t)\left(\frac{1}{2m}(\mathbf{p} - m\mathbf{u}(\mathbf{r}, t))^2 - \mu(\mathbf{r}, t)\right)\right] , \tag{1.8}$$

with $\mathbf{u}$ the velocity of the fluid. Although the above equation is not an equilibrium solution of the Boltzmann equation, it cancels the collisional term. The vanishing of collisional term here does not mean that there are no collisions but the opposite: there are enough collisions to maintain *locally* the thermodynamic equilibrium, with a well-defined temperature, velocity and chemical potential, at every position of the fluid.

From the local equilibrium distribution (1.8), one can derive conservation equations, by taking the n^{th} momenta of the Boltzmann equation. This is achieved by multiplying Eq. (1.2) by $\mathbf{p}^n$ ($n = 0, 1, 2$) and integrating over the momentum space:

1. 0^{th} momentum. Equation of continuity:

$$\frac{\partial}{\partial t} n(\mathbf{r}, t) + \nabla \mathbf{j}(\mathbf{r}, t) = 0 \tag{1.9a}$$

   with $\mathbf{j}(\mathbf{r}, t) = \int d^3\mathbf{p} (\mathbf{p}/m) f(\mathbf{r}, \mathbf{p}, t)$ the current density.

2. 1^{st} momentum. Momentum conservation:

$$m \frac{\partial}{\partial t} \mathbf{j}(\mathbf{r}, t) + \int d^3\mathbf{p} \, (\mathbf{p}\nabla) \left(\frac{\mathbf{p}}{m} f(\mathbf{p}, \mathbf{r}, t) \right) = -\nabla U(\mathbf{r}, t) n(\mathbf{r}, t) \tag{1.9b}$$

3. 2^{nd} momentum. Energy conservation:

$$\frac{\partial}{\partial t} \mathcal{E}(\mathbf{r}, t) + \nabla \int d^3\mathbf{p} \frac{\mathbf{p}}{m} \frac{p^2}{2m} f(\mathbf{p}, \mathbf{r}, t) = -\nabla U(\mathbf{r}, t) \mathbf{j}(\mathbf{r}, t) \tag{1.9c}$$

   with $\mathcal{E}(\mathbf{r}, t) = \int d^3\mathbf{p} (p^2/2m) f(\mathbf{r}, \mathbf{p}, t)$ the energy density.

For the description of acoustic waves, we shall concentrate on the small amplitude oscillations of the fluid. This is achieved by expanding the physical quantities around their equilibrium values, $x(\mathbf{r}, \mathbf{p}, t) = x^0 + \delta x(\mathbf{r}, \mathbf{p}, t)$, and keeping only terms to linear order in δx (we consider the fluid to be initially at rest; $v^0 = 0$). Then, noticing that any integrands with odd power of $(\mathbf{p} - m\mathbf{v})$ vanish, Eqs. (1.9a) - (1.9c) yield to linear order:

$$\frac{\partial}{\partial t} n(\mathbf{r}, t) = -n^0 \nabla \mathbf{v}(\mathbf{r}, t) \,, \tag{1.10a}$$

$$m \frac{\partial}{\partial t} j(\mathbf{r}, t) = -\nabla \mathcal{P}(\mathbf{r}, t) - n^0 \nabla U(\mathbf{r}, t) \,, \tag{1.10b}$$

$$\frac{\partial}{\partial t} \mathcal{E}(\mathbf{r}, t) = -(\mathcal{E}^0 + \mathcal{P}^0) \nabla \mathbf{v}(\mathbf{r}, t) \,, \tag{1.10c}$$

with $\mathcal{P} = 2\mathcal{E}/3$, and to linear order, $\mathbf{j}(\mathbf{r}, t) = n^0 \mathbf{v}(\mathbf{r}, t)$. Solving the above equations one finally finds the following wave equation,

$$\frac{\partial^2 n(\mathbf{r}, t)}{\partial t^2} = c^2 \nabla^2 n(\mathbf{r}, t) + n \nabla^2 U(\mathbf{r}, t) \,, \tag{1.11}$$

with the classical sound velocity $c = \sqrt{5 k_B T/(3m)}$.

Before closing this section, it is insightful to discuss the nature of the classical sound. From Eqs. (1.10a) and (1.10c), one finds

$$\frac{1}{n}\frac{\partial n(\mathbf{r},t)}{\partial t} = \frac{3}{5}\frac{\partial P(\mathbf{r},t)}{\partial t}\,. \tag{1.12}$$

This equation corresponds to the isentropic condition $PV^{5/3} = \text{const}$, reflecting that the sound wave propagates adiabatically. One can indeed verify that the sound speed is given by the adiabatic compressibility of an ideal fluid, $c^2 = \frac{1}{m}\frac{\partial P}{\partial n}|_s$.

It is also worth noticing that the above approach based on the Boltzmann equation neglects the effects of interaction (see Eq. (1.9c) in which $\mathcal{E}$ includes only the kinetic energy), and is therefore valid for weakly-interacting fluids only. As one shall see in the next section, the formulation of the hydrodynamic equation for the quantum fluids follows essentially the same procedure, starting from the conservation equations after assuming local equilibrium of the gas. However we shall not adopt any equation of state, making the superfluid hydrodynamics more general than the classical description sketched in this section.

1.1.3 Collisionless sound in classical fluids

The Boltzmann equation can also be solved in the absence of collisions, by putting explicitly the collisional term on the right-hand side of Eq. (1.2) to zero. The collisionless Boltzmann equation, also referred to the Vlaslov equation in the literatures, has been intensively used in the context of plasma physics, to treat the long-range character of Coulomb interactions [24, §6] [26, Ch. 3]. The effects of interaction are taken into account through an effective potential,

$$U_{\text{eff}}(\mathbf{r}) = U_{\text{ext}}(\mathbf{r}) + U_{\text{int}}(\mathbf{r})\,. \tag{1.13}$$

In particular, we consider the interaction to be in the form,

$$U_{\text{int}}(\mathbf{r}) = \int d^3\mathbf{r}' V(\mathbf{r}-\mathbf{r}')n(\mathbf{r}')\,. \tag{1.14}$$

Let us calculate the solution to the Boltzmann equation, under an external perturbation $U_{\text{ext}}(x) = \delta U_{\text{ext}}(q,\omega)e^{i(qx-\omega t)}$, propagating along the x direction. Then, for sufficiently small value of δU_{ext}, the induced fluctuations oscillate at the same frequency as the perturbation:

$$f(\mathbf{p},\mathbf{r},t) = f^0(\mathbf{p}) + \delta f(\mathbf{p},q,\omega)e^{i(qx-\omega t)} \tag{1.15}$$

where $f^0(\mathbf{p})$ is an equilibrium distribution function satisfying Eq. (1.7). To linear order in the perturbation, the Boltzmann equation now reads,

$$i(qv_x-\omega)\delta f(\mathbf{p},q,\omega) - ik\delta U_{\text{eff}}(q,\omega)\frac{\partial f^0(\mathbf{p})}{\partial p_x} = 0\,, \tag{1.16}$$

where the small amplitude deviation of the effective potential is

$$\delta U_{\text{eff}}(q,\omega) = \delta U_{\text{ext}}(q,\omega) + v(q)\int d^3\mathbf{p}'\delta f(\mathbf{p}',q,\omega)\,, \tag{1.17}$$

with $v(q) = \int d^3\mathbf{s}V(\mathbf{s})e^{-iqs_x}$ the Fourier component of the interaction potential. The density perturbation induced by the external potential $\delta n = \int d^3\mathbf{p}\delta f$ is found to be,

$$\begin{aligned}\delta n(q,\omega) &= \delta U_{\text{eff}}(q,\omega)\int d^3\mathbf{p}'\frac{q}{qv_x-\omega}\frac{\partial f^0(\mathbf{p}')}{\partial p_x}\\ &\equiv -\delta U_{\text{eff}}\chi^0(q,\omega)\end{aligned} \tag{1.18}$$

where we have introduced the response function of the referential system χ_0. Finally, from Eq. (1.16), one finds

$$\begin{aligned}\delta n(q,\omega) &= -\delta U_{\text{ext}}\frac{\chi^0(q,\omega)}{1-v(q)\chi^0(q,\omega)}\\ &\equiv -\delta U_{\text{ext}}\chi(q,\omega)\,.\end{aligned} \tag{1.19}$$

The sound velocity can be calculated from the pole of the response function $\chi(q,\omega)$:

$$1 - v(q)\chi^0(q,\omega) = 0. \tag{1.20}$$

1.2 Bose-Einstein condensation and superfluidity

Since the first realization of Bose-Einstein condensation (BEC) over two decades ago [2,3], the scientific field of ultracold atomic gases has been constantly growing, by gathering the interest of both experimental and theoretical communities [4, 7, 27]. The occurrence of BEC is associated to the macroscopic occupation of a given single-particle state, while the other states remain microscopically occupied. A striking feature of BEC is that it is a purely statistical phenomenon, arising from the very bosonic nature of the particles, regardless the interaction between them. As a result, BEC occurs when the quantum nature of the particles becomes dominant, i.e. when the thermal de Broglie wavelength,

$$\lambda_T = \sqrt{\frac{2\pi\hbar^2}{mk_BT}} \tag{1.21}$$

becomes comparable to the interparticle distance. Experimentally, such configuration can be achieved by both lowering the temperature or increasing the atomic density. That is the dilute Bose gas, which is the system of interest in this thesis.

1.2.1 Long-range order and density matrices

In order to discuss the phenomenon of BEC from the microscopic point of view, it is meaningful to introduce the one body density matrix [7, §1]

$$n^{(1)}(\mathbf{r},\mathbf{r}') = \langle \hat{\Psi}^\dagger(\mathbf{r})\hat{\Psi}(\mathbf{r}')\rangle \,, \tag{1.22}$$

where $\hat{\Psi}(\mathbf{r})$ ($\hat{\Psi}^\dagger(\mathbf{r})$) is the field operator destroying (creating) a particle at the spatial coordinate $\mathbf{r}$. The $\langle \ldots \rangle$ denotes the statistical average, taken in the grand-canonical ensemble (see below). By definition, the diagonal elements of the density matrix correspond to the real space density:

$$n^{(1)}(\mathbf{r},\mathbf{r}) = n(\mathbf{r}) \,. \tag{1.23}$$

The field operators can be expressed in the basis of single-particle wave functions as follows [28]

$$\hat{\Psi}(\mathbf{r}) = \sum_i \varphi_i(\mathbf{r})\hat{a}_i \,, \tag{1.24}$$

where $\hat{a}_i$ ($\hat{a}_i^\dagger$) is the annihilation (creation) operator of a single particle in the state described by φ_i. Using this expression, the one body density matrix Eq. (1.22) now takes the form

$$n^{(1)}(\mathbf{r},\mathbf{r}') = \sum_i n_i \varphi_i^*(\mathbf{r})\varphi_i(\mathbf{r}') \,, \tag{1.25}$$

with $n_i = \langle \hat{a}_i^\dagger \hat{a}_i \rangle$ the occupation number of the state φ_i. For simplicity, we consider the uniform system in which the single-particle wave functions are given by plane-waves, $\varphi_i(\mathbf{r}) = e^{i\mathbf{k}_i\mathbf{r}}/\sqrt{V}$. In the thermodynamic limit where $N, V \to \infty$ with $N/V = \text{const}$, the one body density matrix will depend only on the modulus of the relative distance $\mathbf{s} = \mathbf{r} - \mathbf{r}'$.

The onset of BEC is characterized by the macroscopic occupation of the lowest lying single-particle mode $n_{i=0} = N_0$, with N_0 being of the same order as the total atoms number N. Equation (1.25) therefore becomes

$$n^{(1)}(s) = n_0 + \sum_{\mathbf{p}\neq 0} n_{\mathbf{p}} e^{\frac{i}{\hbar}\mathbf{p}\cdot\mathbf{s}} \,, \tag{1.26}$$

with $n_0 = N_0/V$. For a system in the thermodynamic limit, the sum in Eq. (1.26) can be replaced by an integration and one can verify that

$$\lim_{s\to\infty} n^{(1)}(s) = n_0 \,. \tag{1.27}$$

This is the off-diagonal long-range order nature of the condensate. It is worth stressing that the long-range order defines uniquely the condensate. As one shall

see in the chapter devoted to two-dimensional systems, the enhancement of thermal fluctuations in low dimensional system, and the consequent breaking of long-range order, prevails the gas from having a BEC at finite-temperature in two dimensions.

By taking the Fourier transform of Eq. (1.22), one obtains the momentum distribution function:

$$\begin{aligned} n(\mathbf{p}) &= \frac{V}{(2\pi\hbar)^3}\int d^3\mathbf{s} n^{(1)}(s) e^{-\frac{i}{\hbar}\mathbf{p}\cdot\mathbf{s}} \\ &= \langle\hat{\Psi}^\dagger(\mathbf{p})\hat{\Psi}(\mathbf{p})\rangle\,, \end{aligned} \tag{1.28}$$

with $\hat{\Psi}(\mathbf{p}) = (2\pi\hbar^3)^{-1}\int d^3\mathbf{r}\hat{\Psi}(\mathbf{r})e^{-i\mathbf{p}\cdot\mathbf{r}/\hbar}$. Using the expression (1.26) for $n^{(1)}(\mathbf{s})$ one finds,

$$n(\mathbf{p}) = N_0\delta(\mathbf{p}) + \frac{V}{(2\pi\hbar)^3}n_{\mathbf{p}}\,. \tag{1.29}$$

An explicit expression for the occupation number in the non-interacting gas will be given in the next section.

Finally, let us introduce the two-body density matrix:

$$n^{(2)}(\mathbf{r},\mathbf{r}') = \langle\hat{\Psi}^\dagger(\mathbf{r})\hat{\Psi}^\dagger(\mathbf{r}')\hat{\Psi}(\mathbf{r})\hat{\Psi}(\mathbf{r}')\rangle\,. \tag{1.30}$$

The two body density matrix characterizes the correlation between two particles at distance $\mathbf{r}-\mathbf{r}'$, and hence is closely related to the two-body correlation functions introduced in Sec. 1.1.1.

1.2.2 The ideal Bose gas

For a non-interacting uniform Bose gas, one can evaluate the momentum distribution (1.29) in the thermodynamic equilibrium [7, 23]. This is achieved by working out in the grand-canonical ensemble, and one finds the Bose-Einstein distribution function:

$$f(\mathbf{p}) = \frac{1}{e^{\beta\left(\frac{p^2}{2m}-\mu\right)}-1}\,, \tag{1.31}$$

where μ is the chemical potential fixed by the normalization condition $n = V^{-1}\sum_{\mathbf{p}} f(\mathbf{p})$. When the chemical potential becomes equal to the lowest-lying single-particle state ε_0, the distribution function diverges, signaling that this state becomes macroscopically occupied. This is the mechanism behind BEC. For a uniform gas, $\varepsilon_0 = 0$ and consequently BEC occurs when one reaches the critical density:

$$n_{\mathrm{BEC}} = \frac{g_{3/2}(1)}{\lambda_T^3}\,, \tag{1.32}$$

where we have introduced the Bose special integral,

$$g_p(z) = \frac{1}{\Gamma(p)} \int_0^\infty dx x^{p-1} \frac{1}{e^x z^{-1} - 1}\,, \tag{1.33}$$

with $\Gamma(p)$ the Gamma function. By definition, $g_p(1) = \zeta(p)$ is the Riemann's zeta function, and one can rewrite Eq. (1.32) in terms of the critical temperature,

$$T_{\rm BEC} = \frac{2\pi\hbar^2}{m} \left(\frac{n}{\zeta(3/2)} \right)^{2/3} . \tag{1.34}$$

As for the two-body density matrix (1.30), one can show that for an ideal Bose gas it is directly related to the one-body density matrix as [7, 29]:

$$n^{(2)}(\mathbf{r}, \mathbf{r}') = n(\mathbf{r}) n(\mathbf{r}') + |n^{(1)}(\mathbf{r}, \mathbf{r}')|^2 - n_0(\mathbf{r}) n_0(\mathbf{r}')\,. \tag{1.35}$$

In particular, we consider here the following two limits:

1. $T = 0$. All the atoms are condensed ($n_0(\mathbf{r}) = n(\mathbf{r})$) and

$$n^{(2)}(\mathbf{r}, \mathbf{r}) = n^2(\mathbf{r})\,. \tag{1.36}$$

2. $T > T_{\rm BEC}$. None of the atoms are condensed ($n_0(\mathbf{r}) = 0$) and

$$n^{(2)}(\mathbf{r}, \mathbf{r}) = 2n^2(\mathbf{r})\,. \tag{1.37}$$

The factor 2 in Eq. (1.37) is referred to bosonic bunching (or exchange effect), and arises from the statistical nature of bosons, which prefer to occupy the same state. For fermions, one would instead have the opposite effect, with the fermions avoiding staying in the same state, due to Pauli exclusion principle. It is worth noticing from Eq. (1.36) that the exchange effect is suppressed in the presence of a condensate. In the following chapters, we will come back to the physical interpretation of the two-body matrix, which plays a crucial role in low dimensions (Chap. 3).

1.2.3 Weakly interacting Bose gas

We now turn to the effects of interaction, which has been discarded so far. For this purpose, we start from a brief review of the two-body problem, introducing the s-wave scattering length. After that, we develop the Bogoliubov theory for weakly interacting bosons at zero temperature.

The two-body problem

Let us consider the binary collision of two particles with mass m_1 and m_2 [30, §122]. In the center of mass frame, the scattering problem is described by the following Shrödinger equation:

$$\left(-\frac{\hbar^2}{2\mu}\nabla^2 + V(\mathbf{r})\right)\Psi(\mathbf{r}) = E\Psi(\mathbf{r})\,, \tag{1.38}$$

with $1/\mu = 1/m_1 + 1/m_2$ the reduced mass. Equation (1.38) shows that in the center of mass frame, the two-body problem reduces to a single-particle problem with a scattering center $V(\mathbf{r})$. Let us consider that the interatomic potential is central $V(|\mathbf{r}|)$, an assumption which is true for the weakly interacting Bose gases (unless one considers long-range dipolar interaction [31]). Then, Eq. (1.38) reduces to the radial equation

$$\left(-\frac{\hbar^2}{2\mu}\frac{\partial^2}{\partial r^2} + V_{\text{eff}}(r)\right)u_l(r) = E_l u_l(r)\,, \tag{1.39}$$

where we have factorized $\Psi(\mathbf{r}) = R_l(r)Y_l^m(\theta,\phi)$, introducing the spherical harmonics Y_m^l, and $u_l(r) = rR_l(r)$ is the radial wave-function. The effective potential reads

$$V_{\text{eff}} = V(r) + \frac{\hbar^2 l(l+1)}{2\mu r^2}\,. \tag{1.40}$$

The description of the two-body problem is particularly simplified when one considers the dilute gas [32]. Indeed, as we have already pointed out, in such system the inter-particle distance is very large, so that the interaction is effectively small. Moreover, the diluteness implies that the actual shape of the inter-atomic potential is unimportant. In what follows we can therefore limit ourself to the study of collisions far from the scattering center. In that region, the incoming particle can be described by a plane-wave, whereas the scattered particle must be described by an out-going spherical wave. For indistinguishable bosons ($m_1 = m_2 = m$), the wave function takes therefore the asymptotic form:

$$\Psi(\mathbf{r}) \to \left(e^{i\mathbf{kr}} + e^{-i\mathbf{kr}}\right) + \frac{e^{ikr}}{r}\left[f(k,\theta) + f(k,\pi-\theta)\right]\,, \tag{1.41}$$

where θ is the scattering angle and we have taken into account the symmetric nature of bosons, and introduced the scattering amplitude $f(k,\theta)$ [30, §135]. In the limit of low scattering energy, one may only consider the $l = 0$ contribution in the effective potential Eq. (1.40), corresponding to the s-wave regime. In such regime the scattering amplitude becomes independent of k and θ:

$$\lim_{k\to 0} f(k,\theta) = -a_s\,, \tag{1.42}$$

with a_s the s-wave scattering length. Therefore, for a dilute gas, one can choose an arbitrary shape of the interacting potential, as long as it recovers the relations (1.41) and (1.42).

Let us now evaluate the scattering amplitude, from a perturbative solution of the Schrödinger equation (1.38). Decomposing the wave function into $\Psi = \Psi_0 + \Psi_1$, where Ψ_0 is the plane-wave solution of the free particle problem ($V = 0$), Eq. (1.38) becomes

$$\left(\nabla^2 + k^2\right) \Psi_1(\mathbf{r}) = \frac{2mV(\mathbf{r})}{\hbar^2} \Psi_0(\mathbf{r}) \,. \tag{1.43}$$

The above equation is nothing but the Poisson equation. In the dilute limit, its solution is given by

$$\Psi_1(r) \simeq -\frac{m}{2\pi\hbar^2} \frac{e^{ikr}}{r} \int d^3\mathbf{r}' V(\mathbf{r}') e^{i\mathbf{k}\mathbf{r}'} \,. \tag{1.44}$$

By comparing with Eq. (1.41), one identifies that

$$f(k,\theta) + f(k,\pi-\theta) = -\frac{m}{2\pi\hbar^2} \int d^3\mathbf{r}' V(\mathbf{r}') e^{i\mathbf{k}\mathbf{r}'} \,. \tag{1.45}$$

This is the (first order) Born approximation for the scattering amplitude.

Finally, based on our discussion about the s-wave regime, we find convenient to choose the following potential to model the two-bodies interaction [32]:

$$V(\mathbf{r}) = g\delta(\mathbf{r}) \,, \tag{1.46}$$

with g the interaction coupling constant defined as $g = 4\pi\hbar^2 a_s/m$, so as to recover result (1.42) for the scattering amplitude.

Bogoliubov theory

The gas of weakly interacting bosons is described by the following model Hamiltonian, written in the second quantization form [7, 33, §25]:

$$\begin{aligned} \hat{H} = &\int d^3\mathbf{r} \left(\frac{\hbar^2}{2m} \nabla\hat{\Psi}^\dagger(\mathbf{r}) \nabla\hat{\Psi}(\mathbf{r}) \right) \\ &+ \frac{1}{2} \int d^3\mathbf{r} d^3\mathbf{r}' \left(\hat{\Psi}(\mathbf{r})^\dagger \hat{\Psi}(\mathbf{r}')^\dagger V(\mathbf{r}-\mathbf{r}') \hat{\Psi}(\mathbf{r}') \hat{\Psi}(\mathbf{r}) \right) \end{aligned} \tag{1.47}$$

with $V(\mathbf{r})$ the two-body potential. As we saw in the previous section, the interaction potential can be conveniently replaced by the contact type potential $V(\mathbf{r}) = g\delta(\mathbf{r}-\mathbf{r}')$. Restricting us to the uniform gas occupying a volume V,

and expressing the field operators in the plane-wave basis as in Eq. (1.24), the Hamiltonian becomes

$$\hat{H} = \sum_{\mathbf{k}} \varepsilon_{\mathbf{k}} \hat{a}^\dagger_{\mathbf{k}} \hat{a}_{\mathbf{k}} + \frac{g}{2V} \sum_{\mathbf{k},\mathbf{k}',\mathbf{q}} \hat{a}^\dagger_{\mathbf{k}} \hat{a}^\dagger_{\mathbf{k}'+\mathbf{q}} \hat{a}_{\mathbf{k}'} \hat{a}_{\mathbf{k}+\mathbf{q}} \,, \tag{1.48}$$

with $\varepsilon_{\mathbf{k}} = \hbar^2 k^2/(2m)$ the single-particle kinetic energy. A major assumption in solving the above Hamiltonian consists to replace the operator for the lowest lying mode $\hat{a}_0$ ($\hat{a}^\dagger_0$) by the number of condensate atoms N_0. This is the *Bogoliubov prescription*, motivated by the macroscopic occupation of the condensate state [34].

Let us consider the ground state of the gas, at zero temperature. Then, one may expect the depletion of the condensate due to interactions to be small, since for an ideal gas all the atoms are found to be in the condensate state at $T = 0$. We can therefore keep in Eq. (1.47) only quadratic terms in the particle operator $\hat{a}_{\mathbf{k}\neq 0}$, and neglect higher order terms. From momentum conservation, one also dismisses the terms in which only one operator $\hat{a}_{\mathbf{p}\neq 0}(\hat{a}^\dagger_{\mathbf{p}\neq 0})$ appears, so as to rewrite the Hamiltonian in the form:

$$\hat{H} = \frac{g}{2V} N_0^2 + \sum_{\mathbf{k}\neq 0} \varepsilon_{\mathbf{k}} \hat{a}^\dagger_{\mathbf{k}} \hat{a}_{\mathbf{k}} + \frac{2g}{V} N_0 \sum_{\mathbf{k}\neq 0} \hat{a}^\dagger_{\mathbf{k}} \hat{a}_{\mathbf{k}} + \frac{g}{2V} N_0 \sum_{\mathbf{k}\neq 0} \left(\hat{a}^\dagger_{\mathbf{k}} \hat{a}^\dagger_{-\mathbf{k}} + \hat{a}_{\mathbf{k}} \hat{a}_{-\mathbf{k}} \right) . \tag{1.49}$$

To leading order in g, one can replace N_0 by N in the last two terms of Eq. (1.49), while it has to be replaced by

$$N_0^2 \simeq N^2 - 2N \sum_{\mathbf{k}\neq 0} \hat{a}^\dagger_{\mathbf{k}} \hat{a}_{\mathbf{k}} \,, \tag{1.50}$$

in the first term in order to keep the same accuracy. It is worth noticing that the last terms of Eq. (1.49) do not preserve the number of atoms, meaning that in the Bogoliubov approach the condensate plays the role of a reservoir. Furthermore, as we will see later, the ground-state energy associated with the Hamiltonian (1.49) exhibits a ultraviolet divergence, due to the momentum sum. Finally, the Bogoliubov Hamiltonian is given by,

$$\hat{H} = \frac{g}{2V} N^2 + \sum_{\mathbf{k}\neq 0} \varepsilon_{\mathbf{k}} \hat{a}^\dagger_{\mathbf{k}} \hat{a}_{\mathbf{k}} + \frac{2g}{V} N \sum_{\mathbf{k}\neq 0} \hat{a}^\dagger_{\mathbf{k}} \hat{a}_{\mathbf{k}} + \frac{g}{2V} N \sum_{\mathbf{k}\neq 0} \left(\hat{a}^\dagger_{\mathbf{k}} \hat{a}^\dagger_{-\mathbf{k}} + \hat{a}_{\mathbf{k}} \hat{a}_{-\mathbf{k}} \right) . \tag{1.51}$$

We now diagonalize the Hamiltonian, by performing the following canonical (Bogoliubov) transformations:

$$\begin{aligned} \hat{a}_{\mathbf{k}} &= u_{\mathbf{k}} \hat{\alpha}_{\mathbf{k}} + v^*_{-\mathbf{k}} \hat{\alpha}^\dagger_{-\mathbf{k}} \,, \\ \hat{a}^\dagger_{\mathbf{k}} &= u^*_{\mathbf{k}} \hat{\alpha}^\dagger_{\mathbf{k}} + v_{-\mathbf{k}} \hat{\alpha}_{-\mathbf{k}} \,. \end{aligned} \tag{1.52}$$

These new creation and annihilation operators obey the Bose statistics, and consequently,

$$|u_{\mathbf{k}}|^2 - |v_{-\mathbf{k}}|^2 = 1\,. \tag{1.53}$$

Inserting Eq. (1.52) into the Hamiltonian Eq. (1.51), one finds that the off-diagonal terms $\hat{\alpha}\hat{\alpha}$ ($\hat{\alpha}^\dagger\hat{\alpha}^\dagger$) vanish for the following values of the quasi-particle amplitudes:

$$u_{\mathbf{k}}, v_{-\mathbf{k}} = \pm\left(\frac{\varepsilon_{\mathbf{k}} + gn}{2E_{\mathbf{k}}} \pm \frac{1}{2}\right)^{1/2}\,, \tag{1.54}$$

where the Bogoliubov spectrum of elementary excitations is given by

$$E_{\mathbf{k}} = \sqrt{\varepsilon_{\mathbf{k}}^2 + 2gn\varepsilon_{\mathbf{k}}}\,. \tag{1.55}$$

The long wavelength excitation mode of the Bogoliubov gas corresponds to a sound mode, $\lim_{\mathbf{k}\to 0} E_{\mathbf{k}} = c_0 k$, with

$$c_0 = \sqrt{\frac{gn}{m}}\,, \tag{1.56}$$

the Bogoliubov phonon mode velocity. This sound mode arises from the macroscopic coherence of the condensate, and therefore has a collisionless nature. It corresponds to the Goldstone mode of the weakly-interacting Bose gas, associated with the spontaneous breaking of Gauge symmetry (see Eq. (1.69) below). Instead for higher mode, the excitation spectrum is described by the single-particle kinetic energy, $\lim_{\mathbf{k}\to\infty} E_{\mathbf{k}} = \varepsilon_k$.

Finally, the Hamiltonian (1.51) in its diagonalized form reads

$$\hat{H} = E_0 + \sum_{\mathbf{k}\neq 0} E_{\mathbf{k}}\hat{\alpha}_{\mathbf{k}}^\dagger\hat{\alpha}_{\mathbf{k}}\,, \tag{1.57}$$

with the ground-state energy

$$E_0 = \frac{g}{2V}N^2 + \frac{1}{2}\sum_{\mathbf{k}\neq 0}\left[E_{\mathbf{k}} - gn - \varepsilon_{\mathbf{k}}\right] \tag{1.58}$$

$$= \frac{g}{2V}N^2\left[1 + \frac{128}{15\sqrt{\pi}}(na^3)^{1/2}\right]\,. \tag{1.59}$$

where we have performed the momentum integration in going to the second line. As we have already stressed, this integration is ultraviolet divergent and has to be cured by a proper renormalization of the coupling constant. This problem arises from the Born approximation we have made in the previous section, which includes only the lowest order contribution to the coupling constant. Since we are developing a second-order perturbation theory, one needs to include also second-order contribution in the Born approximation for the interacting potential. This

is achieved by replacing the coupling constant g in the first term of Eq. (1.58) by [33, §6]:

$$gn \to gn\left(1 + \frac{g}{V}\sum_{\mathbf{k}\neq 0}\frac{m}{\hbar}\frac{1}{p^2}\right) . \tag{1.60}$$

The last term of Eq. (1.59), the Lee-Huang-Yang (LHY) correction, characterizes the effects of quantum fluctuations [35]. It arises from the inclusion of the last terms of Eq. (1.48), in which annihilation and creation operators appear by pairs. As for the depletion of the condensate, one finds from Eq. (1.50) that in the ground-state

$$\begin{aligned} n_0 &= n - \frac{1}{V}\sum_{\mathbf{k}\neq 0}\langle \hat{a}^\dagger_{\mathbf{k}}\hat{a}_{\mathbf{k}}\rangle \\ &= n\left[1 - \frac{8}{3\sqrt{\pi}}(na^3)^{1/2}\right] . \end{aligned} \tag{1.61}$$

The Bogoliubov theory therefore shows that the system of interacting particles Eq. (1.48) can be mapped into an effective Hamiltonian of non-interacting quasi-particles Eq. (1.57). In the subsequent chapters, we will see how to extend the present model to finite-temperature.

1.2.4 Superfluidity

Zero temperature

The phenomenon of superfluidity was first observed by Kapitza [36], Allen and Misener [37] in 1938, and theorized later by London [38], Tisza [39], and Landau [8] (for an historical overview, see Ref. [40]). In the initial experiment of Kapitza, they observed a non-viscous flow of liquid Helium trough capillaries when the fluid was cooled down to 2K. Landau later showed that for a moving quantum fluid, the process of spontaneous creation of excitations was energetically favorable only under a very specific condition. In particular, he found that as far as the velocity of the fluid is smaller than a critical value

$$v_c = \min_{\mathbf{p}} \frac{E_{\mathbf{p}}}{p} , \tag{1.62}$$

the spontaneous emission of excitations, thus the dissipation of energy, is not possible. This is the Landau's criterion of superfluidity. In such regime, the fluid is said to behave as a superfluid, flowing without any friction. For an ideal Bose gas, in which the excitation spectrum is given by the single-particle kinetic energy

$E_{\mathbf{p}} = p^2/(2m)$, Eq. (1.62) gives a zero critical velocity, meaning that the non-interacting gas is not superfluid. Instead, for a weakly interacting Bose gas, one finds from Eq. (1.55) that

$$v_c = c_0 \,, \tag{1.63}$$

with c_0 the phonon velocity (1.56).

Connection to Bose-Einstein condensation

The above analysis underlines that BEC and superfluidity are distinct phenomena, which are not to be confused. Nevertheless, one can show that both phenomena are closely related to each other [7]. To see this connection, let us write down the equation of motion for the field operator, in the Heisenberg picture,

$$i\hbar \frac{\partial \hat{\Psi}(\mathbf{r},t)}{\partial t} = [\hat{\Psi}(\mathbf{r},t), \hat{H}] = \left[-\frac{\hbar^2}{2m}\nabla^2 + V_{\rm ext}(\mathbf{r},t) + g|\hat{\Psi}(\mathbf{r},t)|^2 \right] \hat{\Psi}(\mathbf{r},t) \,, \tag{1.64}$$

where we have used the Hamiltonian (1.47) assuming contact-like interaction and an external potential $V_{\rm ext}(\mathbf{r},t)$. In order to look for the solutions of the equation of motion, let us recall the Bogoliubov prescription introduced earlier. In terms of the field operator, the Bogoliubov ansatz can be expressed as

$$\hat{\Psi}(\mathbf{r}) \simeq \Psi_0(\mathbf{r}) + \delta\hat{\Psi}(\mathbf{r}) \,, \tag{1.65}$$

where $\Psi_0(\mathbf{r})$ is the wave function of the condensate. It is a complex classical field,

$$\Psi_0(\mathbf{r},t) = \sqrt{n_0(\mathbf{r},t)} e^{iS(\mathbf{r},t)} \,. \tag{1.66}$$

Similarly to the Bogoliubov theory, at zero temperature one can safely approximate $\hat{\Psi}$ by Ψ_0. This leads us to the celebrated Gross-Pitaevskii equation [41, 42]:

$$i\hbar \frac{\partial \Psi_0(\mathbf{r},t)}{\partial t} = \left[-\frac{\hbar^2}{2m}\nabla^2 + V_{\rm ext}(\mathbf{r},t) + g|\Psi_0(\mathbf{r},t)|^2 \right] \Psi_0(\mathbf{r},t) \,, \tag{1.67}$$

extensively used in the literature for the investigation of zero-temperature Bose gas dynamics (for a review, see Ref. [4]).

Let us start looking to the stationary solution of Eq. (1.64). The Bogoliubov ansatz is in fact equivalent to the the identity $\langle\hat{\Psi}\rangle = \Psi_0$, and one can rewrite the classical field in terms of the time evolution operators as

$$\Psi_0(\mathbf{r},t) = \langle e^{\frac{i}{\hbar}\hat{H}t} \hat{\Psi}(\mathbf{r}) e^{-\frac{i}{\hbar}\hat{H}t} \rangle \tag{1.68}$$

As we have already pointed out, the orthogonality between the left and right states does not imply a zero average, since one considers the condensate to act as

a reservoir, in which adding or subtracting a particle does not modify the physics. Finally, the stationary solution takes the form

$$\Psi_0(\mathbf{r},t) = \Psi_0(\mathbf{r})e^{-\frac{i}{\hbar}\mu t}\,. \tag{1.69}$$

We also briefly note that the explicit choice for the phase of the order parameter $S(\mathbf{r},t)$ as we have seen here, corresponds to the spontaneous breaking of Gauge symmetry [43].

Let us now consider a uniform condensate at rest. Then, neglecting the contribution of thermal and quantum depletions, the equilibrium solution of Eq. (1.64) is given by the stationary solution $\Psi_0(\mathbf{t}) = \sqrt{n_0}e^{-i\mu t/\hbar}$. In the moving frame instead, in which the fluid moves with velocity $\mathbf{v}$, one can verify that

$$\Psi_0'(\mathbf{r},t) = \sqrt{n_0}e^{iS'(\mathbf{r},t)}\,, \tag{1.70}$$

with the new phase given by

$$S'(\mathbf{r},t) = \frac{1}{\hbar}\left[m\mathbf{v}\mathbf{r} - \left(\frac{1}{2}mv^2 + \mu\right)t\right]\,, \tag{1.71}$$

is a solution of Eq. (1.64). Thus, the velocity of the fluid is given by

$$\mathbf{v}_s = \frac{\hbar}{m}\nabla S \tag{1.72}$$

and can be identified to the superfluid velocity. Because of the divergence, the flow is irrotational ($\nabla \times \mathbf{v}_s = 0$). It is worth stressing that Eq. (1.72) has been derived by assuming the existence of an order parameter Eq. (1.66) only, and therefore is general to any superfluid.

Finite-temperature

In Sec. 1.2.3 we have seen that the gas of interacting bosons can be regarded as a gas of non-interacting quasi-particles (excitations). Therefore, at finite but sufficiently small temperature, one can assume the thermodynamic properties of the fluid to be described by those excitations. Although the superfluid does not create any new excitations, quasi-particles can be thermally excited. Then, these quasi-particles can collide with the capillary, eventually exchanging energy and momentum, therefore acting as a viscous fluid. Thus at finite temperature, the gas can be described by a two-fluid picture, in which both a non-viscous superfluid and a viscous normal fluid coexist [33, §23]:

$$n = n_s + n_n\,, \tag{1.73}$$

with n_s and n_n, the superfluid and normal components of the fluid, respectively.

Although the superfluid velocity is related to the phase of the condensate wave function, it does not imply that the superfluid density is connected to the condensate density. Actually, identifying the normal fluid to the gas of excitations, one can show that the normal atoms density is given by the formula

$$n_n = -\frac{1}{3m}\frac{1}{(2\pi\hbar)^3}\int d^3\mathbf{p}\, p^2 \frac{dN_{\mathbf{p}}(E)}{dE}\,, \tag{1.74}$$

where $N_{\mathbf{p}}(E)$ is the distribution of excitations, which according to the Bogoliubov theory, follows non-interacting Bose statistics. One can verify that for an ideal Bose gas $E_{\mathbf{p}} = p^2/(2m)$, Eq. (1.74) yields $n_n = n$ for any temperatures, so that $n_s = 0$.

1.3 Sound propagation in quantum fluids

We now discuss the propagation of sound waves in quantum fluids. In this respect, we will first give the two-fluid equation for the hydrodynamic sounds, which are derived from general considerations, and apply to any superfluids. Next, we will discuss the sound propagation in the collisionless regime, by reviewing some general concepts of linear response theory.

1.3.1 Two-fluid hydrodynamics

The hydrodynamic equations for the sound waves in a quantum fluid are obtained in a similar fashion to the classical gas Sec. 1.1.2. We start from the assumption of local thermodynamic equilibrium, so as to derive the conservation equations holding in every point of the fluid [7, §6.6] [1, §141]. However, as we have discussed before, a major difference comes from the consideration of two separated and independent fluids: the normal fluid and the superfluid. Consequently, the current density is given by:

$$\mathbf{j}(\mathbf{r},t) = n_s\mathbf{v}_s + n_n\mathbf{v}_n\,. \tag{1.75}$$

Both the continuity equation and the momentum conservation take the same form as the classical fluid, Eqs. (1.9a) and (1.9b),

$$\frac{\partial}{\partial t}n(\mathbf{r},t) + \nabla\mathbf{j}(\mathbf{r},t) = 0\,, \tag{1.76a}$$

$$m\frac{\partial}{\partial t}\mathbf{j}(\mathbf{r},t) + \nabla P(\mathbf{r},t) = 0\,, \tag{1.76b}$$

where we have omitted the external field. Important considerations about the superfluid arise in the equation for the superfluid velocity $\mathbf{v}_s$, which is related to the chemical potential as (see Eqs. (1.69), (1.70))

$$m\frac{\partial \mathbf{v}_s}{\partial t} + \nabla\mu = 0\,, \tag{1.76c}$$

and the equation for the entropy per unit volume,

$$\frac{\partial s}{\partial t} + \nabla(s\mathbf{v}_n) = 0\,, \tag{1.76d}$$

reflecting that the superfluid component does not carry any entropy. From Eqs. (1.76a) and (1.76b) one finds the wave equation for the pressure/density:

$$m\frac{\partial^2 n}{\partial t^2} = \nabla^2 P\,. \tag{1.77}$$

On the other hand, Eqs. (1.76c) and (1.76d) together with the Gibbs-Duhem relation

$$dP = nd\mu + sdT\,, \tag{1.78}$$

leads to the wave equation for the entropy/temperature:

$$\frac{\partial^2 \bar{s}}{\partial t^2} = \frac{1}{m}\frac{n_s}{n_n}\bar{s}^2\nabla^2 T \tag{1.79}$$

where $\bar{s} = s/n$ is the entropy per particle. This last equation makes the key difference with the classical hydrodynamic equations derived earlier. We now linearize Eqs. (1.77) and (1.79), by looking for plane-wave solutions $x(\mathbf{r},t) = x_0 + \delta x e^{i(kx-\omega t)}$. Using the expansion

$$\delta n = \left.\frac{\partial n}{\partial P}\right|_T \delta P + \left.\frac{\partial n}{\partial T}\right|_P \delta T\,, \quad \delta\bar{s} = \left.\frac{\partial \bar{s}}{\partial P}\right|_T \delta P + \left.\frac{\partial \bar{s}}{\partial T}\right|_P \delta T\,, \tag{1.80}$$

to express the equations in terms of the variables P and T, one finds

$$\left(1 - c^2\frac{\partial n}{\partial P}\right)\delta P - \omega^2\frac{\partial n}{\partial T}\delta T = 0\,, \tag{1.81a}$$

$$\left(\frac{n_s}{n_n}\bar{s}^2 - c^2\frac{\partial \bar{s}}{\partial T}\right)\delta T - \omega^2\frac{\partial \bar{s}}{\partial P}\delta P = 0\,. \tag{1.81b}$$

These two coupled equations can be recast to a single quartic equation, and finally using some general thermodynamic identities one finds:

$$c^4 - \left[\frac{1}{mn\kappa_s} + \frac{n_s T\bar{s}^2}{mn_n\bar{c}_v}\right]c^2 + \frac{n_s T\bar{s}^2}{mn_n\bar{c}_V}\frac{1}{mn\kappa_T} = 0\,, \tag{1.82}$$

where $\kappa_{s(T)}$ is the adiabatic (isothermal) compressibility, and $\bar{c}_V$ the specific heat at constant volume per particle. Equation (1.82) is the Landau's two-fluid hydrodynamic equation, which possesses two positive solutions, referred as to the first and second sound. Here, the terminology second sound is used to designate the sound wave that arises from the presence of a superfluid, and which vanishes otherwise. It is worth stressing that in deriving Eq. (1.82), we have only assumed general properties of the superfluid (irrotational flow and zero entropy). Landau's two-fluid equation is therefore very general, being applicable for any superfluid systems regardless the statistics of the particles or the interaction. The specific properties of the fluid arises only in the behavior of the thermodynamic quantities entering in Eq. (1.82). The proper determination of the equation of state of the system under consideration is therefore essential and the subsequent chapters will be devoted for the development of reliable thermodynamic theories.

Before closing this section, let us consider some general solutions of Eq. (1.82) [9]. First, as one approaches the superfluid to normal transition point $T \to T_c$, the superfluid density becomes small $n_s \to 0$ [1]. In this regime the inequality $c_1 \gg c_2$ holds, where c_1 and c_2 are the first and second sound, respectively. By neglecting the c^0 (c^4) term in Eq. (1.82) one obtains to lowest order in n_s,

$$c_1 = \sqrt{\frac{1}{mn\kappa_s}}\,, \qquad c_2 = \sqrt{\frac{n_s T\tilde{s}^2}{mn_n\bar{c}_P}}\,, \tag{1.83}$$

with $\bar{c}_P$ the specific heat at constant pressure per particle. Next, above T_c, $n_s = 0$, and the second sound vanishes, whereas the first sound is described by the classical gas expression $c_1^2 = \partial P/\partial n|_{\tilde{s}}$. Finally, we have previously seen that the two wave equations (1.77) and (1.79) are coupled to each other. From Eq. (1.81) it is found that this coupling is negligible if

$$\alpha T = \left(\frac{\kappa_T}{\kappa_s} - 1\right) \ll 1\,, \tag{1.84}$$

where $\alpha = -n^{-1}\partial n/\partial T|_P$ is the thermal expansion coefficient. In that case, Eqs. (1.77) and (1.79) take the form of independent wave equations for the density and the entropy, respectively, and Eq. (1.83) yields the correct speed of sounds. Generally, condition (1.84) is satisfied as one approaches $T = 0$ since $\kappa_T \simeq \kappa_s$. Other important examples of incompressible fluids are the strongly interacting systems, such as liquid Helium or unitary Fermi gas, for which Eq. (1.83) provides the correct behavior of the sounds speed in a wide range of temperature.

[1] A notable exception is the two-dimensional Bose gas, as one shall discuss in Sec. 3

1.3.2 Linear response theory

In Sec. 1.1.3, we have seen that the investigation of the density response function provides valuable information about the behavior of sound wave in the collisionless regime. In this section, we will introduce the linear response theory, which provides a direct way to calculate the response of the system to any type of external perturbation. Contrary to the classical density response function derived from the collisionless Boltzmann equation (1.19), the linear response formalism can in principle be applied both in the hydrodynamic and collisionless regime. In particular, one can derive general sum rules, which offer a powerful tool to investigate the dynamic properties of the system. We here follow the development of Ref. [7, §7], and focus in particular to the density response of the gas.

Generality

Let us consider a many-body system described by the Hamiltonian $\hat{H}_0$, being under an external perturbation described by the Hamiltonian $\hat{H}_{\rm pert}$. The expectation value of a physical quantity of interest, described by an operator $\hat{F}$, is given by

$$\langle \hat{F}^\dagger \rangle = \frac{1}{Z} \mathrm{Tr}\left[\hat{\rho}\hat{F}^\dagger\right] , \tag{1.85}$$

with $\hat{\rho} = e^{-\beta(\hat{H}_0+\hat{H}_{\rm pert})}$ the density matrix and $Z = \mathrm{Tr}[\hat{\rho}]$ the partition function. Then, by applying linear perturbation theory to evaluate the trace, one arrives to the Kubo formula [28, §32] [44, §1.2]:

$$\langle \hat{F}^\dagger \rangle = \langle \hat{F}^\dagger \rangle_0 - \frac{i}{\hbar}\int_{-\infty}^{t} dt' \mathrm{Tr}\left\{\hat{\rho}_0\left[\hat{H}_{\rm pert}(t'), \hat{F}^\dagger(t)\right]\right\} , \tag{1.86}$$

where the expectation value on the right-hand side is calculated with respect to the unperturbed system $\hat{H}_0$, and the operators are taken in the interaction picture $\hat{\alpha}(t) = e^{\frac{i}{\hbar}\hat{H}_0 t}\hat{\alpha}e^{-\frac{i}{\hbar}\hat{H}_0 t}$. Hereafter we omit the subscript 0 for the expectation values.

Now, we consider the particular case in which the perturbation has an explicit time-dependence given by

$$\hat{H}_{\rm pert} = -\lambda \hat{G} e^{-i\omega t} e^{\eta t} + \mathrm{h.c.} , \tag{1.87}$$

where λ is the amplitude of the external field, $\hat{G}$ a given operator, and $e^{\eta t}$ with small positive value of η ensures that as $t \to -\infty$ the perturbation vanishes. The fluctuation $\delta\langle \hat{F}^\dagger \rangle$ of an operator of physical interest $\hat{F}$ induced by such perturbation oscillates at the same frequency ω as the external field. We introduce the linear response function $\chi_{F^\dagger G}$, defined as

$$\delta\langle \hat{F}^\dagger \rangle = \lambda e^{-i\omega t} e^{\eta t} \chi_{F^\dagger G} + \mathrm{h.c.} + \lambda^* e^{i\omega t} e^{\eta t} \chi_{F^\dagger G^\dagger} . \tag{1.88}$$

To calculate χ, we use the Kubo formula (1.86), and consider that at $t \to -\infty$ the system is in thermal equilibrium at temperature T. Then, the trace is evaluated as a canonical ensemble average:

$$\begin{aligned}\mathrm{Tr}\left[\hat{\rho}_0 \hat{H}_{\mathrm{pert}}(t')\,\hat{F}^\dagger(t)\right] &= \sum_n e^{-\beta E_n}\langle n|\hat{H}_{\mathrm{pert}}(t')\hat{F}^\dagger(t)|n\rangle \\ &= -\lambda e^{-i(\omega-i\eta)t'}\sum_{n,m} e^{-\beta E_n} e^{i\omega_{nm}(t'-t)}\langle n|\hat{G}|m\rangle\langle m|\hat{F}^\dagger|n\rangle\,,\end{aligned} \tag{1.89}$$

where $|n\rangle$ and E_n are the eigenstate and eigenvalue of the unperturbed Hamiltonian $\hat{H}_0|n\rangle = E_n|n\rangle$, and $\omega_{nm} = (E_n - E_m)/\hbar$. In the last line we have also used the completeness relation $\sum_m |m\rangle\langle m| = 1$. Performing the time integration in Eq. (1.86), the response function is found to be

$$\chi_{F^\dagger G} = -\frac{1}{\hbar} Z^{-1}\sum_{m,n} e^{-\beta E_m}\left[\frac{\langle m|\hat{F}^\dagger|n\rangle\langle n|\hat{G}|m\rangle}{\omega-\omega_{nm}+i\eta} - \frac{\langle m|\hat{G}|n\rangle\langle n|\hat{F}^\dagger|m\rangle}{\omega+\omega_{nm}+i\eta}\right]. \tag{1.90}$$

For future purpose it is useful to introduce the dynamic structure factor,

$$S_F(\omega) = Z^{-1}\sum_{m,n} e^{-\beta E_m}|\langle n|\hat{F}|m\rangle|^2\delta(\hbar\omega - \hbar\omega_{nm})\,, \tag{1.91}$$

which embodies valuable informations about the excitation spectrum of the fluctuation. In what follows, we consider the simplest case in which $\hat{F} = \hat{G}$. In that case, the connection between the response function and the dynamic structure factor is straightforward:

$$\chi_F(\omega) = -\int_{-\infty}^{\infty} d\omega'\left[\frac{S_F(\omega')}{\omega-\omega'+i\eta} - \frac{S_{F^\dagger}(\omega')}{\omega+\omega'+i\eta}\right]. \tag{1.92}$$

Density response function

For the study of the sound propagation, the fluctuation we are interested in corresponds to the density one. Let us therefore consider the density operator for a uniform system

$$\hat{\rho}_{\mathbf{q}} = \frac{1}{V}\sum_{\mathbf{p}} \hat{a}^\dagger_{\mathbf{p}-\hbar\mathbf{q}}\hat{a}_{\mathbf{q}}\,. \tag{1.93}$$

The associated fluctuation operator is given by $\delta\hat{\rho}_{\mathbf{q}} = \hat{\rho}_{\mathbf{q}} - \langle\hat{\rho}_{\mathbf{q}}\rangle$, with $\langle\hat{\rho}_{\mathbf{q}}\rangle = 0$ at equilibrium if $\mathbf{q} \neq 0$. Then, the density response function $\hat{F} = \delta\hat{\rho}^\dagger_{\mathbf{q}}$ is given from Eq. (1.90) as

$$\chi(\mathbf{q},\omega) = -\frac{1}{\hbar V} Z^{-1}\sum_{m,n} e^{-\beta E_m}\left[\frac{|\langle m|\delta\hat{\rho}_{\mathbf{q}}|n\rangle|^2}{\omega-\omega_{nm}+i\eta} - \frac{|\langle m|\delta\hat{\rho}^\dagger_{\mathbf{q}}|n\rangle|^2}{\omega+\omega_{nm}+i\eta}\right]. \tag{1.94}$$

From Eq. (1.91) one can further obtain the dynamic structure factor

$$S(\mathbf{q},\omega) = Z^{-1}\sum_{m,n} e^{-\beta E_m}|\langle n|\delta\hat{\rho}^\dagger_{\mathbf{q}}|m\rangle|^2\delta(\hbar\omega - \hbar\omega_{nm})\,. \tag{1.95}$$

The evaluation of the response function requires the solution of the Schrödinger equation in order to evaluate the eigenstates of the unperturbed system. However, insightful informations about the response function can be extracted by the method of sum-rule [45], which provides a convenient way to evaluate the moments of the dynamic structure factor:

$$m_p(\mathbf{q}) = \hbar^{p+1}\int_{-\infty}^{\infty} d\omega\omega^p S(\mathbf{q},\omega)\,. \tag{1.96}$$

In particular, two sum rules related to the density response will be extensively used in the following chapters. The first one, known as the f-sum rule, comes from the particle conservation of the system

$$m_1(\mathbf{q}) = n\frac{\hbar^2 q^2}{2m}\,, \tag{1.97}$$

with n the total atoms density. The energy weighted momentum characterizes the high-frequency behavior of the response function, and one has consequently

$$\lim_{\omega\to\infty}\chi(\mathbf{q},\omega) = \frac{n}{m}\frac{q^2}{\omega^2}\,. \tag{1.98}$$

The second one is the compressibility sum rule, which connects the dynamic property of the system to the thermodynamic one:

$$\lim_{\mathbf{q}\to 0} m_{-1}(\mathbf{q}) = \frac{1}{2}n^2\kappa_T\,, \tag{1.99}$$

where κ_T is the isothermal compressibility of the gas. The inverse energy-weighted momentum is instead related to the static response as

$$\lim_{\mathbf{q}\to 0}\chi(\mathbf{q},\omega=0) = n^2\kappa_T\,. \tag{1.100}$$

1.3.3 Quantum Boltzmann equation

So far, we have considered distinctly the two extreme regimes which are the collisionless and collisional hydrodynamic regimes. However, as we have seen for the classical gas, a unified description of the transport phenomena is in principle possible starting from transport equations. Although we will not give the details

here, one can actually show that not only the classical particles, but also quantum particles obey the Boltzmann equation (1.2) [24, 46]. In that case, the collisional integral (1.4) has to be adapted to include the statistical nature of the particles, and for the bosons it takes the form

$$\left.\frac{\partial f}{\partial t}\right|_{\text{coll}} = \frac{\sigma}{\pi m^2 (2\pi\hbar)^3} \int d^3\mathbf{p}_2 d^3\mathbf{p}'_1 d^3\mathbf{p}'_2 \delta(\mathbf{p}+\mathbf{p}_2-\mathbf{p}_{1'}-\mathbf{p}_{2'}) \times \delta(\varepsilon_{\mathbf{p}}+\varepsilon_{\mathbf{p}_2}-\varepsilon_{\mathbf{p}_{1'}}-\varepsilon_{\mathbf{p}_{2'}}) \times \left[(1+f)(1+f_2)f_{1'}f_{2'} - (1+f_{1'})(1+f_{2'})f_1 f_2\right] , \tag{1.101}$$

where we have expressed the scattering function in terms of the differential cross section σ and Dirac δ-functions, to take into account energy and momentum conservation, and adopted the short-hand notation $f_1 = f(\mathbf{r}, \mathbf{p}_1, t)$. This collisional term is referred to the Uehling-Uhlenbeck formula [47, 48], and together with Eq. (1.2) they form the quantum Boltzmann equation for bosons. The additional $(1+f_1)(1+f_2)$ terms take into account the bosonic bunching, in which the colliding atoms preferentially scatter into states already occupied by other atoms. One can verify that Eq. (1.101) vanishes for the following class of solutions:

$$f(\mathbf{p},\mathbf{r},t) = \left[e^{\beta(\mathbf{r},t)\left(\frac{1}{2m}(\mathbf{p}-m\mathbf{u}(\mathbf{r},t))^2-\mu(\mathbf{r},t)\right)}-1\right]^{-1} . \tag{1.102}$$

In particular, the thermodynamic equilibrium solution in absence of an external potential is given by the Bose-Einstein distribution function (1.31).

We briefly note that the quantum Boltzmann equation as defined in the last paragraph, does not include the physics of the condensate. For this purpose, one needs an additional equation to describe the transport properties of the BEC. This is achieved by solving the quantum Boltzmann equation together with the Gross-Pitaevskii equation (1.67), and by including the effects of collisions between condensate and thermal atoms through a second collisional integral analogous to Eq. (1.101) [49–51]. This is the general idea behind the finite-temperature non-equilibrium theory developed by Zaremba, Nikuni and Griffin, referred to the ZNG model [46]. The analysis of sound dynamics in the framework of ZNG approach is out of the scope of this thesis, for two reasons. First, the ZNG solutions in the hydrodynamic and collisionless limits correspond, respectively, to the solutions obtained within the Landau equation (1.82) and linear response Eq. (1.94), evaluated within the Random Phase Approximation. In this thesis, we shall focus on the two limits, using the later approaches. Secondly, the ZNG framework being based on the existence of a well-defined condensate, it is *a priori* not suitable for the investigation of 2D Bose gas, carried in Chap. 3, for which BEC does not occur. From this point of view, a reliable description of the dynamics in the 2D

Bose gas is provided by stochastic approaches, such as the stochastic (projected) Gross-Pitaevskii equation [52–54].

1.3.4 From the hydrodynamic to the collisionless regime

In this section we briefly discuss how to assess in which regime between the hydrodynamic one and collisionless one a fluid belongs. The most straightforward way for this purpose is to introduce the collisional time τ, defined from the single relaxation time approximation for the collisional term of Eq. (1.2) as

$$\left.\frac{\partial f}{\partial t}\right|_{\text{coll}} \simeq -\frac{f(\mathbf{r},\mathbf{p},t) - f^0(\mathbf{r},\mathbf{p})}{\tau}\,, \tag{1.103}$$

with f^0 the distribution function at equilibrium. The above approximation simplifies the expression of the collisional term by assuming an exponential decay of the out-of-equilibrium distribution toward its equilibrium value, with characteristic time τ. As briefly discussed in Sec. 1.1.1, the fluid is said to be in the collisional hydrodynamic regime if the mean time between two collisions, τ, is much larger than the typical time-scale of the fluid dynamics, ω^{-1}, so as to ensure the local equilibrium picture. Oppositely, the fluid is in the collisionless regime, if τ is sufficiently large, so that the collision integral described by Eq. (1.103) becomes negligible. Hence,

$$\begin{aligned} &\omega\tau \ll 1 \qquad \text{Hydrodynamic} \\ &\omega\tau \gg 1 \qquad \text{Collisionless} \end{aligned}$$

where in our interest, $\omega = ck$ is the sound frequency, with velocity c and wavevector k. It is important to underline that the term *collisionless* does not mean *non-interacting*. In presence of inter-atomic interaction, one can adopt the quasi-particle picture, in which the particle is dressed with a self-consistent field arising from the interaction with all the other atoms (U_{eff} in Sec. (1.1.3)) [45]. Then, the hydrodynamic regime will correspond to a regime in which the restoring force to the equilibrium state arises from the instantaneous collisions between these non-interacting quasi-particles, as described by the collisional integral of Eq. (1.4). As for the collisionless regime, the restoring force is instead brought about by the aforementioned self-consistent field, which under an external perturbation will depend on position and time. One can hence stress that, a non-interacting gas can propagate in the hydrodynamic regime, while in the collisionless regime not, since the self-consistent field would not exist.

Let us give an estimate for the relaxation time, based on the collisional integral Eq. (1.101) [46, §11.3]. In particular, we are interested in the scattering out term,

since it represents the number of atoms per unit time colliding in the element volume $d^3\mathbf{r}d^3\mathbf{p}$ and leaving it. Therefore,

$$\Gamma = \frac{1}{(2\pi\hbar)^3}\int d^3\mathbf{p}\left(\frac{\partial f}{\partial t}\right)_{\text{out}}, \tag{1.104}$$

represents the number of atoms colliding per unit volume and unit time. On the other hand, by definition τ is the mean time between two collisions, and thus dt/τ the probability for an atom to collide in an interval of time dt. It follows that $n(\mathbf{r})d^3\mathbf{r}dt/\tau$ is the number of atoms in the unit volume $d^3\mathbf{r}$ experiencing a collision in the time interval dt. Therefore,

$$\Gamma = \frac{n(\mathbf{r},t)}{\tau(\mathbf{r},t)}\,. \tag{1.105}$$

For the normal Bose gas in equilibrium, Γ is obtained from Eq. (1.101) replacing f by its equilibrium value f^0. After performing the integral over the δ-functions, one finds (see for instance Refs. [23, 46])

$$\frac{1}{\tau_{22}} = \frac{\sigma}{4\pi(2\pi\hbar)^6}\int d^3\mathbf{p}_1\int d^3\mathbf{p}_2\int d\Omega|\mathbf{v}_1-\mathbf{v}_2|f_1^0f_2^0(1+f_3^0)(1+f_4^0)\,, \tag{1.106}$$

where $\mathbf{p}_{3,4}$ are functions of $\mathbf{p}_{1,2}$ according to energy and momentum conservation. In the classical limit, one can find by using the Maxwell-Boltzmann distribution Eq. (1.6) for f^0,

$$\frac{1}{\tau_{\text{MB}}} = \sqrt{2}\sigma v_{\text{th}}n\,, \tag{1.107}$$

with $v_{\text{th}} = \sqrt{8k_BT/(\pi m)}$ the mean velocity. The cross-section is instead related to the scattering amplitude $f(k,\theta)$ of Eq. (1.41) as $d\sigma/d\Omega = |f(k,\theta)|^2$ and in the s-wave regime, $\sigma = 8\pi a^2$.

1.4 Overview of sound experiments in ultracold quantum gases

Before closing this chapter, let us review the existing works in the field of sound propagation in ultracold quantum gases, and formulate our motivation. Measurements of sound speed in atomic gases have been achieved since the early age of BEC, as a fundamental tool to study the collective behavior of the Bose gas, as well as to probe the superfluid property of the system.

For weakly interacting Bose gas, a first experimental measurement at zero temperature has been achieved at MIT [55]. The experimental protocol consists

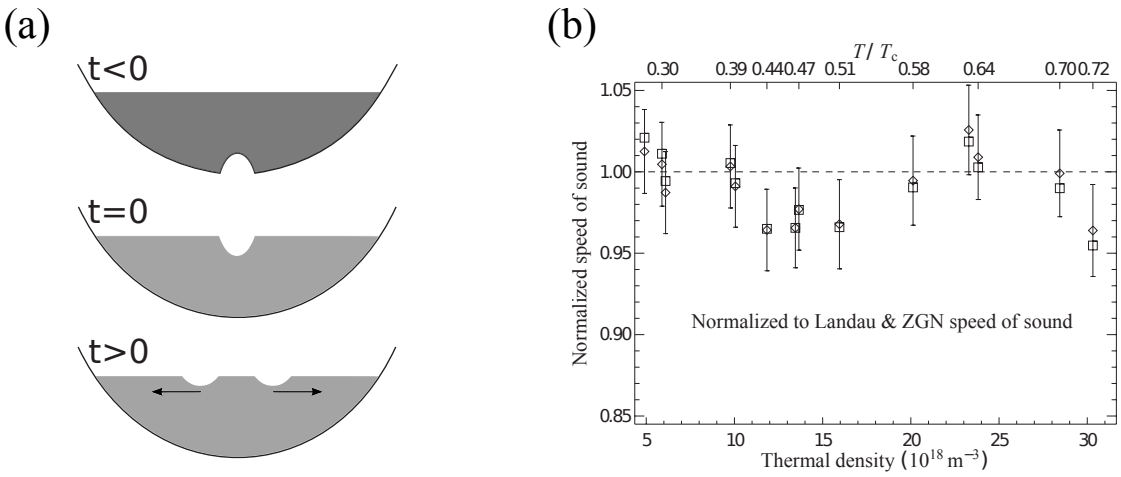

Figure 1.1: (a) Experimental sketch to excite sound wave in weakly interacting Bose gas. At $t < 0$ a density depletion is created by means of a repulsive beam. At $t = 0$ the beam is suddenly turned off, and the density perturbation is responsible for the propagation of a density depletion for time $t > 0$. (b) Measured sound velocity as a function of thermal density (temperature). The sound speed is normalized with respect to the prediction for the second sound calculated from Landau theory, showing a good agreement with the hydrodynamic theory (see Chap. 2). Figures from Ref. [56]

in applying a local density perturbation through a laser beam, at the center of a harmonically trapped gas, and observe how such density defect propagates in space and time (see Fig. 1.1(a)). Their measurement was in close agreement with the prediction of Bogoliubov theory for the speed of phonon Eq. (1.56), when taking into account the effects of trap inhomogeneity. Lately, the same experiment has been performed at finite temperature [56]. The temperature dependence of the sound speed was found to correspond with the prediction of Landau's theory (1.82) for the second sound, deviating from the Bogoliubov phonon result. However, in that experiment the first sound mode was not observed, querying the hydrodynamicity of the fluid. More recently, uniform Bose gases trapped in box-like potential became available [57, 58], together with new experiments on sound measurement [59].

On the other hand, the propagation of sound waves has been also investigated in the context of ultracold Fermi atoms [11]. Although Fermi particles do not condense due to Pauli exclusion principle, atoms of different hyperfine states interacting attractively can form pairs and exhibit a superfluid transition [5, 60]. In particular, in the unitary regime of the gas, where the s-wave scattering length

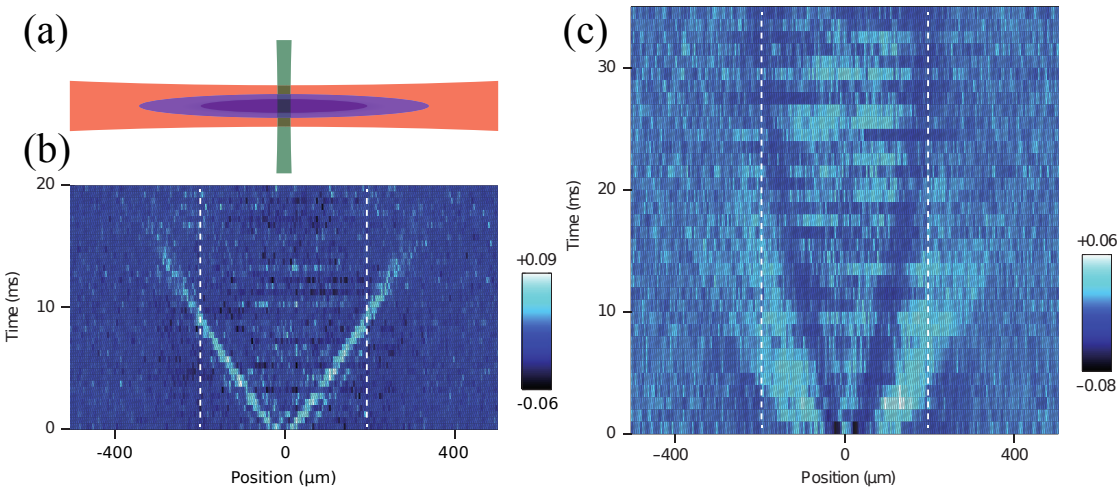

Figure 1.2: (a) Experimental sketch to excite sound waves in strongly interacting Fermi gas. The protocol is similar to that of Fig. 1.1, however the laser beam (green) induces a local density or thermal perturbation, depending on the studied mode. (b) Measured density depletion for the first sound mode (color scale) as a position in the trap at different time step. The first sound is excited through a density probe. (c) Same figure as (b) but for the second sound mode, excited through a temperature probe. Figures from Ref. [11]

diverges, strongly interacting fermions gain a universal description, in which all the thermodynamic quantities can be expressed through a single parameter; the Fermi wave vector [61–63]. The strong interaction among the atoms implying both hydrodynamicity and small thermal expansion coefficient Eq. (1.84), the first and second sounds can be regarded in these systems as uncoupled density and entropy modes, at any temperature [64]. Therefore, for the first sound, which is essentially an oscillation of the total density, a localized density perturbation similar to that of Bose gas has been used to excite it. Instead for the second sound, due to its entropic nature, a local thermal perturbation (heating) has been used to excite it. In this regime, the second sound is still weakly coupled to the density mode, so that it can be observed by measuring the induced density depletion. The experimental protocol is summarized in Fig. 1.2. The measured experimental data were in agreement with the theoretical predictions obtained within the Landau theory, calculated using the universal thermodynamics. This permitted to further extract the superfluid density from the second sound speed, providing the first experimental measurement of superfluid density for ultracold Fermi gases.

Finally, during the last decade, a growing interest has emerged in the field of low-dimensional quantum gases [7, §22-§23]. In particular, many experimen-

tal [65–72] and theoretical [12, 14, 15, 73–76] works have been devoted to the Berezeinskii-Kosterlitz-Thouless (BKT) phase transition in two dimensions, associated with the presence of topological defects. The BKT phase has the peculiarity to exhibit a jump of the superfluid density as one crosses the transition point (see Chap. 3), while the other thermodynamic quantities evolve smoothly at the transition. In analogy to the unitary Fermi gas, theoretical speculation for the observation of the BKT jump through a measurement of the second sound velocity has been made in the pioneering work of Ref. [16]. Stimulated by this prediction, experimental measurement of sound velocity in a uniform two-dimensional Bose gas was recently carried by the group of Collège de France in Paris [17]. However, while the measured sound velocity was in agreement with Landau's prediction in the superfluid phase, it did not exhibit the expected jump at the superfluid transition point, keeping a finite value of sound speed also in the normal phase.

Chapter 2

Sound propagation in three-dimensional Bose gases

In this chapter, we review the propagation of sound in the three-dimensional Bose gas, both in the hydrodynamic and collisionless regimes. This will allow us to handle with the theoretical tools introduced in Chap. 1. As we have already discussed, the determination of the equation of state is essential for the solution of the Landau's equation. Therefore, we will start by developing the finite-temperature Hartree-Fock theory for the weakly interacting Bose gas. As for the collisionless sound, it will be calculated from the pole of the density response function, evaluated within the Random Phase Approximation (RPA).

2.1 Weakly interacting Bose gas at finite temperature

2.1.1 Hartree-Fock theory

We develop in this section the Hartree-Fock (HF) theory for the weakly interacting Bose gas at finite temperature. Our starting point in deriving the HF equations is the Hamiltonian Eq. (1.48). For the description of the static properties of the gas, it is necessary to work in the grand-canonical ensemble, since due to the presence of a condensate, the total number of atoms is not conserved [77]. The key assumption in deriving the finite-temperature mean-field theory, is to assume the macroscopic occupation of the condensate state through the Bogoliubov ansatz, but without treating the non-condensate component as a negligible quantity, like we did in Sec. 1.2.3. Instead, the non-condensate operators are treated in a mean-field fashion, by neglecting the quadratic order terms in the fluctuations around

their mean value ($[a^\dagger_{\mathbf{k}}\hat{a}_{\mathbf{k}'} - \langle a^\dagger_{\mathbf{k}}\hat{a}_{\mathbf{k}'}\rangle]^2 \simeq 0$):

$$\begin{aligned}\hat{a}^\dagger_{\mathbf{k}}\hat{a}^\dagger_{\mathbf{k}'+\mathbf{q}}\hat{a}_{\mathbf{k}'}\hat{a}_{\mathbf{k}+\mathbf{q}} &= \left[\langle\hat{a}^\dagger_{\mathbf{k}}\hat{a}_{\mathbf{k}'}\rangle + \left(a^\dagger_{\mathbf{k}}\hat{a}_{\mathbf{k}'} - \langle a^\dagger_{\mathbf{k}}\hat{a}_{\mathbf{k}'}\rangle\right)\right] \\ &\quad\times\left[\langle\hat{a}^\dagger_{\mathbf{k}'+\mathbf{q}}\hat{a}_{\mathbf{k}+\mathbf{q}}\rangle + \left(\hat{a}^\dagger_{\mathbf{k}'+\mathbf{q}}\hat{a}_{\mathbf{k}+\mathbf{q}} - \langle\hat{a}^\dagger_{\mathbf{k}'+\mathbf{q}}\hat{a}_{\mathbf{k}+\mathbf{q}}\rangle\right)\right] \\ &\simeq \left(n_{\mathbf{k}}\hat{a}^\dagger_{\mathbf{k}+\mathbf{q}}\hat{a}_{\mathbf{k}+\mathbf{q}} + n_{\mathbf{k}+\mathbf{q}}\hat{a}^\dagger_{\mathbf{k}}a_{\mathbf{k}} - n_{\mathbf{k}}n_{\mathbf{k}+\mathbf{q}}\right)\delta_{\mathbf{k},\mathbf{k}'}\,, \end{aligned} \tag{2.1}$$

(the subscripts are all taken to be different from 0) where we have used the orthogonality $\langle\hat{a}^\dagger_i\hat{a}_j\rangle = \delta_{ij}$, and $n_{\mathbf{k}} = \langle\hat{a}^\dagger_{\mathbf{k}}\hat{a}_{\mathbf{k}}\rangle$ is the occupation number. In deriving Eq. (2.1), we have further ignored the anomalous components, corresponding to the terms in which the creation and annihilation operators appear by pairs (Hartree-Fock approximation). Then, after the replacement (2.1), one obtains for the grand canonical Hamiltonian $\hat{K} = \hat{H} - \mu\hat{N}$:

$$\hat{K} = \frac{g}{2V}N_0^2 - \frac{g}{V}\tilde{N}^2 - \mu N_0 + \sum_{\mathbf{k}\neq 0}\left(\varepsilon_{\mathbf{k}} + 2gn - \mu\right)\hat{a}^\dagger_{\mathbf{k}}\hat{a}_{\mathbf{k}}\,, \tag{2.2}$$

with $\tilde{N} = N - N_0 = \sum_{\mathbf{k}\neq 0} n_{\mathbf{k}}$ the number of non-condensed atoms. The thermodynamic potential is obtained according to $\Omega = \beta^{-1}\ln Z$, where $Z = \mathrm{Tr}(e^{-\beta\hat{K}})$ is the grand partition function. The Hamiltonian being already diagonal, the trace immediately follows:

$$\Omega = \Omega_0 + \frac{1}{\beta}\sum_{\mathbf{k}}\ln\left(1 - e^{-\beta(\varepsilon_{\mathbf{k}}+2gn-\mu)}\right)\,, \tag{2.3}$$

with $\Omega_0 = gN_0^2/(2V) - g\tilde{N}^2/(2V) - \mu n_0$.

From the thermodynamic relation $N = -\partial\Omega/\partial\mu$, one finds $n = n_0 + \tilde{n}$, where the thermal atoms density reads

$$\tilde{n} = \frac{1}{(2\pi\hbar)^3}\int_0^\infty d^3\mathbf{p}\frac{1}{e^{\beta\varepsilon_{\mathbf{p}}}z^{-1} - 1} = \frac{1}{\lambda_T^3}g_{3/2}(z)\,, \tag{2.4}$$

with $z = e^{\beta(\mu-2gn)}$ the fugacity, and $g_{3/2}(z)$ the Bose special function Eq. (1.33). As for the chemical potential, it is obtained in the BEC phase from the saddle-point equation $\partial\Omega/\partial n_0|_{T,\tilde{n}} = 0$, according to:

$$\mu = gn_0 + 2g\tilde{n}\,, \tag{2.5}$$

whereas in the absence of a condensate, it is given by the number equation (2.4), by putting $n_0 = 0$,

$$\mu = \mu^{\mathrm{IBG}} + 2gn\,, \tag{2.6}$$

with $\mu^{\rm IBG}$ the ideal Bose gas chemical potential. Therefore, in the HF description, the particles are evolving freely in a mean-field, created by the presence of other atoms. It is worth noticing that this mean-field is felt differently from the condensed and thermal atoms, since the latter has a factor 2 (see Eq. (2.5)), arising from the exchange effect. A normal Bose gas undergoes Bose-Einstein condensation, when the chemical potential approaches the lowest-lying single-particle state, $\varepsilon_0 + 2gn$. Therefore according to Eq. (2.6), HF theory predicts BEC to occur when $\mu = 2gn$, thus at the same critical temperature as the ideal gas; Eq. (1.34). Actually, the many-body correction to the critical temperature can not be obtained in the framework of perturbation theories, and one needs to resort to non-perturbative approaches, such as the universal relations [78, 79] or *ab-initio* calculations [80].

For future purpose, it is useful to derive an analytical expression for the thermal atoms density, valid in the temperature regime where $k_B T \gg |\mu - 2gn|$. Let us introduce a characteristic scale $\beta|\mu - 2gn| \ll \tilde{x} \ll 1$, so as to divide the integration domain of Eq. (2.4) into two parts:

$$\begin{aligned}\Gamma(3/2) g_{3/2}(z) &= \int_0^{\tilde{x}} dx \sqrt{x} \frac{1}{e^x z^{-1} - 1} + \int_{\tilde{x}}^{\infty} dx \sqrt{x} \frac{1}{e^x z^{-1} - 1} \\ &\simeq \int_0^{\tilde{x}} dx \frac{\sqrt{x}}{x + \beta|\mu - 2gn|} + \int_{\tilde{x}}^{\infty} dx \sqrt{x} \frac{1}{e^x - 1} \\ &= -\pi \sqrt{\beta|\mu - 2gn|} + \zeta(3/2)\Gamma(3/2)\,, \end{aligned} \tag{2.7}$$

where in the last line we have used that the second integral is that of an ideal gas. Using the value $\Gamma(3/2) = \sqrt{\pi}/2$, we arrive at:

$$\tilde{n} \simeq n_T^0 - \frac{2\sqrt{\pi}}{\lambda_T^3} \sqrt{\beta|\mu - 2gn|}\,, \tag{2.8}$$

with $n_T^0 = \zeta(3/2)/\lambda_T^3$ the ideal Bose gas thermal atoms density.

2.1.2 Results

We now show the numerical results for the key thermodynamic quantities. These are evaluated for the interaction parameter

$$\eta \equiv gn/(k_B T_{\rm BEC}) = 0.05\,. \tag{2.9}$$

The chosen η corresponds to the typical value of the gas parameter, $na^3 \sim 10^{-6}$, found in dilute Bose gas experiments [4]. Figure 2.1 shows the results for the condensate density and the chemical potential. We compare the predictions from the Hartree-Fock theory, together with the calculations from the beyond mean-field

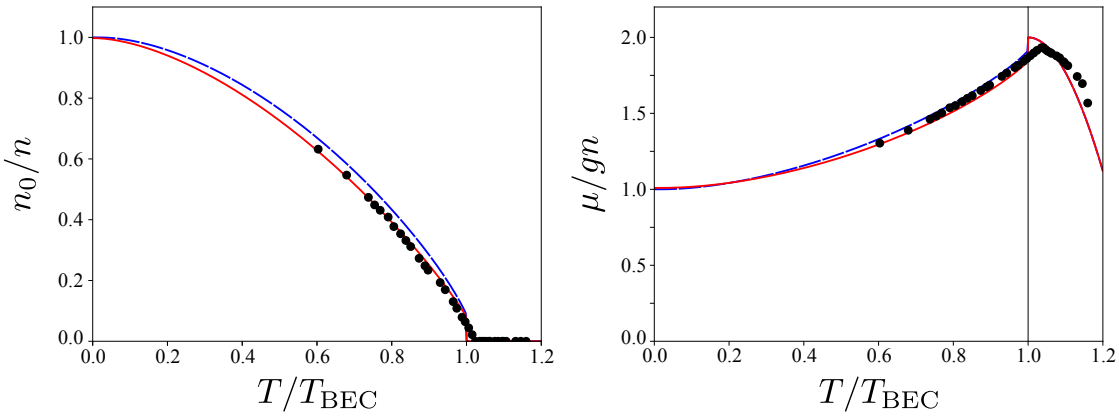

Figure 2.1: Left panel: condensate density $n_0 = n - \tilde{n}$ as a function of temperature, for interaction parameter $\eta = 0.05$. Right panel: chemical potential μ as a function of temperature. Blue dashed line is the HF theory prediction. The red solid line shows the result of the Popov theory and the black dots are the universal relations prediction, from Ref. [83].

Popov theory and the universal relations. The Popov approach is known to be the best available second-order perturbation theory to describe the weakly interacting Bose gas at finite temperature, and includes both the effects of thermal and quantum fluctuations, through the proper treatment of the anomalous averages. Its derivation, as well as some of the important outcomes, are given in Appendix A.1. As for the universal relations (UR), it describes the region in the vicinity of the phase transition, where perturbative theory fails due to strong fluctuations but a universal description of the weakly interacting Bose gas exists [81–83]. The equation of state in the vicinity of the critical density n_{BEC} depends on a single variable, $n - n_{\mathrm{BEC}} = f(X)$, with X given by [83]

$$X = \frac{\hbar^6(\mu - \mu_{\mathrm{BEC}})}{m^3(k_B T)^2 g^2}\,, \tag{2.10}$$

with μ_{BEC} the chemical potential at the critical point. Explicit results for the universal functions f in 3D was calculated using the classical Monte-Carlo simulations in Ref. [83]. The universal relations become extremely useful in two dimension, where a mean-field description is obsolete, and we will come back to discuss the problem in Chap. 3.

The left panel of Fig. 2.1 shows the condensate density, calculated from Eq. (2.4). The HF result is found to agree qualitatively well with the other approaches in the whole temperature region. We briefly note that the unphysical jump of the condensate density observed in both the HF and Popov results is an artifact of

these theories, arising from the inclusion of beyond quadratic order terms in the coupling constant. Indeed, let us recall the high-temperature expansion (2.4):

$$n - n_0 \simeq n_T^0 - \frac{\alpha\sqrt{\pi}}{\lambda_T^3}\sqrt{\beta g n_0}\,, \tag{2.11}$$

with $\alpha = 2\sqrt{\pi}$ or $\sqrt{2\pi}$ for the HF or Popov theory, respectively (see Eq. (2.8) and Eq. (A.25) in the Appendix). The solution for n_0 in Eq. (2.4) can be easily found:

$$\frac{n_0(T \to T_{\rm BEC}^-)}{n} = \eta\frac{\alpha^2}{\zeta(3/2)^2}\,, \tag{2.12}$$

$$\frac{n_0(T \to T_{\rm BEC}^+)}{n} = 0\,, \tag{2.13}$$

yielding therefore a jump proportional to η, given by (2.9). Such problem would not arise if one includes the effects of interaction up to second order in g only, and use the ideal gas value $n_0^0 = n - n_T^0$ for the condensate density entering in the square root of Eq. (2.11) (see Appendix A for further discussion).

It is useful to estimate the region in which strong fluctuations near the critical point spoil the mean-field description. From the perturbation theory, one can estimate the first correction to the thermodynamics due to the fluctuations to be small if [84, §146]

$$\frac{|\mu - 2gn|}{k_B T_{\rm BEC}} \gg \eta^2\frac{8\pi}{\zeta(3/2)^2}\,, \tag{2.14}$$

For $\eta = 0.05$ one finds that in the BEC phase, $|\mu - 2gn|/(k_B T_{\rm BEC}) \ll 0.09$ corresponding to $T \ll 0.99 T_{\rm BEC}$.

In the right panel of Fig. 2.1 we make a similar comparison for the chemical potential. As expected from Eq. (2.5), the chemical potential evolves monotonically from gn at zero temperature to $\sim 2gn$ at the critical temperature.

This comparison shows that the HF theory is well suited for the description of the weakly interacting Bose gas at finite-temperature, giving essentially the same results as the more sophisticated Popov or UR approaches. However, we anticipate that this will be no longer true for the description of binary Bose mixtures. The breakdown of HF theory for the mixtures, and the development of the Popov theory to overcome these failures, will be the main topic discussed in Chap. 4.

2.2 Hydrodynamic sounds in a 3D Bose gas

The theoretical tool being settled, we can now investigate the propagation of sound waves in the hydrodynamic regime. The Landau's two-fluid equation (1.82) is

solved by evaluating the thermodynamic quantities:

$$\begin{aligned} \bar{c}_V &= \frac{T}{N}\frac{\partial S}{\partial T}\bigg|_n , \qquad \kappa_T = \frac{1}{n}\frac{\partial n}{\partial P}\bigg|_T \\ \kappa_S &= \frac{1}{n}\frac{\partial n}{\partial P}\bigg|_S = \left[\frac{1}{\kappa_T} + \frac{k_B T}{\bar{c}_V n}\left(\frac{\partial P}{\partial T}\right)_n^2\right]^{-1} \end{aligned} \tag{2.15}$$

with $P = -\Omega/V$ the pressure evaluated from Eq. (2.3), and we have expressed all the thermodynamic derivatives in terms of the canonical variables (n, T). As for the entropy, according to the non-interacting single particles picture, it can be evaluated from the ideal gas formula:

$$S = k_B \sum_{\mathbf{k}} \beta E_{\mathbf{k}} f(E_{\mathbf{k}}) - \ln\left(1 - e^{-\beta E_{\mathbf{k}}}\right) , \tag{2.16}$$

with $E_{\mathbf{k}} = \varepsilon_{\mathbf{k}} + 2gn - \mu$. Finally, a crucial quantity is the superfluid density, given by Eq. (1.74). Within the HF theory one simply finds $n_s = n_0$. The HF theory therefore does not distinguish the superfluid from the condensate.

Figure 2.2 shows the calculated speeds of sound, in units of the zero-temperature Bogoliubov sound velocity $c_0 = \sqrt{gn/m}$. We find that the second sound velocity (red dashed line) is always smaller than the first sound (blue solid line), and vanishes at T_{BEC}. One can observe at $T \simeq 0.05 T_{\mathrm{BEC}}$ the occurrence of a hybridization of the two sound modes (see inset) [85]. Although the HF theory is not expected to be valid in such a degenerate regime, we have checked that the same hybridization occurs within the Popov approach. This is understood if we remind that for any superfluid, in the region where $T \to 0$, the first and second sound modes are decoupled and correspond, respectively, to a density and entropy oscillation of the system. However, as the temperature increases, the thermal expansion coefficient Eq. (1.84) takes a non-negligible value, and one can not ignore anymore the coupling between the two modes. This is shown in Fig. 2.3 where the thermal expansion coefficient is found to increase with the temperature. The hybridization point therefore signals the departure from the uncoupled sound waves picture. We briefly note that, in the low-temperature regime $k_B T \ll gn$, the thermodynamic properties are governed by the phonon excitations, which are not captured in the HF framework. Actually by using phonon thermodynamics (see Appendix A.1.2), one finds that at zero temperature $c_2 = c_1/\sqrt{3}$.

For a weakly interacting Bose gas, a good estimate for the sound velocities at intermediate temperatures is obtained by considering that all the thermodynamic quantities entering in the Landau's equation, except the isothermal compressibility and the superfluid density, are described by that of the ideal gas [9]. In that case

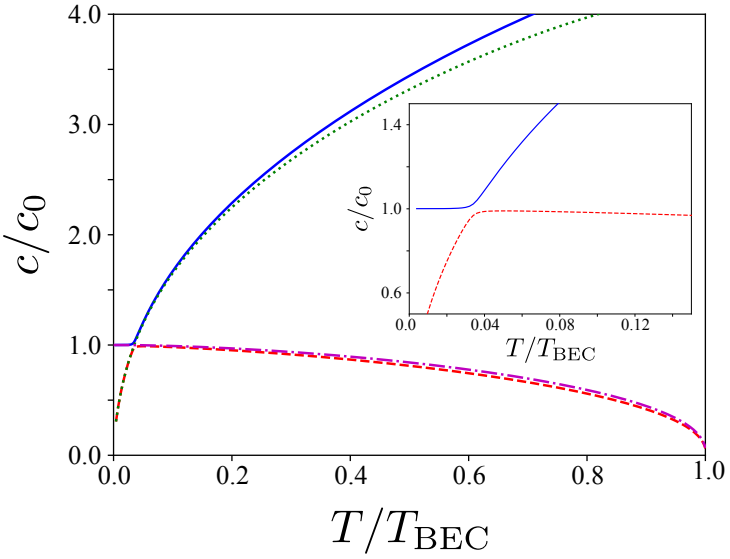

Figure 2.2: Hydrodynamic sound velocities for a weakly interacting Bose gas, normalized to the zero-temperature Bogoliubov sound $c_0 = \sqrt{gn/m}$. The interaction parameter is chosen to be $\eta = 0.05$. Blue solid and red dashed lines: first and second sounds evaluated from the Landau's two-fluid equation (1.82), respectively. Green dotted and cyan dotted-dashed lines: first and second sounds calculated from the weakly interacting Bose gas approximated expressions (2.18). The inset emphasizes the hybridization point near $k_B T = gn$.

the following identity holds:

$$\frac{1}{mn\kappa_s} + \frac{n_s T\bar{s}^2}{mn_n\bar{c}_v} = \frac{nT\bar{s}^2}{mn_n\bar{c}_v}\,. \tag{2.17}$$

Using the above expression in the Landau's equation (1.82), one finds the approximated results,

$$c_{1,\rm WI} = \sqrt{\frac{nT\bar{s}^2}{n_n m\bar{c}_v}}, \qquad c_{2,\rm WI} = \sqrt{\frac{n_s}{n}\frac{1}{mn\kappa_T}}\,. \tag{2.18}$$

These approximations of the sound velocities are shown in Fig. 2.2 as green dotted ($c_{1,\rm WI}$) and cyan dot-dashed ($c_{2,\rm WI}$) lines. Equation (2.18) correctly describes the sound velocities down to the hybridization point.

Finally, it is useful for the experimental perspective to assess how sensitive are the sound modes to a density probe. This is achieved by looking to the density response function of the system. In the deep hydrodynamic regime, which is under consideration here, sound propagates without any damping. This implies that the

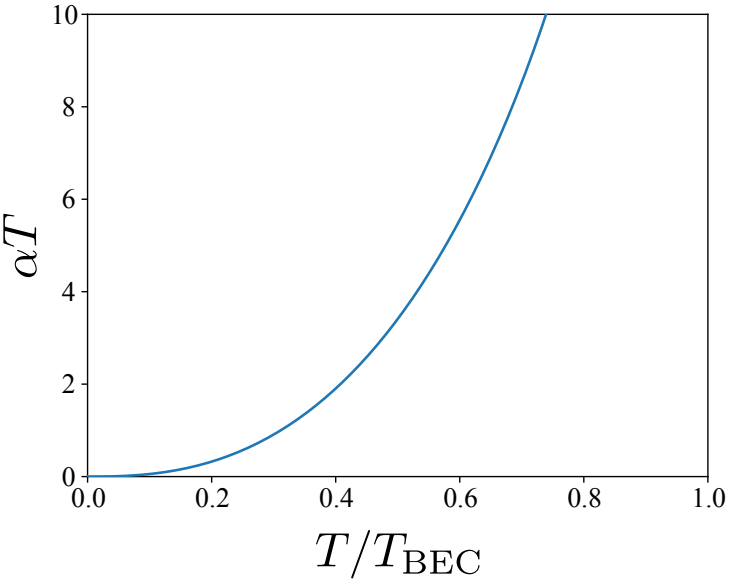

Figure 2.3: Thermal expansion coefficient αT Eq. (1.84), for a weakly interacting Bose gas with interaction parameter $\eta = 0.05$.

dynamic structure factor Eq. (1.95) in the two-fluid picture can be modeled by two delta-peaks [86]:

$$S(\mathbf{q},\omega) = \frac{nq^2}{2m} Z_1 \delta\left(\omega - c_1 q\right) + \frac{nq^2}{2m} Z_2 \delta\left(\omega - c_2 q\right) . \tag{2.19}$$

The factors in front of the delta functions have been chosen so that the amplitudes Z_1 and Z_2 saturate the f-sum rule Eq. (1.97) as $Z_1 + Z_2 = 1$. On the other hand, the two sound modes also exhaust the compressibility sum rule Eq. (1.99). The relative contribution $W_{1,2} = Z_{1,2}/c_{1,2}^2$ of each sound mode to the compressibility sum rule is found to be

$$W_1 = \frac{1 - mn\kappa_T c_2^2}{c_1^2 - c_2^2} , \qquad W_2 = \frac{mn\kappa_T c_1^2 - 1}{c_1^2 - c_2^2} . \tag{2.20}$$

Hence, if the ratio W_2/W_1 is larger than unity, second sound can be excited from a density perturbation. We also note that starting from the general inequalities $c_1 \geq c_2$ and $c_1 \geq c_{10}$, the thermal expansion coefficient Eq. (1.84) sets a lower bound for the sum rule,

$$\frac{W_2}{W_1} \geq \alpha T. \tag{2.21}$$

In Fig. 2.4 we show the calculation of the compressibility sum rule amplitude W_2/W_1. As expected from the discussion we have made previously, W_2/W_1 is

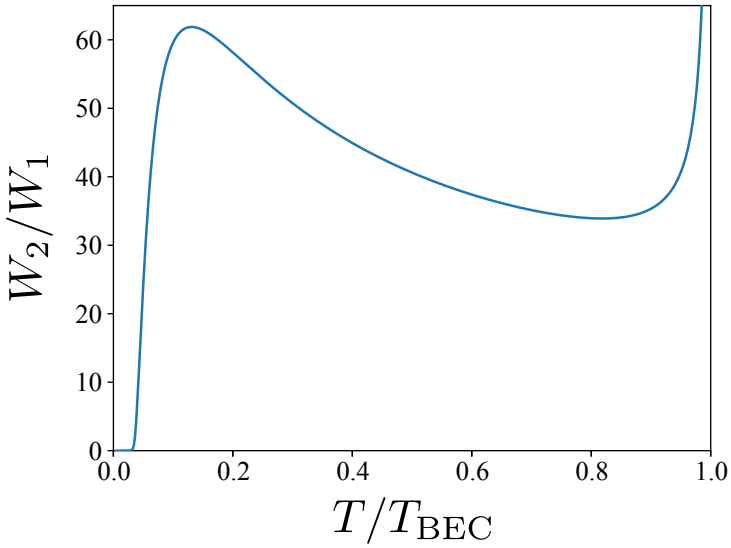

Figure 2.4: Ratio of the compressibility sum rule amplitudes, for $\eta = 0.05$. W_1 (W_2) is the relative contribution of the first (second) sound mode to the compressibility sum rule, Eq. (2.20).

extremely small below the hybridization point, since the second sound corresponds to an entropy wave, uncoupled from the density oscillation of the fluid. Instead, the weight of the second sound becomes abruptly large as one crosses the hybridization point, and remains large up to T_{BEC}. This observation suggests that second sound in a weakly interacting Bose gas can be probed from a density perturbation. This property has been used in the experiment of Ref. [56] to successfully probe the second sound velocity. A more detailed discussion about the comparison between theory and experiment will be carried in the last section of this chapter.

2.3 Collisionless sound in a 3D Bose gas

We now discuss the propagation of sound in the collisionless regime. We have seen in Sec. 1.1.3 that the velocity of a collisionless sound can be determined from the pole of the response function. First, we will give an expression for the density response of a weakly interacting Bose gas, calculated within the Random Phase Approximation (RPA). Then, we will verify that the obtained response function satisfies the sum-rules. Finally, we evaluate the pole of the response function and discuss the nature of the observed sound mode.

2.3.1 Random Phase Approximation

Dynamic mean-field approach

For the description of the weakly interacting Bose gas in the collisionless regime, we start from the general expression (1.18) for the density response to an external perturbation. Let us consider the condensate and normal components of the gas to feel different effective potentials, [46, §5.4]

$$\begin{aligned} \delta n_0(\mathbf{q},\omega) &= -\delta U_{\mathrm{eff},0}(\mathbf{q},\omega)\chi_0^0(\mathbf{q},\omega)\,, \\ \delta\tilde{n}(\mathbf{q},\omega) &= -\delta U_{\mathrm{eff},\tilde{n}}(\mathbf{q},\omega)\chi_{\tilde{n}}^0(\mathbf{q},\omega)\,, \end{aligned} \tag{2.22}$$

where χ_0^0 and $\chi_{\tilde{n}}^0$ are the response functions of the reference system, defined later. The effective interaction is given by the dynamic mean-fields,

$$\begin{aligned} \delta U_{\mathrm{eff},0}(\mathbf{q},\omega) &= \delta U_{\mathrm{ext},0}(\mathbf{q},\omega) + g\delta n_0(\mathbf{q},\omega) + 2g\delta\tilde{n}(\mathbf{q},\omega)\,, \\ \delta U_{\mathrm{eff},\tilde{n}}(\mathbf{q},\omega) &= \delta U_{\mathrm{ext},\tilde{n}}(\mathbf{q},\omega) + 2g\delta n_0(\mathbf{q},\omega) + 2g\delta\tilde{n}(\mathbf{q},\omega)\,. \end{aligned} \tag{2.23}$$

We briefly note that consistently with the discussion made in Secs. 1.2.2 and 2.1.1, the exchange effect for the condensate is suppressed. Consequently, the condensate feels a mean-field $gn_0 + 2g\tilde{n}$ while the thermal component feels $2g(n_0 + \tilde{n})$. The above equations can be solved straightforwardly, and yield the following expressions for the density fluctuations:

$$\delta n_0 = -\left[\delta U_{\mathrm{ext},0}\chi_0 + \delta U_{\mathrm{ext},\tilde{n}}\chi_{0\tilde{n}}\right], \tag{2.24}$$

$$\delta\tilde{n} = -\left[\delta U_{\mathrm{ext},\tilde{n}}\chi_{\tilde{n}} + \delta U_{\mathrm{ext},0}\chi_{0\tilde{n}}\right], \tag{2.25}$$

where the response function in each component is defined to be

$$\chi_0 = \frac{\chi_0^0(1+2g\chi_{\tilde{n}}^0)}{D}\,, \quad \chi_{\tilde{n}} = \frac{\chi_{\tilde{n}}^0(1+g\chi_0^0)}{D}\,, \quad \chi_{0\tilde{n}} = -\frac{2g\chi_0^0\chi_{\tilde{n}}^0}{D}\,, \tag{2.26}$$

with the denominator

$$D(\mathbf{q},\omega) = 1 + g\left[\chi_0^0(1-2g\chi_{\tilde{n}}^0) + 2\chi_{\tilde{n}}^0\right]. \tag{2.27}$$

The zeros of D, corresponding to the poles of the response function, will be analyzed later. If one considers that the external potential acts in the same way on the condensate and on the thermal component ($\delta U_{\mathrm{ext},0} = \delta U_{\mathrm{ext},\tilde{n}} \equiv \delta U_{\mathrm{ext}}$), one has $\delta n = \delta n_0 + \delta\tilde{n} = -\delta U_{\mathrm{ext}}\chi$, with the RPA density response function of the Bose gas given by

$$\chi(\mathbf{q},\omega) = \frac{\chi_0^0(\mathbf{q},\omega) + \chi_{\tilde{n}}^0(\mathbf{q},\omega) - g\chi_0^0\chi_{\tilde{n}}^0(\mathbf{q},\omega)}{D(\mathbf{q},\omega)}\,. \tag{2.28}$$

Bare response function

We now discuss the bare response function $\chi^0(\mathbf{q},\omega)$. For the RPA description, the reference system is chosen to be the Hartree-Fock gas [87]. As one shall see, this choice ensures the consistency with the dynamic mean-fields introduced in Eq. (2.23). In particular, it provides the correct behavior of the compressibility sum rule. Thus, let us start from the general expression for the linear response function Eq. (1.94). In the single-particle description of the HF theory, the eigenstates of the Hamiltonian are fixed by the single-particle occupation number $n_{\mathbf{p}}$ (see Sec. 2.1.1), and the matrix element $\langle m|\hat{a}^\dagger_{\mathbf{p}-\hbar\mathbf{q}}\hat{a}_{\mathbf{p}}|n\rangle$ vanishes unless the energy difference $E_n - E_m$ is equal to the difference of single-particle kinetic energy $\varepsilon_{\mathbf{p}-\hbar\mathbf{q}} - \varepsilon_{\mathbf{p}}$. Consequently, focusing on the first term of Eq. (1.94) only, [7, §7.5]

$$\begin{aligned}\chi^0(\mathbf{q},\omega) &= -\frac{1}{\hbar Z}\sum_{m,n}\frac{e^{-\beta E_m}}{\omega-\omega_{nm}+i\eta}\sum_{\mathbf{p},\mathbf{p}'}\langle m|\hat{a}^\dagger_{\mathbf{p}-\hbar\mathbf{q}}\hat{a}_{\mathbf{p}}|n\rangle\langle n|\hat{a}^\dagger_{\mathbf{p}'}\hat{a}_{\mathbf{p}'-\hbar\mathbf{q}}|m\rangle + (\cdots)\\ &= -\frac{1}{Z}\sum_m\sum_{\mathbf{p}}\frac{e^{-\beta E_m}}{\hbar\omega-(\varepsilon_{\mathbf{p}-\hbar\mathbf{q}}-\varepsilon_{\mathbf{p}})+i\eta}\langle m|\hat{a}^\dagger_{\mathbf{p}-\hbar\mathbf{q}}\hat{a}_{\mathbf{p}}\hat{a}^\dagger_{\mathbf{p}}\hat{a}_{\mathbf{p}-\hbar\mathbf{q}}|m\rangle + (\cdots)\\ &= -\sum_{\mathbf{p}}\frac{f(\varepsilon_{\mathbf{p}-\hbar\mathbf{q}})f(\varepsilon_{\mathbf{p}})+f(\varepsilon_{\mathbf{p}-\hbar\mathbf{q}})}{\hbar\omega-(\varepsilon_{\mathbf{p}-\hbar\mathbf{q}}-\varepsilon_{\mathbf{p}})+i\eta}+(\cdots)\,,\end{aligned} \tag{2.29}$$

where we have assumed $\mathbf{q}\neq 0$. The second term denoted by $(\cdots)$ follows essentially the same calculation, and one finally obtains

$$\chi^0(\mathbf{q},\omega)=\sum_{\mathbf{p}}\frac{1}{\hbar\omega+(\varepsilon_{\mathbf{p}}-\varepsilon_{\mathbf{p}+\hbar\mathbf{q}})+i\eta}\left[f(\varepsilon_{\mathbf{p}+\hbar\mathbf{q}})-f(\varepsilon_{\mathbf{p}})\right]\,, \tag{2.30}$$

with $\eta\to 0^+$. The equilibrium distribution function is given by the Bose-Einstein distribution function with the HF mean-field energy

$$f(\varepsilon_{\mathbf{p}})=\frac{1}{e^{\beta(\varepsilon_{\mathbf{p}}+2gn-\mu)}-1}\,. \tag{2.31}$$

As seen before, one needs to consider separately the contribution from the condensate $\mathbf{p}=0$ and the thermal part. Therefore $\chi^0=\chi^0_0+\chi^0_{\tilde{n}}$ with

$$\begin{aligned}\chi^0_0(\mathbf{q},\omega) &= n_0\left[\frac{-1}{\hbar\omega-\varepsilon_{\hbar\mathbf{q}}+i\eta}+\frac{1}{\hbar\omega+\varepsilon_{\hbar\mathbf{q}}+i\eta}\right]\,,\\ \chi^0_{\tilde{n}}(\mathbf{q},\omega) &= \int\frac{\mathrm{d}^3\mathbf{p}}{(2\pi\hbar)^3}\frac{f(\varepsilon_{\mathbf{p}+\hbar\mathbf{q}/2})-f(\varepsilon_{\mathbf{p}-\hbar\mathbf{q}/2})}{\hbar\omega-\hbar\mathbf{p}\mathbf{q}/m+i\eta}\,.\end{aligned} \tag{2.32}$$

In the long wavelength limit ($q\to 0$), the response function takes the form (we assume the sound to propagate in the x-direction, $\mathbf{q}=q\mathbf{e}_x$):

$$\chi^0(\omega/q)=-\frac{n_0}{m}\left(\frac{q}{\omega}\right)^2+\int\frac{\mathrm{d}^3\mathbf{p}}{(2\pi\hbar)^3}\frac{1}{\omega/q-p_x/m+i\eta}\frac{\partial f(\varepsilon_p)}{\partial p_x}\,, \tag{2.33}$$

depending on the ratio ω/q only. We can simplify the integration of the thermal part by using the cylindrical coordinate (with x the longitudinal axis) and one finally gets,

$$\chi^0(\omega/q) = -\frac{n_0}{m}\left(\frac{q}{\omega}\right)^2 - \frac{1}{\hbar^3(2\pi)^2}\int_{-\infty}^{\infty} \mathrm{d}p_x \frac{p_x}{\omega/q - p_x/m + i\eta} f(\varepsilon_{p_x})\,. \tag{2.34}$$

Before going to the next section, we briefly note from Eq. (2.28) that at zero temperature, $\chi = \chi_0^0/(1 + g\chi_0^0)$. The pole of the response function then gives the Bogoliubov dispersion relation, Eq. (1.55):

$$\hbar\omega = \sqrt{\left(\frac{\hbar^2 q^2}{2m}\right)^2 + \frac{\hbar^2 g n}{m} q^2}\,, \tag{2.35}$$

or equivalently, from the long-wavelength expression (2.34), the Bogoliubov phonon velocity Eq. (1.56), $\omega/q = \sqrt{gn/m}$.

2.3.2 Sum rules

f-sum rule

We start from the verification of the f-sum rule (1.98), which for the system under consideration is given by

$$\chi_i^0(q, \omega \to \infty) = \frac{n_i q^2}{m\omega^2}, \tag{2.36}$$

where the subscript i refers to the total ($\emptyset$), thermal ($\tilde{n}$) or condensate (0) response function.

First, one can immediately see from Eq. (2.34) that χ_0^0 already satisfies the sum rule. As for the non-condensate part,

$$\chi_{\tilde{n}}^0(q, \omega \to \infty) \simeq \int \frac{d^3\mathbf{p}}{(2\pi\hbar)^3} \frac{q}{\omega}\left(1 + \frac{q p_x}{m\omega}\right)\frac{\partial f}{\partial p_x}\,. \tag{2.37}$$

Noticing that the first term of Eq. (2.37) vanishes from the oddness of $\partial f/\partial p_x$, and integrating by part, the f-sum rule for the thermal part is also found to be satisfied. Finally,

$$\chi(q, \omega \to \infty) \simeq \chi_0(q, \omega \to \infty) + \chi_{\tilde{n}}(q, \omega \to \infty) = \frac{n q^2}{m\omega^2}\,. \tag{2.38}$$

Compressibility sum rule

We next verify the compressibility sum rule, Eq. (1.100) $\chi(\mathbf{q} \to 0, \omega = 0) = n^2\kappa_T$. Let us start from the bare response function χ^0, which the long wavelength expression (2.34) already takes into account the $q \to 0$ limit. It is immediate to see that

$$\chi_0^0(\omega/q = 0) \to \infty. \tag{2.39}$$

This is an expected behavior, since the isothermal compressibility of an ideal Bose gas is infinite. For the normal part, it can be expressed in terms of the Bose integral as

$$\chi_{\tilde{n}}^0(0) = \frac{\beta}{\lambda_T^3} g_{1/2}(z). \tag{2.40}$$

In the normal phase above $T_{\rm BEC}$, $\chi = \chi_{\tilde{n}} = \chi_{\tilde{n}}^0/(1+2g\chi_{\tilde{n}}^0)$ and one has consequently

$$\kappa_T(T > T_{\rm BEC}) = \frac{1}{n^2} \frac{\frac{\beta}{\lambda_T^3} g_{1/2}(z)}{1 + 2g\frac{\beta}{\lambda_T^3} g_{1/2}(z)}. \tag{2.41}$$

Below $T_{\rm BEC}$ instead, one can use the inequality $\chi_0^0(0) \gg \{\chi_{\tilde{n}}^0(0),\ 1\}$ so that the pole of the response function reduces to $D \simeq g\chi_0^0(0)[1 - 2g\chi_{\tilde{n}}^0(0)]$ and Eq. (2.28) becomes:

$$\kappa_T(T < T_{\rm BEC}) = \frac{1}{gn^2} \frac{1 - g\frac{\beta}{\lambda_T^3} g_{1/2}(z)}{1 - 2g\frac{\beta}{\lambda_T^3} g_{1/2}(z)}. \tag{2.42}$$

It is worth noticing from the above equation that, the compressibility of the Bose gas in the BEC phase becomes finite in presence of interaction. In particular, $\kappa_T(T = 0) = (gn^2)^{-1}$ at zero temperature.

Thermodynamic compressibility

Let us evaluate the isothermal compressibility within the HF thermodynamics, in order to verify the consistency of the RPA approach. From the thermodynamic identity $\mu = \partial P/\partial n|_T$, the isothermal compressibility can be expressed as

$$\kappa_T = \frac{1}{n^2} \frac{\partial n}{\partial \mu}\Big|_T. \tag{2.43}$$

Above $T_{\rm BEC}$, the total density is $n = \tilde{n}$, and from Eq. (2.4),

$$\frac{\partial \tilde{n}}{\partial \mu} = \frac{\beta}{\lambda_T^3} \left(1 - 2g\frac{\partial \tilde{n}}{\partial \mu}\right) g_{1/2}(z)\,, \tag{2.44}$$

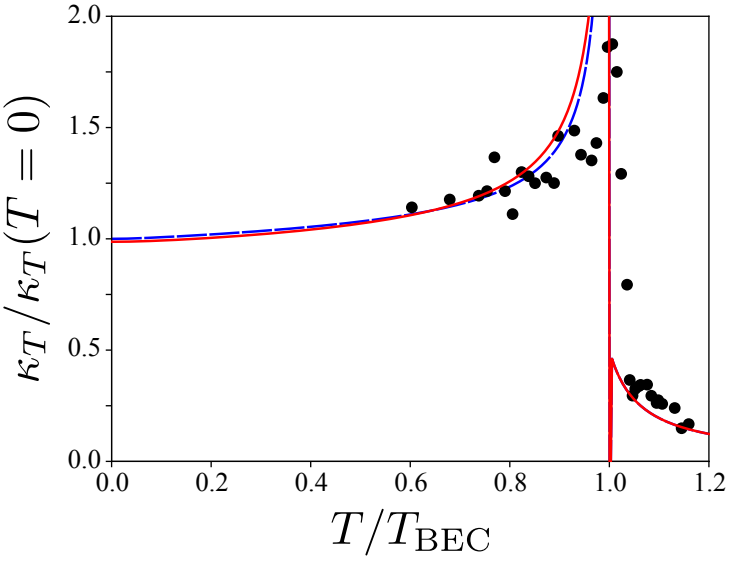

Figure 2.5: Isothermal compressibility as a function of temperature, for interaction parameter $\eta = 0.05$. Red solid line: self-consistent Popov theory. Blue dashed line: HF theory.

where we have used the Bose integral property $\partial g_s(z)/\partial z = g_{s-1}(z)/z$. After some algebra we obtain

$$\kappa_T(T > T_{\rm BEC}) = \frac{1}{n^2}\frac{\beta}{\lambda_T^3}\frac{g_{1/2}(z)}{1 + 2g\frac{\beta}{\lambda_T^3}g_{1/2}(z)}, \tag{2.45}$$

namely, Eq. (2.42). For $T < T_{\rm BEC}$ we instead use the equation of state (2.5) to express the total density as $n = \frac{\mu}{g} - \tilde{n}$ and using Eq. (2.44) for $\partial\tilde{n}/\partial\mu$, one finds,

$$\kappa_T(T < T_{\rm BEC}) = \frac{1}{gn^2}\frac{1 - g\frac{\beta}{\lambda_T^3}g_{1/2}(z)}{1 - 2g\frac{\beta}{\lambda_T^3}g_{1/2}(z)} \tag{2.46}$$

which is the same expression as Eq. (2.42).

We show in Fig. 2.5 the calculated isothermal compressibility, with the HF prediction drawn as a blue dashed-line. For comparison, we also show the predictions from the Popov theory (see Appendix A.1) and the universal relations. We briefly note that the presence of the factor 2 in the denominator of Eq. (2.46) is crucial for the increase of the compressibility at finite temperature. This is the direct consequence of the exchange effect, which is responsible for the increase of the interaction energy with respect to the value predicted at $T = 0$ when the whole

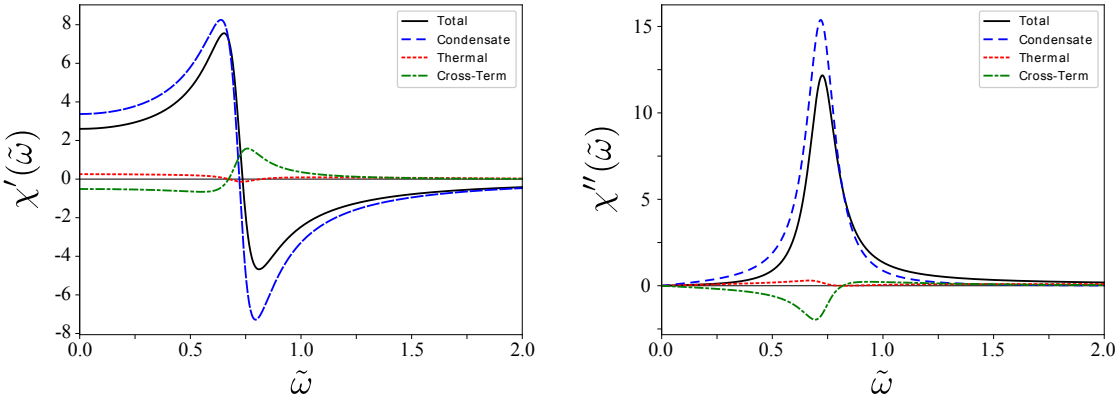

Figure 2.6: RPA response function evaluated for $\eta = 0.05$, as a function of dimensionless frequency $\tilde{\omega} = \omega/(kc_0)$. Left and right panels are the real and imaginary part of the response function at $T = 0.7T_{\rm BEC}$, respectively. Black solid line: total response χ. Blue dashed line: response function of the condensate χ_0. Red dotted line: response function of the thermal part $\chi_{\tilde{n}}$. Green dotted-dashed line: cross-term response function $\chi_{0\tilde{n}}$.

system is fully Bose condensed. This effect explicitly shows up in the temperature dependence of the chemical potential Eq. (2.5) and in the density dependence of the non-condensed component through the fugacity, Eq. (2.4). It is worth noticing that if one employs the lowest order HF theory by taking $\mu \simeq g(n + n_T^0)$, one misses the additional density dependence responsible for the enhancement of κ_T. The temperature dependence of the single-component compressibility plays a major role in describing the magnetic phase transition in the binary mixture, as one shall discuss in Chap. 4.

2.3.3 Results

Response function

In Fig. 2.6 we show the real and imaginary part of the response function, evaluated at $T = 0.7T_{\rm BEC}$. As one can see, the main contribution to the total response function comes from the condensate part, in agreement with our previous discussion about the compressibility sum rule. Numerical study shows that this statement remains true for all the range of temperature $T < T_{\rm BEC}$, including the close vicinity of $T_{\rm BEC}$.

Evaluation of sound velocity

We now turn to the analytical study of the pole of the response function. After some algebra, the pole equation (2.27) reads

$$D = (1 + 2g\chi_{\tilde{n}}^0)\left[1 + g\chi_0^0 \frac{1 - 2g\chi_{\tilde{n}}^0}{1 + 2g\chi_{\tilde{n}}^0}\right] = 0. \tag{2.47}$$

The thermal part of the response function being small in the BEC phase, $g\chi_{\tilde{n}}^0 \ll 1$, one can expand the denominator of Eq. (2.47) as:

$$D \simeq (1 + 2g\chi_{\tilde{n}}^0)\left[1 + g\chi_0^0(1 - 2g\chi_{\tilde{n}}^0)^2\right] \tag{2.48}$$

The RPA response function hence possesses two poles. As already discussed, under a density perturbation, the response of a weakly interacting Bose gas in the BEC phase is mainly governed by the condensate part. We therefore focus on the second pole of Eq. (2.48), arising from the presence of a condensate. Inserting expression (2.34) for χ_0^0, the condensate pole equation yields [1]

$$1 - g\frac{n_0}{m}\left(\frac{q}{\omega}\right)^2 (1 - 2g\chi_{\tilde{n}}^0)^2 = 0\,. \tag{2.49}$$

Thus the pole $\bar{c} = \omega/q$ is given by,

$$\bar{c} = c - i\Gamma = c_B\left(1 - 2g\chi_{\tilde{n}}^0(\bar{c})\right), \tag{2.50}$$

where we have introduced the temperature-dependent Bogoliubov sound velocity $c_B = \sqrt{gn_0(T)/m}$. At zero temperature, within the HF theory, $c_B(T = 0) = c_0$. Assuming that the quality factor $Q \equiv c/\Gamma$ is small, one can decouple the real and complex part of the pole equation into

$$c = c_B\left(1 - 2g\chi_{\tilde{n}}^{0\,\prime}(c)\right), \tag{2.51}$$

$$\Gamma = 2g\chi_{\tilde{n}}^{0\,\prime\prime}(c). \tag{2.52}$$

The sound mode described by Eq. (2.50) corresponds to a *collisionless* sound. It is associated to the coherent motion of the fluid, coming from quasi-particles (phonon) excitation. Unlike the hydrodynamic sounds sustained by the incoherent collisions between atoms, the restoring force in the collisionless mode arises from the average mean-field produced by the other atoms. The collisionless sound is

[1] We actually have checked, using the Fourier transform method developed in Chap. 3, that the collective mode arising from the thermal response $1 + 2g\chi_{\tilde{n}}^0 = 0$, has a negligibly small amplitude at any temperatures, for the chosen interaction parameter. The response becomes significant only for $\eta \sim 1$, where the validity of the HF approach becomes questionable.

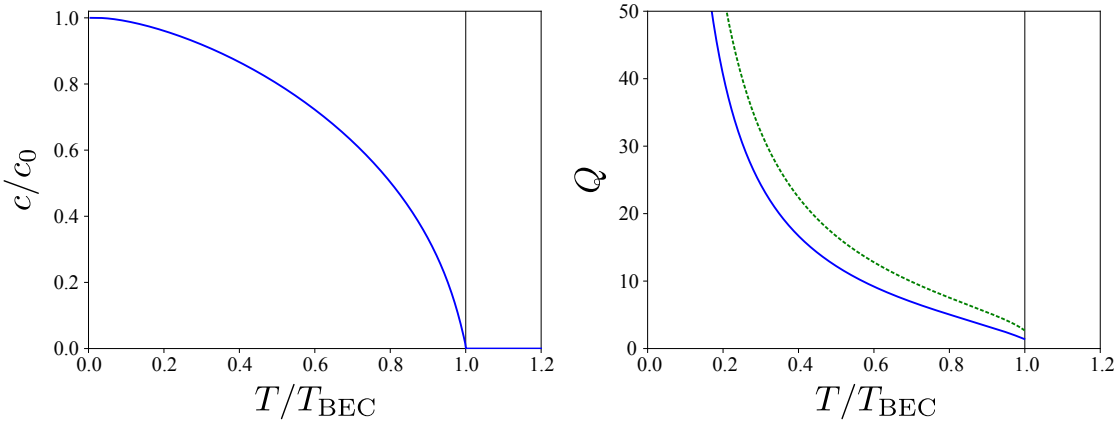

Figure 2.7: Left panel: sound velocity calculated from the pole of the response function Eq. (2.51), with interaction parameter $\eta = 0.05$. Right panel: quality factor $Q = c/\Gamma$. The blue solid line is the pole solution Eq. (2.52) whereas the green dotted line is the theoretical prediction for the Landau damping from Ref. [90].

also referred sometimes to the quasi-particle sound [88], or zero sound [89]. This last nomenclature comes from the analogous effect in the interacting Fermi gas, described by the Fermi liquid theory [45].

In order to understand the origin of the damping Eq. (2.52), it is useful to recall the general RPA expression (2.32) for $\chi^0_{\tilde{n}}$, and rewrite:

$$\Gamma = 2g\pi \int \frac{\mathrm{d}^3\mathbf{p}}{(2\pi\hbar)^3} \left[f(\varepsilon_{\mathbf{p}}) - f(\varepsilon_{\mathbf{p}+\hbar\mathbf{q}})\right] \delta\left(\hbar\omega + \varepsilon_{\mathbf{p}} - \varepsilon_{\mathbf{p}+\hbar\mathbf{q}}\right). \tag{2.53}$$

The above equation shows that the decay corresponds to a process in which the sound mode $\hbar\omega$ is absorbed by a thermal excitation $\varepsilon_{\mathbf{p}}$, which shifts to another thermal excitation $\varepsilon_{\mathbf{p}+\hbar\mathbf{q}}$. This is the Landau damping, which is a finite-temperature effect, but not associated to any thermalization processes [90, 91], in contrast to the collisional damping.

In the left panel of Fig. 2.7 we show the sound velocity evaluated solving the pole equation (2.51). Because the collisionless sound evaluated in the present section corresponds to the response of the condensate, its velocity vanishes at T_{BEC}. In the right panel of Fig. 2.7, we also plot the theoretical prediction for the damping rate Eq. (2.52). For comparison, Landau damping expression from Ref. [90] is also shown. The discrepancy between the two predictions are due to the neglect of the anomalous pair density in our HF theory.

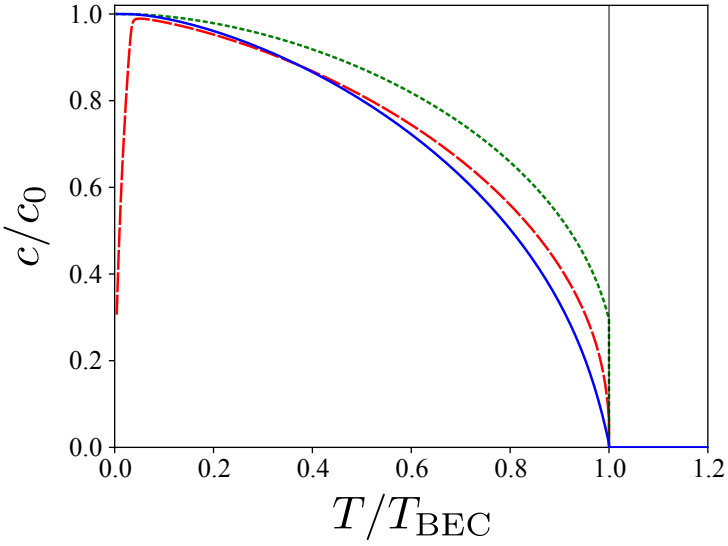

Figure 2.8: Sound velocity in units of zero-temperature Bogoliubov sound $c_0 = \sqrt{gn/m}$ for $\eta = 0.05$. Blue solid line: RPA prediction (2.51). Red dashed line: second sound predicted from Landau's two-fluid hydrodynamics calculated using HF thermodynamics. Green dashed line: generalized Bogoliubov sound $c_B = \sqrt{gn_0/m}$.

2.4 Comparative study of hydrodynamic and collisionless sounds

Before closing this chapter, we show in Fig. 2.8 a comparison between the hydrodynamic second sound, the collisionless sound and the temperature-dependent Bogoilubov sound $c_B = \sqrt{gn_0(T)/m}$. Remarkably, all the three velocities have the same temperature dependence, making them qualitatively similar. This can be easily understood if we recall the approximated expression (2.18) for the second sound speed, $c_{2,\mathrm{WI}} = \sqrt{n_s/(mn^2\kappa_T)}$. In the HF approach, $n_s = n_0$. Moreover, as it can be seen from Fig. 2.5, for a weakly interacting gas the compressibility is almost temperature independent, except in the close vicinity of the phase transition: $\kappa_T \simeq (gn^2)^{-1}$. Thus one arrives to $c_2 \simeq c_B$. As for the collisionless sound, Eq. (2.51) also indicates that $c_{\mathrm{less}} \simeq c_B$.

In the experiment of Ref. [56], the sound speed measured from a density probe was compared to the prediction for the Bogoliubov sound c_B (left panel of Fig. 2.9) and the hydrodynamic second sound of Landau theory, c_2 (right panel). It was found that the experimental points are better described by the Landau theory, therefore supporting the observation of the second sound. However, due to the

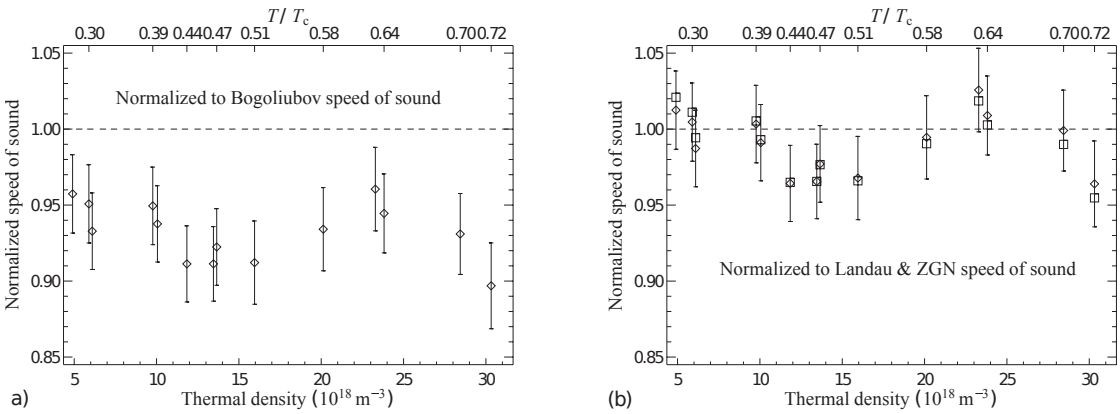

Figure 2.9: Experimental results of Ref. [56] for the measurement of sound velocity as a function of temperature (thermal atoms density). Left panel: measured sound velocity normalized to the (temperature-dependent) Bogoliubov sound, c_B. Right panel: the same experimental points normalized to the hydrodynamic sound prediction of Landau theory and ZNG approach (see main text). From Ref. [56].

experimental uncertainty, it is difficult to claim the observation of the second sound in favor to the collisionless one. Actually, the experiment could not investigate the temperature region below the hybridization point where the difference of both sounds become clear, nor observe the existence of a first sound mode. From this point of view, one way to assess the collisional nature of the sound wave would be to investigate the damping rate of the mode. Indeed, the hydrodynamic sound is not expected to show any damping in the deep collisional regime, in contrast to the collisionless sound, which as we have seen previously, is governed by the Landau damping.

Finally, let us briefly comment that the dynamic approach of Zaremba, Nikuni and Griffin, reduces to the RPA formalism developed in this chapter, in the collisionless regime [46, §13]. In the hydrodynamic regime, it has been also shown that ZNG is equivalent to the Landau's two-fluid hydrodynamics, when the thermodynamic quantities entering the equation is evaluated using the HF theory [92]. In particular, it was found that in a weakly interacting Bose gas, the second sound mainly corresponds the oscillation of the condensate, ans has been interpreted as the hydrodynamic continuation of the collisionless sound.

Chapter 3

Sound propagation in two-dimensional Bose gases

This chapter is devoted to the study of sound propagation in a two-dimensional (2D) Bose gas. Very recently, measurements of sound dynamics have become available in uniform 2D Bose gases [17]. Such system is of particular interest since, in 2D, BEC does not occur, as a consequence of the Hohenberg-Mermin-Wagner theorem. As we will see, the 2D Bose gas still exhibits a superfluid phase transition at finite-temperature, the Berezinskii-Kosterlitz-Thouless (BKT) phase transition, which is of infinite order and does not show any discontinuity in the thermodynamic quantities. Remarkably, the superfluid density exhibits a universal jump at the transition, and this motivates us to investigate the second sound, which we predict to vanish abruptly at the BKT transition. In particular, we investigate the interaction dependence of the speed of sound, to observe how the nature of the sound mode evolves as one goes from the weakly interacting to the strongly interacting regime. On the other hand, the experiment of Ref. [17] did not reveal the occurrence of any jump in the sound velocity, its value remaining finite also in the normal phase. We therefore develop a collisionless theory for the 2D Bose gas, and compare our result to the experimental one.

3.1 The BKT phase transition

3.1.1 The ideal Bose gas in 2D

One of the most striking feature in the 2D Bose gas, is the absence of a condensate associated to the off-diagonal long range order of the system [13, 73]. This can be understood if one recalls the expression for the equation of state of an ideal gas,

discussed in Sec. 1.2.2:

$$n\lambda_T^d = g_{d/2}(e^{\beta\mu})\,, \tag{3.1}$$

where the quantity $D = n\lambda_T^d$ is called the phase space density. In the three dimensional case ($d = 3$), we have seen that $g_{3/2}(z)$ saturates at $\mu = 0$, and an increase of the phase-space density beyond the critical value $g_{3/2}(1)$ is only made possible by the emergence of a condensate state. However in 2D, the phase space density takes the explicit form

$$D = -\ln\left(1 - e^{\beta\mu}\right)\,, \tag{3.2}$$

and a solution for the fugacity with a negative chemical potential exists for any values of D, prevailing the atoms to macroscopically occupy a single-state.

More formally, one can look at the off-diagonal long-range behavior of the one-body density matrix Eq. (1.22):

$$n^{(1)}(s) = \frac{1}{(2\pi)^2}\int d^2\mathbf{k}\frac{e^{i\mathbf{k}\cdot\mathbf{s}}}{e^{\beta(\varepsilon_\mathbf{k}-\mu)}-1}\,. \tag{3.3}$$

Since we are interested in the long-range behavior of the system, one can focus on the long wavelength modes $k \to 0$. Further assuming that the system is in the degenerate regime, $|\mu|/k_BT \ll 1$, one can approximate the distribution function by $f(\varepsilon_k) \sim 2m\hbar^{-2}k_BT/(k^2 + k_c^2)$ with $k_c = \sqrt{2m|\mu|/\hbar^2}$. Then one finds

$$n^{(1)}(s) \propto e^{-s/l_c} \tag{3.4}$$

with $l_c = k_c^{-1} \simeq \lambda_T e^{D/2}/\sqrt{4\pi}$. Equation (3.4) clearly suggests that contrary to the 3D case, the 2D Bose gas does not exhibit any long-range order at finite temperature. However, it is interesting to notice that the length scale over which $n^{(1)}$ decays (i.e. the correlation length l_c) increases exponentially as one decreases the temperature. This observation suggests that in a real finite-size system, one might reach a regime in which the correlation length is comparable to the system size ($l_c \sim L$), so that the correlations span the entire volume. As one shall see below, the decay of the correlations is further reduced when one includes the effects of interactions.

3.1.2 Weakly interacting Bose gas in 2D

Suppression of density fluctuations

A crucial ingredient in understanding the thermodynamic behavior of a two-dimensional Bose gas, is the presence of a *quasi*-condensate, associated to the suppression of density fluctuations. In this section, we mainly follow the argument developed by Hadzibabic and Dalibard in Ref. [12].

In order to discuss the interacting gas, let us consider that like in 3D, the interaction between two atoms can be modeled by a contact type interaction $V(\mathbf{r}) = g_{2D}\delta(\mathbf{r})$, with g_{2D} the two-dimensional coupling constant. This assumption holds for the general experimental set-up, where the transverse confinement is tight enough to ensure the 2D kinematics. The details about the interaction in 2D is given in the appendix B, and here we only notice that as a peculiarity of the 2D Bose gas, one can define a dimensionless coupling constant,

$$\tilde{g} = \frac{m}{\hbar^2} g_{2D}\,. \tag{3.5}$$

Under these assumptions, the model Hamiltonian for the 2D gas is the same as that of the 3D gas, Eq. (1.47). The interaction energy is therefore given by (for the remaining of this chapter we use the notation $g \equiv g_{2D}$ for the 2D coupling constant)

$$E_{\rm int} = \frac{g}{2}\int d^2\mathbf{r}\left\langle \hat{\Psi}(\mathbf{r})^\dagger \hat{\Psi}(\mathbf{r})^\dagger \hat{\Psi}(\mathbf{r})\hat{\Psi}(\mathbf{r})\right\rangle = \frac{g}{2}L^2 n^{(2)}(0)\,, \tag{3.6}$$

where we have used the definition of the two-body density matrix $n^{(2)}(\mathbf{r})$ (1.30). We briefly remind that its value is comprised between n^2 and $2n^2$, depending on whether the density fluctuations are suppressed ($n^{(2)} = n^2$) or not ($n^{(2)} = 2n^2$; Gaussian fluctuations). An estimate for the cost of density fluctuations is obtained by looking to the change of internal energy when adding an atom to the system:

$$\frac{\partial E_{\rm int}}{\partial N} = gn\,. \tag{3.7}$$

Consequently, the relative fluctuation cost with respect to the thermal energy is given by

$$\frac{gn}{k_B T} = \frac{\tilde{g}}{2\pi} D\,. \tag{3.8}$$

The above equation suggests that at sufficiently low temperature, in which $D \gg 2\pi/\tilde{g}$, density fluctuations can be strongly suppressed. This suppression plays a key role in developing the quasi-condensate mean-field theory [93,94]. As we show in details in Appendix C.1, phase fluctuations are instead not suppressed, and this leads to a *quasi*-long range behavior of the one-body density matrix in the superfluid phase:

$$n^{(1)}(s) \propto \left(\frac{R_c}{s}\right)^{1/(n_s\lambda_T^2)}\,, \tag{3.9}$$

with $R_c = \beta\hbar\sqrt{gn_s/m}$, and n_s is the superfluid density. Result (3.9) shows the peculiarity of the 2D interacting system, namely the algebraic decay of the off-diagonal one-body density matrix. In the next section, we will see that the exponent of the density matrix is always smaller than 1/4, involving an extremely slow decay of $n^{(1)}$.

3.1.3 The role of vortices

In the previous section, we have seen that in the degenerate regime of a 2D Bose gas, density fluctuations can be significantly suppressed and one may consider the physics of phase fluctuations only. However, so far we have not discussed how such system undergoes a superfluid transition. In order to understand this point, one needs to take into account an additional ingredient in the 2D physics: the vortex.

Vortices are phase defects arising from the irrotational nature of the superfluid (see Eq. (1.72)). They correspond to a local depletion of the superfluid density, around which the phase of the order parameter varies by a multiple of 2π [7, §5.3]. The most common way to excite vortices consists to rotate (or stir) the system. In this way, vortices have been observed in both Bose [95, 96] and Fermi [97] gases, as a hallmark of superfluidity. In the absence of such external probe, for a vortex line to be thermally excited, its creation has to be energetically favorable. Let us therefore evaluate the free energy associated with the presence of a vortex line $F_v = E_v - TS_v$. First, solving the Gross-Pitaevskii equation (1.67) in a rotating frame, one finds that the velocity around a vortex line is [7, §6.8]:

$$v_s(r) = \frac{\hbar}{m}\frac{s}{r}\,, \tag{3.10}$$

with s an integer, characterizing the quantization of vortices. Furthermore, the size of the vortex core, in which the superfluid is depleted, is found to be given by the healing length $\xi = 1/\sqrt{\tilde{g}n}$. Then, the excitation energy for a $s = 1$ vortex is

$$E_v = \int d^2\mathbf{r} n_s(\mathbf{r}) \frac{1}{2} m v_1^2(r) \simeq \frac{\pi\hbar^2}{m} n_s \ln\left(\frac{R}{\xi}\right)\,, \tag{3.11}$$

where we have considered the system to be a disk of radius R, and the superfluid density to be finite and constant in the region $\xi \leq |\mathbf{r}| \leq R$. As for the entropy, it corresponds to the number of possible configurations for a vortex of size $\pi\xi^2$ to be placed in the system of size πR^2,

$$S_v = k_B \ln\left(\frac{\pi R^2}{\pi\xi^2}\right)\,. \tag{3.12}$$

Thus, one finds for the free energy for the creation of a single vortex to be:

$$F_v = \frac{k_B T}{2}\left(n_s\lambda_T^2 - 4\right)\ln\left(\frac{R}{\xi}\right)\,. \tag{3.13}$$

The creation of a vortex line becomes energetically favorable when [98],

$$n_s\lambda_T^2 = 4\,. \tag{3.14}$$

The logarithmic term in Eq. (3.13) being very large, it means that as soon as $D_s = 4$, a vortex is thermally excited. The vortex corresponding to a local depletion of the superfluid density, n_s consequently decreases and this further favors the creation of new vortices. Therefore, there will be an avalanche effect, which strongly renormalizes the superfluid density to 0 [98]. In other word, one can say that the vortex, corresponding to a phase defect, completely scrambles the phase coherence and so the quasi-long-range order. This is the mechanism behind the superfluid phase transition in 2D, first discussed by Berezinskii, Kosterlitz, and Thouless [14, 15]. The number of vortices is exponentially small in the normal phase just above the phase transition, and this makes the Berezinskii-Kosterlitz-Thouless (BKT) superfluid transition to be of "infinite" order, without exhibiting any discontinuities in the thermodynamic quantities, apart from the superfluid density which abruptly drops to 0 at the critical temperature. The BKT phase transition has been experimentally observed in a variety of systems, including the ^{4}He film [99], the 2D atomic hydrogen [100], and the 2D Bose gas [65, 66].

Equation (3.14) provides a very simple and elegant formula to assess the onset of the phase transition. It is universal, in the sense that it does not depend on the coupling constant, but only on the phase-space density. However, Eq. (3.14) gives the relationship between the superfluid density and the temperature at the critical point only, and it does not tell us at which temperature the BKT phase transition actually occurs. In order to answer to this question, one needs to properly consider the effects of vortices in the phase fluctuations. This can be achieved through a renormalization group calculation, known as the Kosterlitz-Thouless equations [15, 101], or by means of universal relations in the vicinity of the phase transition. Hereafter, we will focus on this later approach.

3.1.4 Universal description of the fluctuating region

The phase transition of any systems is characterized by an increase of the correlation length, so that near the phase transition, the long-wavelength physics becomes dominant [102, §10]. This property allows for a universal description of the phase-transition itself, but also of the critical region around the transition. For a weakly interacting Bose gas, the long-range behavior exhibits the so-called $|\Psi|^4$ universality, which is independent on the nature of the system, being classical or quantum, continuous or discrete [78, 79].

This universality has been used by Svistunov and Prokof'ev to evaluate the BKT critical temperature of the 2D Bose gas [81]. Briefly, the main idea is to separate the equation of state into a universal and a non-universal parts:

$$n = \frac{1}{(2\pi)^2}\left(\int_0^{|\mathbf{k}_{\rm cut}|} d^2\mathbf{k} n_{\mathbf{k}} + \int_{|\mathbf{k}_{\rm cut}|}^{\infty} d^2\mathbf{k} n_{\mathbf{k}}\right) \equiv n_{\rm universal} + n_{\rm ideal}\,, \tag{3.15}$$

where the non-universal part, corresponding to the short-wavelength physics, is essentially described by free particles physics, which can be evaluated straightforwardly. Then, the difference between two distinct systems $\mathcal{A}$ and $\mathcal{B}$ sharing the same universality is given by

$$n^{(\mathcal{A})} - n^{(\mathcal{B})} = n^{(\mathcal{A})}_{\text{ideal}} - n^{(\mathcal{B})}_{\text{ideal}} \,. \tag{3.16}$$

In the work of Svistunov and Prokof'ev, system $\mathcal{A}$ was chosen to be the 2D Bose gas, while system $\mathcal{B}$ a 2D classical lattice. Performing a classical Monte-Carlo calculation, they could evaluate with great precision the critical density for the lattice model, and from Eq. (3.16), that of the 2D Bose gas. In particular, they found that the critical density for the onset of the BKT phase transition is given by the formula

$$n_{\text{BKT}} = \frac{1}{\lambda_T^2} \ln\left(\frac{C}{\tilde{g}}\right) , \tag{3.17}$$

with $C = 380 \pm 3$. This result has further been confirmed in a quantum Monte-Carlo study [80], showing that Eq. (3.17) remains accurate up to very large value of $\tilde{g}$ (~ 2).

3.2 Thermodynamics of 2D Bose gases

3.2.1 Theoretical framework

In order to calculate the hydrodynamic sound velocities by solving the two-fluid equation (1.82), one needs a reliable description of the thermodynamic quantities in 2D. The universality of the weakly interacting Bose gas we have discussed previously, can be used to obtain the equation of state in the critical region. Prokof'ev and Svistunov have calculated the universal behavior for the equation of state of a 2D Bose gas [82], and provided dimensionless functions depending on the variable $x = \mu/(k_B T)$ and $\tilde{g}$ only,

$$\mathcal{D}(x, \tilde{g}) = \lambda_T^2 n \,. \tag{3.18}$$

Using general thermodynamic relations, one can further obtain the reduced pressure

$$\mathcal{P}(x, \tilde{g}) = \frac{\lambda_T^2}{k_B T} P = \frac{1}{k_B T} \int dx \mathcal{D}(x) \,, \tag{3.19}$$

as well as all the thermodynamic quantities needed for the solution of the Landau equation (1.82):

$$\begin{gathered} \bar{s} = 2\frac{\mathcal{P}}{\mathcal{D}} - x, \qquad \kappa_T = \frac{1}{n k_B T}\frac{\mathcal{D}'}{\mathcal{D}}, \qquad \kappa_s = \frac{1}{n k_B T}\frac{\mathcal{D}}{2\mathcal{P}} \\ \bar{c}_V = 2\frac{\mathcal{P}}{\mathcal{D}} - \frac{\mathcal{D}}{\mathcal{D}'}, \qquad \bar{c}_P = \left(2\frac{\mathcal{P}}{\mathcal{D}} - \frac{\mathcal{D}}{\mathcal{D}'}\right) 2\frac{\mathcal{P}\mathcal{D}'}{\mathcal{D}^2}, \end{gathered} \tag{3.20}$$

where $\mathcal{D}' = \partial\mathcal{D}/\partial x$. Universal relations (UR) further provide another dimensionless function $\mathcal{D}_s(x, g) = \lambda_T^2 n_s$, from which one can evaluate the superfluid density. The universal behavior of the weakly interacting Bose gas has also been investigated experimentally [68,103], showing excellent agreement with the predictions of Prokof'ev and Svistunov, in a wide temperature range. In this thesis, we follow the semi-analytical description of Ref. [82], in which the UR description is combined with the 2D Popov theory.

Indeed, while a genuine condensate does not exist in 2D, one can formally introduce the *quasi*-condensate, characterizing the suppression of density fluctuations, according to [104, 105]:

$$n_{qc} = \sqrt{2\langle\hat{n}\rangle^2 - \langle\hat{n}^2\rangle}\,. \tag{3.21}$$

Comparing with Eq. (1.35), one can see that n_{qc} is analogous to n_0 in 3D. However, as we shall see later, the quasi-condensate in 2D takes a non-zero value even when there is no more superfluid. As we show in details in the Appendix C.2, one can then develop a mean-field (Popov) theory for the weakly interacting 2D Bose gas, based on the concept of quasi-condensate. Within the 2D Popov theory, the universal function for the phase-space density is obtained from the implicit formula (see Eq. (C.36) in the Appendix):

$$\mathcal{D} = \frac{2\pi x}{\tilde{g}} + \ln\left(\frac{2\tilde{g}}{\pi}\mathcal{D} - 2x\right)\,. \tag{3.22}$$

To the same accuracy, the superfluid density can be evaluated from Eq. (1.74) as:

$$\mathcal{D}_s = 2\mathcal{D} - \frac{2\pi x}{\tilde{g}} - 1\,. \tag{3.23}$$

We show in Fig. 3.1 a comparison between the 2D Popov theory and the UR, for the isothermal compressibility (left panel) and the superfluid density (right panel). As one can see, the Popov approach catches correctly the temperature dependence of κ_T, up to the BKT critical point. However, the Popov theory fails in describing the behavior of the compressibility in the normal phase, as well as to reproduce the BKT jump of the superfluid density. Thus, in the following, we evaluate all the thermodynamic quantities entering in the Landau equation (1.82) using the 2D Popov theory, except for the superfluid density in the vicinity of the BKT critical point, which we evaluate using the universal approach. Practically, we interpolate between the Popov theory and the UR at an intermediate temperature $T < T_{\mathrm{BKT}}$ (see the red point at $T \simeq 0.6T_{\mathrm{BKT}}$ in the left panel of Fig. 3.1, which corresponds to the point where we "connect" the two theories). Such procedure is found to give essentially the same result as the full UR calculations, at least below T_{BKT}. A detailed discussion about the Popov theory in 2D, as well as a comparative study of the different approaches are presented in Appendix C.2.

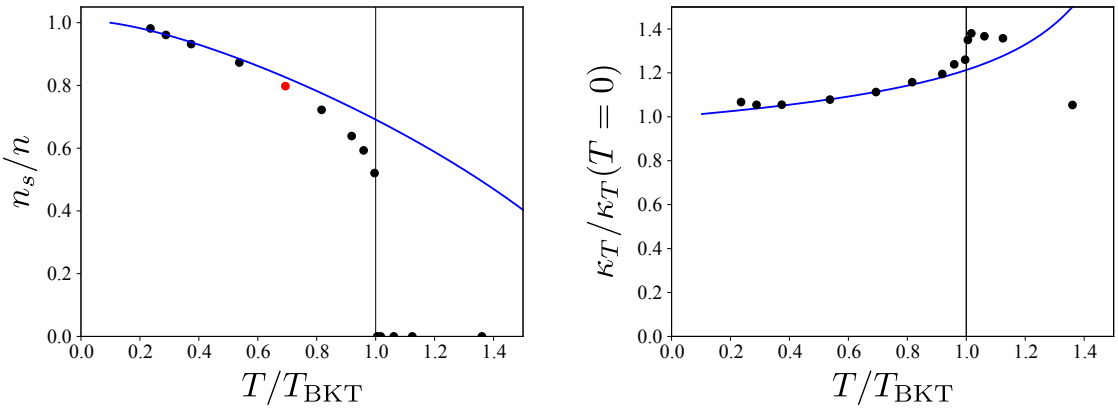

Figure 3.1: Isothermal compressibility (left panel) and superfluid density (right panel) of a 2D Bose gas as a function of temperature, evaluated for $\tilde{g} = 0.1$. The blue solid line is the result from the 2D Popov theory, while the black dots are the predictions from the universal relations of Ref. [82]. The red point in the left panel is an eye-guide to indicate the region where we connect the Popov theory and the UR, in our combined approach (see main text).

3.2.2 Validity domain study

Although UR have been successfully used for the study of the hydrodynamic sound waves in a weakly interacting 2D Bose gas [16], one might ask if the theory is still valid in the strongly interacting regime. Figure 3.2(a) shows the ratio of isothermal and adiabatic compressibilities as a function of the temperature, for different values of the coupling constant, evaluated within the combined Popov-UR approach. From thermodynamic principles, κ_T/κ_s can not be negative [84, §16], and Fig. 3.2(a) shows a clear failure of the universal relation for $g \geq 1$. Still, the behaviour of κ_T/κ_s decreasing with g as shown in the inset of Fig. 3.2(a), has also been observed in the 3D Fermi gas [86], and is physically acceptable. Indeed, the gas is expected to become less compressible as the repulsive interaction between bosons becomes stronger. In Fig. 3.2(b) we show the superfluid density fraction n_s/n for the same values of coupling constant [1]. While the jump turns out to agree [82] with the Nelson-Kosterlitz result (3.14), one observes another unphysical result, with the superfluid density fraction becoming larger than unity at low temperature. This last point directly arises from the limitation of the UR, derived for the fluctuating region near the superfluid phase transition [81, 82]. As the interaction increases, the fluctuating region around T_{BKT} shrinks, reducing the

[1] The reason for the unphysical kink at intermediate temperature in Fig. 3.2(b), comes from the above-mentioned treatment of the combined Popov-UR approach.

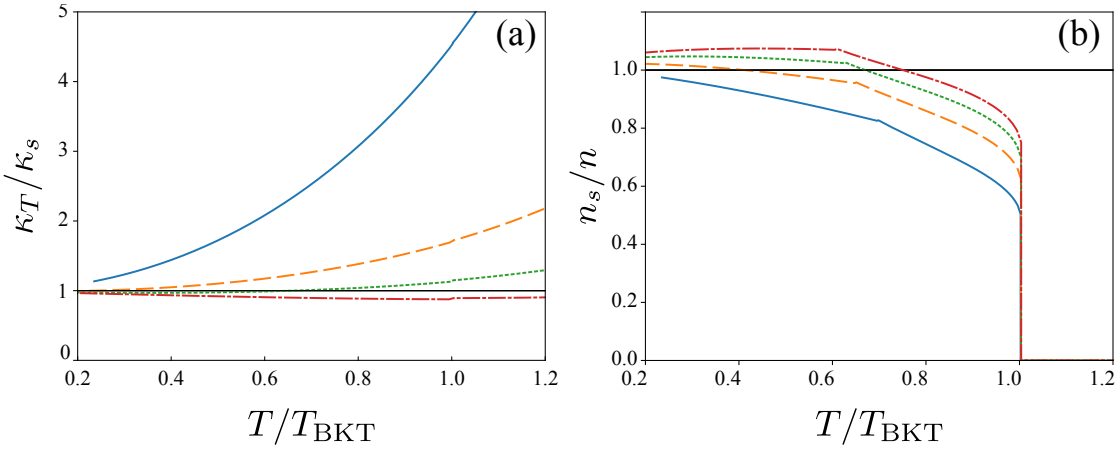

Figure 3.2: (a) Ratio of isothermal and adiabatic compressibilities κ_T/κ_s for different values of g. From top to bottom, $\tilde{g} = 0.1$ (solid line), $\tilde{g} = 0.5$ (dashed line), $\tilde{g} = 1$ (dotted line), $\tilde{g} = 1.5$ (dashed-dotted line). (b) Superfluid density fraction n_s/n for different values of $\tilde{g}$. The values of $\tilde{g}$ are the same as in panel (a). The unphysical kinks observed for $T \simeq 0.6T_{\mathrm{BKT}}$ in the superfluid density is due to the analytical treatment of the dimensionless functions in the universal relations approach [82]. The black solid line is an eye-guide for (a) $\kappa_T/\kappa_s = 1$ and (b) $n_s/n = 1$.

region of validity of the UR. Nevertheless, as we have already mentioned, the UR predicts the correct phase transition temperature, up to $g \simeq 2$, when compared to *ab initio* calculation [80]. Therefore in what follows, we use the UR for the study of the 2D Bose gas, restricting ourself to the temperature region near the phase transition, and to values of $g \leq 1$. We briefly note that, $g \simeq 0.1$ is a typical value of coupling constant for a dilute 2D Bose gas [66], and $0.6 \lesssim g \lesssim 2.8$ corresponds to the BEC regime of a 2D Fermi gas [69, 106], where the system behaves as a gas of bosonic dimers. A direct mapping between our results calculated for the strongly interacting Bose gas and the experimentally relevant 2D Fermi gas can be conveniently achieved using the following relationship [7, §23.4]:

$$g = -4\pi \frac{1}{2\ln(k_{\mathrm{F}} a_{2D}) + \ln(\gamma^2/4\pi)}, \tag{3.24}$$

where $k_{\mathrm{F}} a_{2D}$ is the interaction parameter for a 2D Fermi gas [76], k_{F} and a_{2D} are the Fermi wave vector and the 2D s-wave scattering length, respectively. $\gamma = a_B/a_{2D} \simeq 0.55$ [107] is a constant relating the bosonic scattering length to the fermionic one.

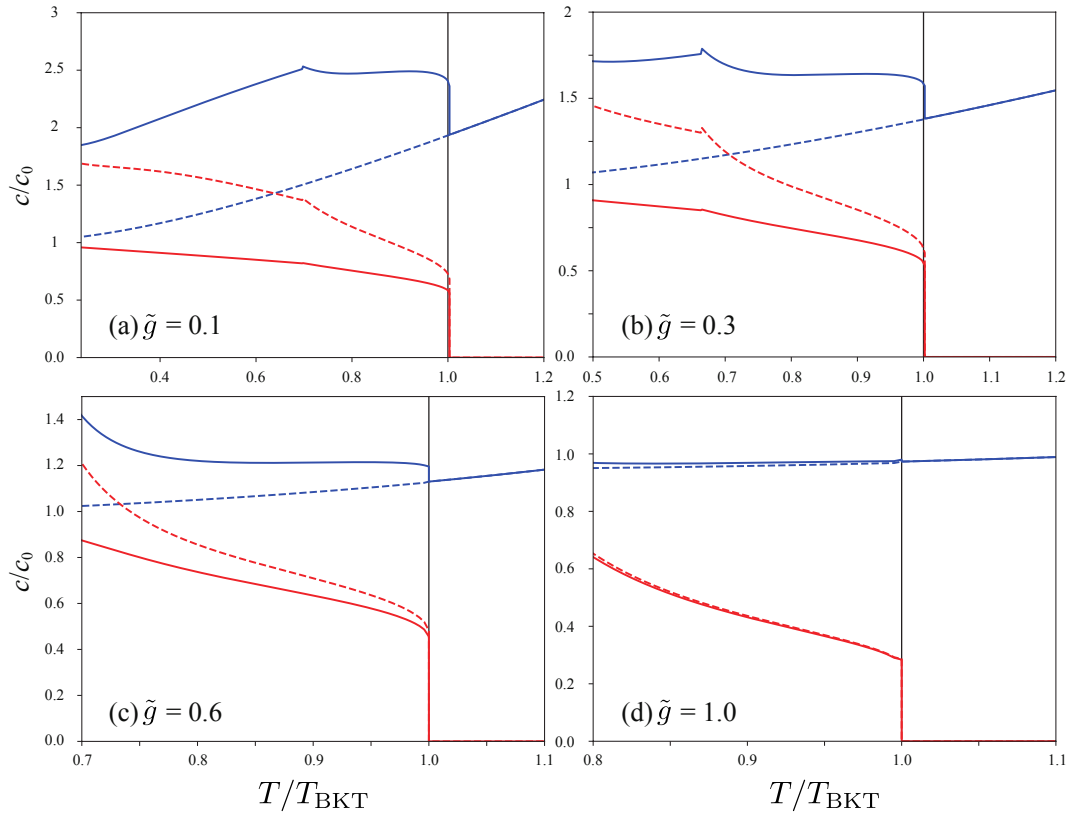

Figure 3.3: First and second sounds as a function of temperature for different values of $\tilde{g}$. The blue and red solid lines correspond to first and second sounds calculated from Eq. (1.82), respectively. The blue and red dashed lines are the approximated form of the first and second sounds for small thermal expansion coefficient, given by Eq. (3.26).

3.3 Hydrodynamic sounds in a 2D Bose gas

We are now in position to investigate the propagation of sound in the hydrodynamic regime. As in the three-dimensional case, the Landau Eq. (1.82) is solved together with the thermodynamic quantities evaluated within the combined Popov-UR approach, Eq. (3.20).

Figure 3.3 shows the first and second sound obtained by solving Eq. (1.82) (solid line), for different values of $\tilde{g}$. The velocities are calculated for fixed total density and expressed in units of the zero temperature Bogoliubov sound velocity $c_0 = \sqrt{\tilde{g}n}/m$. As one can see, both sound velocities show a jump at the transition temperature. This behaviour, originating from the BKT universal jump of the superfluid density, is studied in detail in the following. Panel (a) corresponding

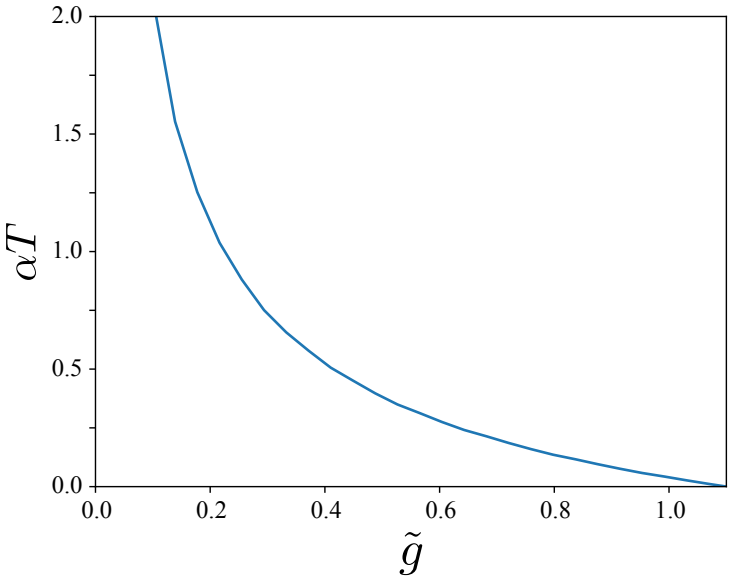

Figure 3.4: Thermal expansion coefficient αT at $T = 0.8T_{\mathrm{BKT}}$ as a function of the 2D coupling constant $\tilde{g}$.

to $\tilde{g} = 0.1$ has already been studied within the same approach in [16]. In order to understand the evolution of the sound modes with the coupling constant, one recall the two-fluid Landau equation (1.82). As we have already discussed in Sec. 1.3.1, the two sound modes are decoupled if the thermal expansion coefficient is negligibly small:

$$\alpha T = \left(\frac{\kappa_T}{\kappa_s} - 1 \right) \ll 1 \,. \tag{3.25}$$

In that case the first and second sound modes take the form of density and entropy waves respectively,

$$c_{10}^2 = \frac{1}{mn\kappa_s}, \qquad c_{20}^2 = \frac{n_s T \bar{s}^2}{m n_n \bar{c}_p}. \tag{3.26}$$

Figure 3.3(a) and 3.3(b) show that the calculated velocities strongly deviate from Eq. (3.26) (shown as dashed-line), revealing the strong coupling between the density and entropy modes in the highly compressible regime where the condition $\alpha T \ll 1$ is violated. Figure 3.4 shows that as the coupling constant increases, the gas evolves from a weakly interacting to a strongly interacting behaviour, becoming less compressible. As a consequence Eq. (3.26) becomes more and more accurate, as shown in panels (c) and (d). The transition between the weakly interacting and the strongly interacting regime is then expected to take place for values of the 2D coupling constant corresponding to $\tilde{g} \sim 0.5$. This regime

can be reached in a 2D Bose gas with Feshbach resonance [67] or in the BEC side of the BEC-BCS crossover in 2D superfluid Fermi gases [106]. It is worth noticing that the already mentioned unphysical violation of the thermodynamic relation $\kappa_T/\kappa_s \geq 1$ predicted by the use of universal relations for large values of the coupling constant, has little effect on the sound speeds, while the violation of the condition $n_s \leq n$ has dramatic unphysical consequences due to the resulting negativity of the normal density. The proper estimate of the sound velocities in the strongly interacting regime should then be based on more realistic estimates of the superfluid density. Accurate calculations of the superfluid density as well as of the relevant thermodynamic functions of 2D Fermi gases, based on quantum Monte Carlo simulations [80, 108] or many-body theories [109–111], would in particular allow for a safer evaluation of the sound velocities along the whole BCS-BEC crossover.

In the 2D Bose gas too, one can approximate the thermodynamic quantities entering in the two-fluid equation except the isothermal compressibility and the superfluid density, by those of an ideal Bose gas. We rewrite here the results found in Sec. 2.2,

$$c_{1,\mathrm{WI}} = \sqrt{\frac{nT\bar{s}^2}{n_n m \bar{c}_v}}, \qquad c_{2,\mathrm{WI}} = \sqrt{\frac{n_s}{n}\frac{1}{mn\kappa_T}}\,. \tag{3.27}$$

Figure 3.5 shows, again, the sound velocities for the same values of the coupling constant, but compared this time, to Eq. (3.27) (dotted-lines). As expected, the approximation successfully describes the exact sound speeds for small $\tilde{g}$. In contrast to Fig. 3.3, Eq. (3.27) becomes less accurate as one increases $\tilde{g}$. However, panel (d) shows that the approximated velocities approach again the exact solutions, for $T \leq T_{\mathrm{BKT}}$. This is a proper behaviour to the 2D system, where the BKT jump of the superfluid density, scaling as $n_s/n = 4/\ln(C/\tilde{g})$ (see Eqs. (3.14) and (3.17)), is responsible for $n_s \simeq n$ over the whole range of temperature, as observed in Fig. 3.2(b). This assumption, in addition to $\alpha \simeq 0$ for large value of $\tilde{g}$, leads to $c_{1,\mathrm{WI}} \simeq c_{20}$ (respectively, $c_{2,\mathrm{WI}} \simeq c_{10}$).

While in the 3D case the sound velocities near the phase transition can be estimated by putting $n_s \to 0$, leading to Eq. (3.26), this assumption can not be used in the actual 2D case, due to the presence of the jump. One can however derive a first-order correction to c_{10} and c_{20} from the two-fluid equation (1.82),

$$c^2_{1,\mathrm{BKT}} = c^2_{10}\left(1 + \alpha T \frac{c^2_{20}}{c^2_{10}}\right), \qquad c^2_{2,\mathrm{BKT}} = c^2_{20}\left(1 - \alpha T \frac{c^2_{20}}{c^2_{10}}\right), \tag{3.28}$$

where one has assumed that $\alpha T c^2_{20}/c^2_{10} \ll 1$. This condition is expected to be valid near T_{BKT}, and the results of Eq. (3.28) correctly describe the jump $c(T^-_{\mathrm{BKT}}) - c(T^+_{\mathrm{BKT}})$ of the two velocities in a wide range of values of the coupling constant, as drawn in Fig. 3.6. According to Eq. (3.28), the deviation from c_{10} and c_{20} near

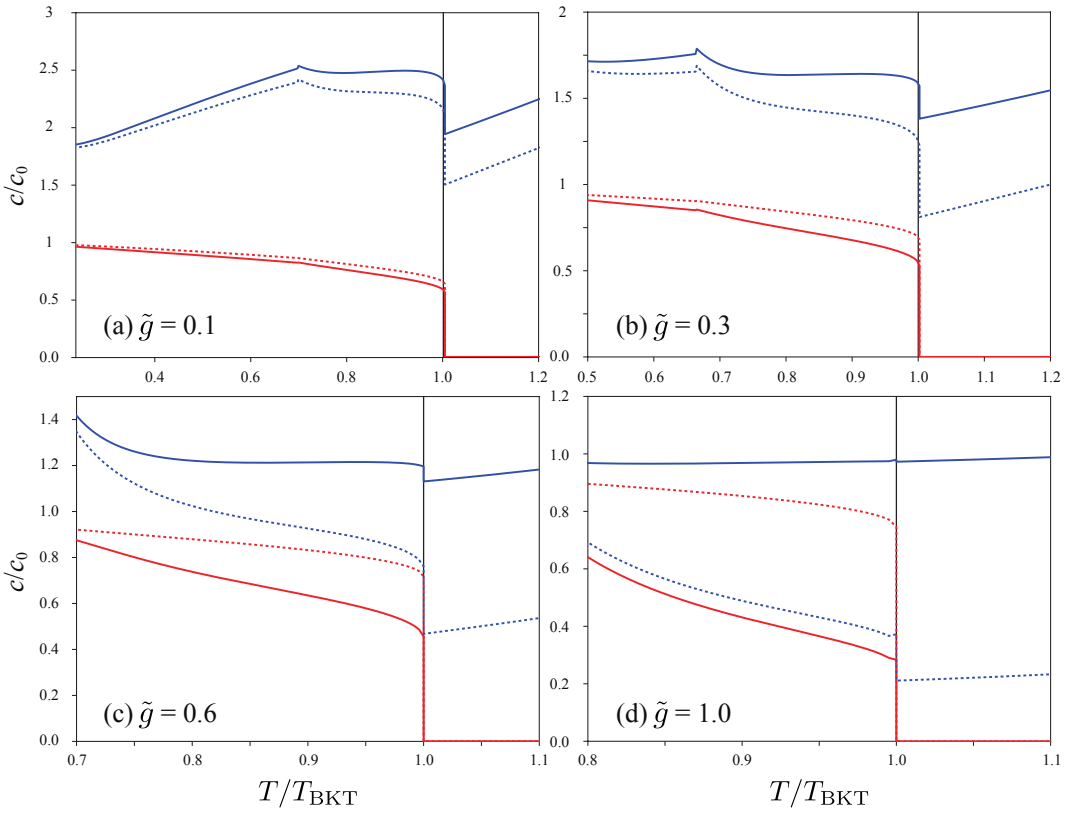

Figure 3.5: First and second sounds as a function of temperature for different values of $\tilde{g}$. Solid lines are the same as Fig. 3.3. The blue and red dotted lines are the approximated form of the first and second sounds for a weakly interacting Bose gas, given by Eq. (3.27).

T_{BKT} is characterized by a factor $\alpha T c_{20}^2/c_{10}^2$. Therefore, not only the BKT jump of the superfluid density (appearing in $c_{20}^2 \propto n_s$), but also the difference between thermal and adiabatic compressibilities, are responsible for the observed gap in the sound velocities. This is explicitly shown in Fig. 3.3(d), where the jump in the first sound mode disappears due to the vanishingly small value of α.

Finally, it is of great interest to understand weather second sound can be excited using a density probe. This is again assessed by calculating the amplitudes of the respective sound modes in the compressibility sum rules, W_1 and W_2. Figure 3.7 shows the ratio of the relative contribution of first and second sound to the compressibility sum rule, Eq. (2.20). We can see from a comparison with Fig. 3.4 that as expected from Eq. (2.21), W_2/W_1 follows the same evolution as κ_T/κ_s. This observation involves that from the experimental point of view, the density

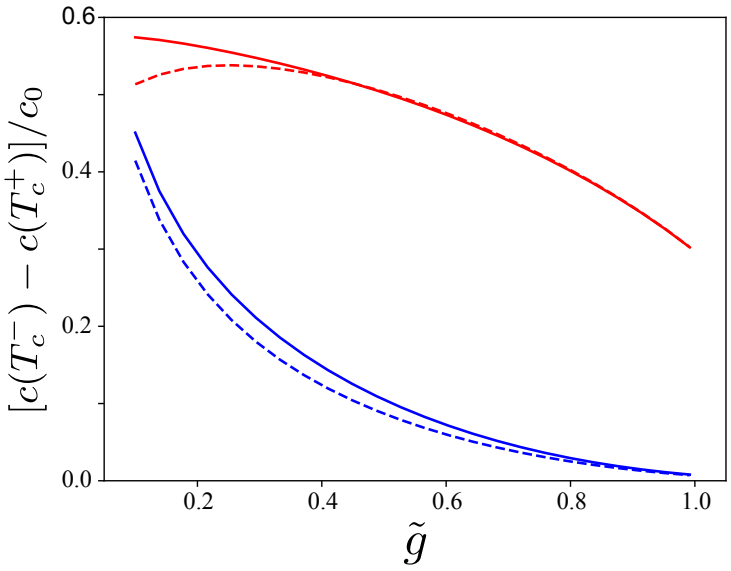

Figure 3.6: BKT jump in sound velocities $c^-_{BKT} - c^+_{BKT}$ as a function of $\tilde{g}$. Sound velocities jump obtained from the solutions of Landau equation (1.82) (solid lines) are compared to the approximated expression Eq. (3.28) (dashed lines).

probe of the second sound becomes more and more difficult as one increase the value of the coupling constant.

3.4 Collisionless sound in a 2D Bose gas

3.4.1 Motivation

We discuss in this section the propagation of sound in the collisionless regime. This discussion is motivated from the recent experiment of Collège de France group in Paris [17], where they have measured the propagation of sound wave in a 2D gas of ^{87}Rb atoms. As shown in Fig. 3.8, while the measured sound lies close to the zero-temperature Bogoliubov sound in the superfluid phase, the velocity does not exhibit any jump and remains finite also above the superfluid transition temperature. This observation is in contradiction with the hydrodynamic theory we have developed in the previous section. The key point for understanding these observations is the role of collisions, which would be essential for the application of two-fluid hydrodynamics. In the quasi-2D regime of [17], one can estimate the

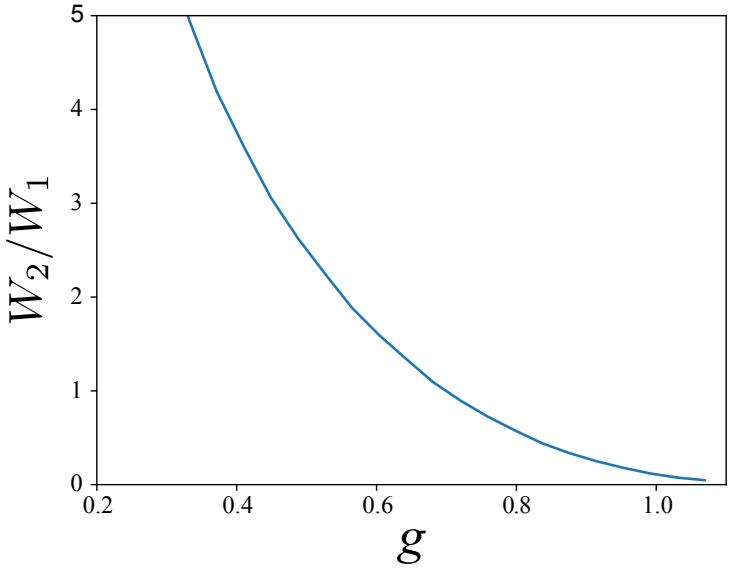

Figure 3.7: Ratio of compressibility sum rule contribution W_2/W_1 at $T = 0.8T_{\mathrm{BKT}}$. W_1 (W_2) is the relative contribution of first (second) sound mode to the compressibility sum rule Eq. (2.20).

collisional parameter to be given by (see Appendix B):

$$\omega\tau \simeq \sqrt{\frac{1}{n\tilde{g}^3}}\frac{2\pi}{L}\,, \tag{3.29}$$

where L is the size of the box. Using the parameters of the experimental set-up:

$$L = 38\mu m\,, \qquad n = 30\mu m^{-2}\,, \qquad \tilde{g} = 0.16\,, \tag{3.30}$$

one gets an estimate for the collisional parameter:

$$\omega\tau \simeq 0.47. \tag{3.31}$$

Thus, the collisional rate is of the same order of the frequency of the excited mode, determined by the box length, and this observation suggests that collisions might not be efficient enough to ensure the collisional hydrodynamic regime. Hence one needs a theory which can describe density waves in the absence of collisions, *above* T_{BKT}, even in the absence of superfluidity.

3.4.2 Collisionless theory of the 2D Bose gas

In Chap. 2, we have found that a collisionless transport theory for the weakly interacting Bose gas can be obtained, starting from the dynamic mean-field approach. Although we have seen that the 2D Bose gas is well described by mean-field

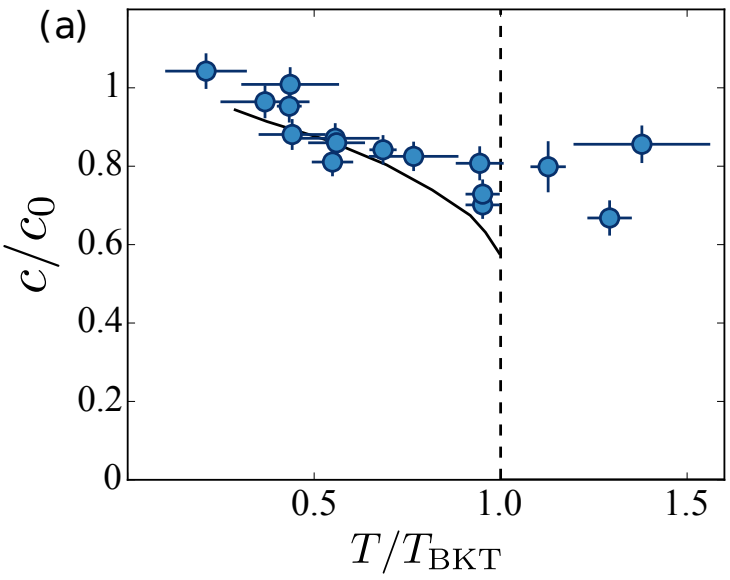

Figure 3.8: Experimental result for the measurement of density sound in a 2D Bose gas, using density probe. The blue dots are the experimental data, the black solid line the theoretical prediction of Sec. 3.3 for the hydrodynamic second sound. Sound velocities are normalized by the Bogoliubov sound velocity c_0. From Ref. [17].

theories based on the concept of quasi-condensate in the superfluid phase, these approaches fail above T_{BKT}, where the physical meaning of the quasi-condensate becomes ambiguous (see Fig. 3.1 where the Popov theory predicts an erroneous divergence of the isothermal compressibility, as well as discussions in Appendix C.2). The experimental measurement showing a discrepancy with the hydrodynamic theory in the normal regime of the gas, one needs an appropriated theory to describe that region.

Kinetic theory

In our work, rather than developing a framework which includes the effects of vortices, we have simplified the description of the Bose gas, assuming that in the temperature region of interest, the system is described by a normal gas with suppressed density fluctuations. This is motivated by the prediction of the universal relations shown in Fig. 3.9, which reveals that the quasi-condensate, characterizing the suppression of density fluctuations Eq. (3.21), is close to the total atoms density even in the normal phase, up to relatively high temperature. Our starting point is therefore the RPA expression for the response function (1.18) of a *normal*

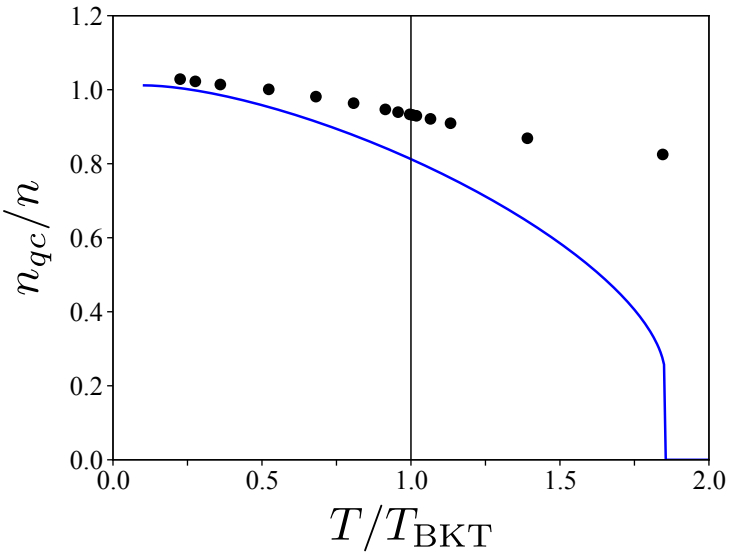

Figure 3.9: Quasi-condensate density as a function of temperature, evaluated for the interaction parameter $\tilde{g} = 0.16$. Blue solid line: prediction from the 2D Popov theory. Black dots: prediction from the universal relations of Ref. [82].

Bose gas:

$$\delta n(\mathbf{q},\omega) = -\delta U_{\mathrm{eff}}(\mathbf{q},\omega)\chi^0(\mathbf{q},\omega)\,, \tag{3.32}$$

with the effective interaction now given by

$$\delta U_{\mathrm{eff}}(\mathbf{q},\omega) = \delta U_{\mathrm{ext}}(\mathbf{q},\omega) + g\delta n(\mathbf{q},\omega)\,, \tag{3.33}$$

namely the dynamic mean-field *in absence* of exchange effect. One immediately obtains,

$$\delta n(\mathbf{q},\omega) = -\delta U_{\mathrm{ext}}(\mathbf{q},\omega)\chi(\mathbf{q},\omega)\,, \tag{3.34}$$

with the density response function given by

$$\chi(\mathbf{q},\omega) = \frac{\chi^0(\mathbf{q},\omega)}{1 - g\chi^0(\mathbf{q},\omega)}\,. \tag{3.35}$$

The response function of the reference system is obtained from the same expression as the 3D Bose gas Eq. (2.30),

$$\chi^0(\mathbf{q},\omega) = \frac{1}{(2\pi\hbar)^2}\int \mathrm{d}^2\mathbf{p}\frac{f(\varepsilon_{\mathbf{p}+\hbar\mathbf{q}/2}) - f(\varepsilon_{\mathbf{p}-\hbar\mathbf{q}/2})}{\hbar\omega - \hbar\mathbf{p}\mathbf{q}/m + i\eta}\,, \tag{3.36}$$

with $\eta \to 0^+$, and the equilibrium distribution function defined as

$$f(\varepsilon_{\mathbf{p}}) = \frac{1}{e^{\beta(\varepsilon_{\mathbf{p}}+gn-\mu)} - 1}\,. \tag{3.37}$$

It is important to stress that, in Eqs. (3.35) and (3.37), the mean-field enters as gn and not $2gn$. This assumption comes from the definition of the quasi-condensate Eq. (3.21), corresponding to the non-Gaussian component of the gas. For the following, it is useful to introduce the effective chemical potential

$$\Lambda = |\mu - gn| = -\mu + gn\,. \tag{3.38}$$

In the long-wavelength limit ($q \to 0$) of interest, the bare response function takes the form (we consider a sound wave propagating in the $\mathbf{q} = q\mathbf{e}_x$ direction):

$$\chi^0(\omega/q) = \frac{1}{(2\pi\hbar)^2}\int_{-\infty}^{\infty} dp_x \frac{F(p_x)}{\omega/q - p_x/m + i\eta}\,, \tag{3.39}$$

where we have introduced

$$F(p_x) \equiv \int_{-\infty}^{\infty} dp_y \frac{\partial f}{\partial p_x} = -\frac{\beta}{m}\int_{-\infty}^{\infty} dp_y \frac{p_x e^{\beta(\frac{p^2}{2m}+\Lambda)}}{\left[e^{\beta(\frac{p^2}{2m}+\Lambda)} - 1\right]^2}\,. \tag{3.40}$$

We briefly note that the same response function Eqs. (3.35) and (3.39) can be obtained starting from the collisionless Boltzmann equation

$$\frac{\partial f}{\partial t} + \mathbf{v}\nabla f - g\nabla_{\mathbf{p}} f \partial_{\mathbf{r}} n(\mathbf{r}) = 0\,, \tag{3.41}$$

and following the same steps as for the classical gas of Sec. 1.1.3 [112]. As for the effective chemical potential Λ, it is obtained from the number equation

$$n = \frac{1}{(2\pi\hbar)^2}\int d^2\mathbf{p} f(\varepsilon_{\mathbf{p}}) = -\frac{1}{\lambda_T^2}\ln\left(1 - e^{-\beta\Lambda}\right)\,, \tag{3.42}$$

and one naturally associates to $-\Lambda$ the chemical potential of an ideal gas.

Sum rules

We first verify the f-sum rule Eq. (1.98). From Eq. (3.35),

$$\chi(q, \omega \to \infty) \simeq \chi^0(q, \omega \to \infty) \tag{3.43}$$

$$\simeq \int \frac{d^2\mathbf{p}}{(2\pi\hbar)^2}\frac{q}{\omega}\left(1 + \frac{qp_x}{m\omega}\right)\frac{\partial f}{\partial p_x} \tag{3.44}$$

In the last equation, the first term vanishes from the oddness of $\partial f/\partial p_x$ and the second term is solved by integrating by part and recalling the number equation (3.42). Finally,

$$\chi(q, \omega \to \infty) = \frac{nq^2}{m\omega^2}. \tag{3.45}$$

We next verify the compressibility sum rule (1.100). The response function (3.39) already assumes the long wave-length limit, and one finds

$$\chi^0(q \to 0, 0) = \frac{\beta}{2\pi\hbar^2} \int_0^\infty dp \frac{e^{\beta(\frac{p^2}{2m}+\Lambda)}}{\left[e^{\beta(\frac{p^2}{2m}+\Lambda)} - 1\right]^2} \,. \tag{3.46}$$

The integration can be performed analytically and one gets,

$$\chi_0(q \to 0, 0) = \frac{m}{2\pi\hbar^2} \frac{1}{e^{\Lambda/T} - 1}. \tag{3.47}$$

The full response function therefore exhausts the compressibility sum-rule:

$$\frac{1}{n^2}\chi(q \to 0, 0) = \frac{1}{n^2} \frac{m}{2\pi\hbar^2} \frac{1}{(e^{\Lambda/T} - 1) + \frac{\tilde{g}}{2\pi}} \equiv \kappa_T \,. \tag{3.48}$$

Thermodynamic compressibility

An alternative way to evaluate the isothermal compressibility is to start from the number equation (3.42), $\kappa_T = n^{-2}(\partial n/\partial\mu)|_T$. In this way, one naturally finds result (3.48) derived from the response function. In fact, the RPA theory we have developed is consistent with the mean-field expression

$$P = \frac{1}{2} g n^2 + \int \frac{d^2\mathbf{p}}{(2\pi\hbar)^2} \frac{p^2}{2m} f(\mathbf{p}) \,, \tag{3.49}$$

for the pressure of the interacting 2D Bose gas.

The isothermal compressibility κ_T is expected to play an important role in characterizing the dynamic behavior of the gas in the collisionless regime, differently from the adiabatic compressibility κ_S which instead describes the propagation of sound in the collisional regime. Figure 3.10 shows the isothermal compressibility evaluated from Eq. (3.48). We also show the results from the 2D Popov theory and the universal relations of Sec. 3.2. Comparing with the prediction of the 2D Popov theory, one can see that although the RPA framework developed in this section does not catch the increasing behavior of the compressibility in the superfluid phase, it smoothly evolves around the critical point, and decreases with the temperature in the normal regime. This behavior confirms our choice of the simplified mean-field theory for the description of the collisionless regime.

Classical field theory

Finally, we also show in Fig. 3.10 the isothermal compressibility calculated within the stochastic (projected) Gross-Pitaevskii equation (SPGPE), from Ref. [21]. In

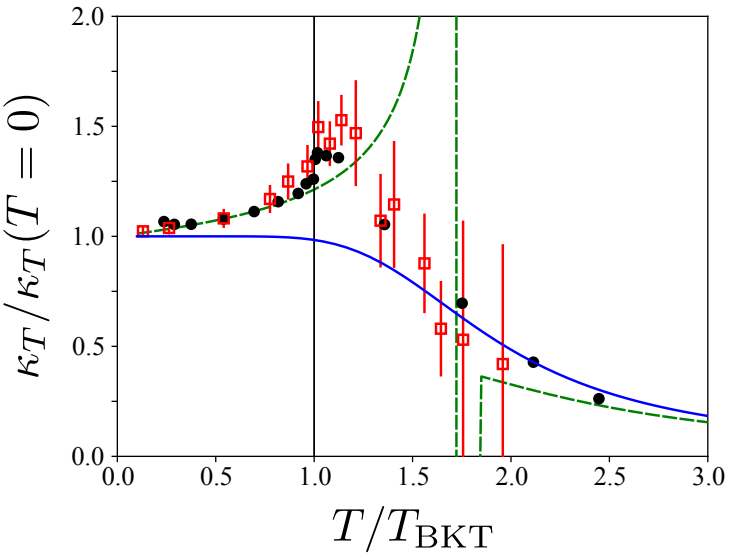

Figure 3.10: Isothermal compressibility evaluated for $\tilde{g} = 0.1$. The blue solid line is the prediction of the RPA theory, while the green dashed line is from the quasi-condensate Popov theory. The red square are predictions from the SPGPE (see main text) [21]. The black dots are from universal relations of Ref. [82].

this approach, the system is divided into two parts, corresponding to the low energy modes, and the high energy modes [54,113]. Owing to the macroscopic occupation of the lowest energy states, the former part can be described by a classical field Ψ, whereas the later part acts as a thermal reservoir of classical atoms. The key point in this approach is that the low energy (coherent) part does not only represent the condensate, but includes a finite number of excited states, up to an energy cutoff. Thus, unlike the ZNG formalism discussed in Sec. 1.3.3 which is based on the presence of a BEC, the SPGPE framework is well suited for the investigation of 2D Bose dynamics [53]. The SPGPE takes a similar form to the Gross-Pitaevskii equation (1.67), with additional thermal dissipation and stochastic fluctuation terms. The equilibrium state at a given temperature is obtained by solving the equation for different noise realizations, and then taking the average. As one can see in Fig. 3.10, although the SPGPE includes the effects of thermal fluctuations in an approximated scheme, it successfully reproduces the characteristic peak of the compressibility near the superfluid transition, in agreement with the UR results.

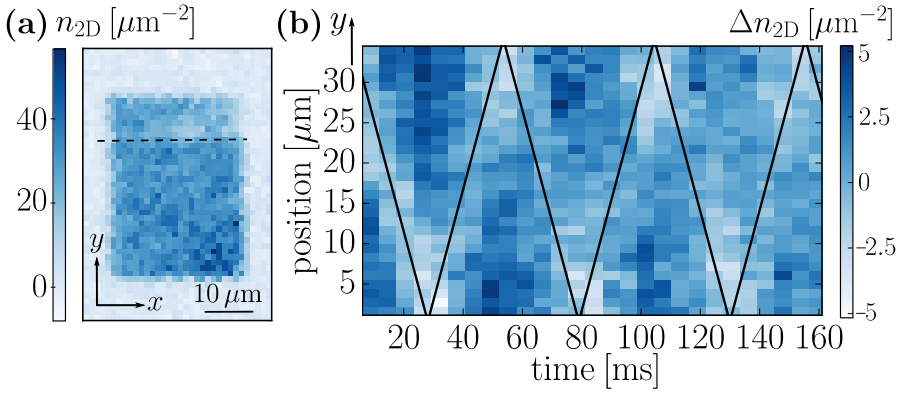

Figure 3.11: Experimental protocol for the excitation of sound wave in 2D Bose gas. (a) Initial density profile of the gas at $t = 0$, with a depleted density in the upper part induced by an external local potential. (b) Time evolution of the density depletion, after removing the external potential. From Ref. [17].

3.4.3 Comparison with the experiments

The velocity of sound as well as its damping rate can in principle be evaluated from the calculation of the pole of the response function Eq. (3.35). However, unlike the 3D case, this is a rather fastidious task (see Appendix D.2). Here, we therefore follow another approach, inspired by the experimental procedure.

Linear response analysis

The experiment of Ref. [17] consists to measure the motion of the gas when a density perturbation is applied (we remind that the initial aim of the experiment was to observe the BKT jump of the second sound, which for a weakly interacting 2D Bose gas is excited through a *density* perturbation, as we have shown in Sec. 3.3). A sketch of the experimental protocol is shown in Fig. 3.11. At $t = -\infty$ the gas in the box has a density depletion, induced by a potential step (panel (a)). This potential step is removed at $t = 0$, letting the density depletion to move freely. The sound velocity is then measured by tracking this density depletion (or equivalently the center of mass oscillation of the gas) in time (panel (b)), as it goes forth and back in the box.

For our calculation, we therefore consider the gas initially at equilibrium in the presence of a weak, spatially periodic, stationary potential, producing a sinusoidal density modulation with a given wave vector $\mathbf{q}$. Then, we investigate the response of the system when the potential is suddenly removed. Such perturbation

is described by the Hamiltonian

$$\begin{aligned}\hat{H}_{\rm pert} &= \lambda\hat{\rho}^\dagger_{\mathbf{q}}\theta(-t) + \text{h.c.} \\ &= \lambda\hat{\rho}^\dagger_{\mathbf{q}}\frac{i}{2\pi}\int_{-\infty}^{\infty} d\omega' \frac{e^{i\omega' t}}{\omega' + i\eta} + \text{h.c.},\end{aligned} \tag{3.50}$$

where in the last line we have used the Fourier transform of the step function. Then, following the same calculation as Sec. 1.3.2 starting from the Kubo formula Eq. (1.86), one obtains for the density response [114, 115]

$$\mathcal{F}(t) = \frac{1}{\pi n^2 \kappa_T}\int_{-\infty}^{\infty} \mathrm{d}\omega \frac{\chi''(k,\omega)}{\omega} e^{i\omega t}\,, \tag{3.51}$$

where we have normalized the signal to its $t = 0$ initial value, fixed by the isothermal compressibility. If the ratio $\chi''(k,\omega)/\omega$ exhibits a narrow peak, as happens at low temperature, then the oscillation will persist for a long time; if instead the same function is broad, then the oscillation is strongly damped. Hence the function $\mathcal{F}(t)$ provides direct information on the velocity of sound and on its damping. In the left panels of Fig. 3.12 we show some typical profile of the function $\chi''(k,\omega)/\omega$ calculated from Eq. (3.35), with $\tilde{g} = 0.16$, below and above the superfluid transition. The figure reveals the occurrence of a peak at $\omega \neq 0$, which is at the origin of a damped oscillatory behavior in the Fourier transform $\mathcal{F}(t)$, shown in the right panels. It is worth noticing on passing that the oscillatory behavior of the function $\mathcal{F}(t)$ is caused by the interaction term in the denominator of $\chi(k,\omega)$. In fact, in the ideal Bose gas ($g = 0$), the function $\chi''(k,\omega)/\omega$ has a peak at $\omega = 0$ and its Fourier transform (3.51) is a monotonously decreasing function (panel (d) in Fig. 3.12). Indeed, one can show that the imaginary part of the ideal gas response function can be written as a sum of Gaussian functions,

$$\chi''^0_{g=0}\left(u = \frac{\omega}{q}\sqrt{\frac{m}{2k_B T}}\right) = \frac{mu}{2\sqrt{\pi}\hbar^2}\sum_{l=1}^{\infty}\sqrt{l}e^{-l(u^2+\beta\Lambda)}\,, \tag{3.52}$$

thus its Fourier transform yields a sum of exponentially decaying functions.

The sound frequency $\tilde{\omega}$ and its damping rate Γ can be extracted from $\mathcal{F}(t)$ by using an appropriated fitting function. In our work, we chose

$$\mathcal{F}^{\rm DHO}(t) = e^{-\Gamma t/2}\left[\cos(\tilde{\omega}t) + \frac{\Gamma}{2\tilde{\omega}}\sin(\tilde{\omega}t)\right], \tag{3.53}$$

as a fitting function, corresponding to the response of a damped harmonic oscillator (see Appendix D.1). The fitting results are shown as red dashed lines in the right panels of Fig. 3.12.

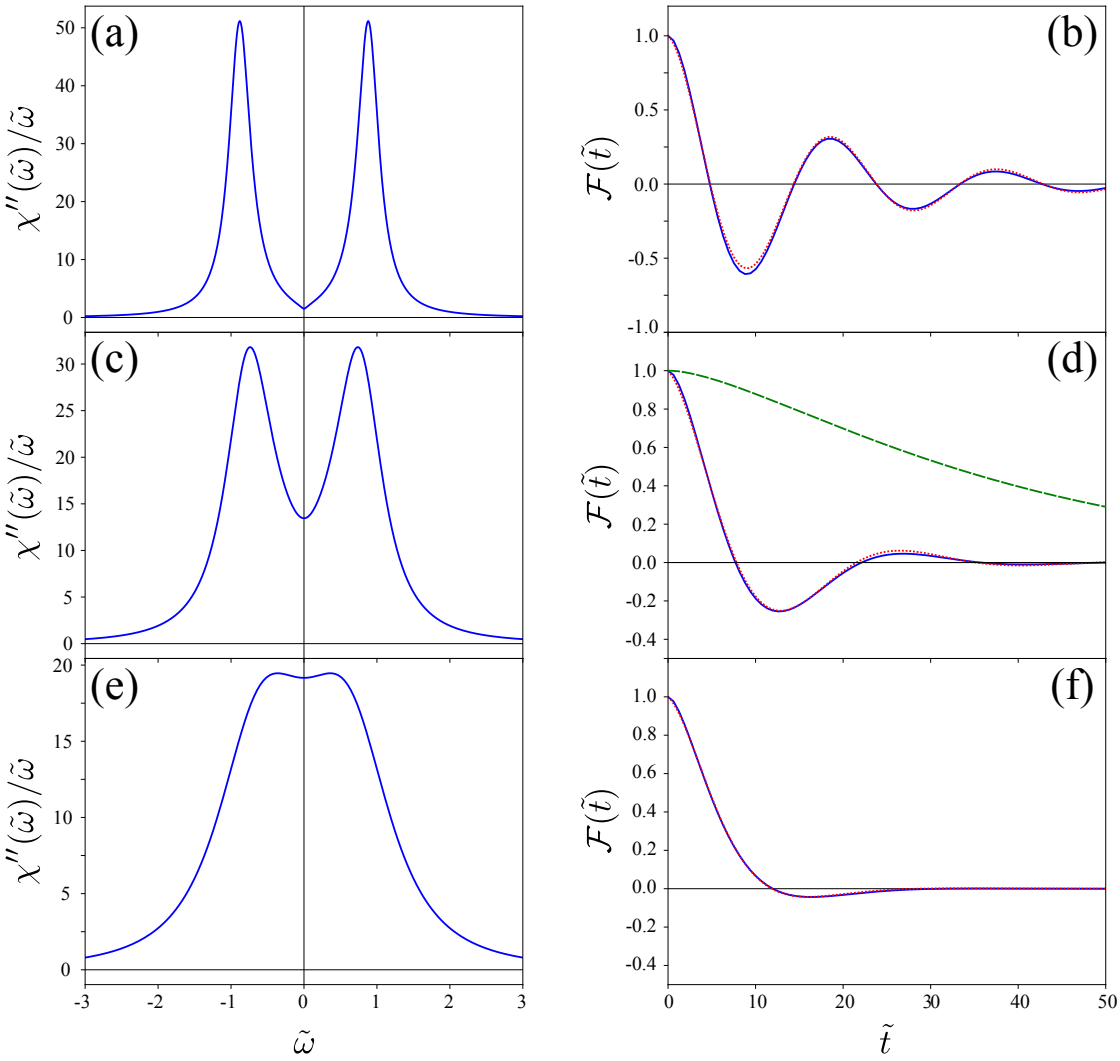

Figure 3.12: Left panels: Imaginary part of the inverse frequency weighted response function, $\chi''(\tilde{\omega})/\tilde{\omega}$, calculated in the RPA with $g = 0.16\hbar^2/m$, as a function of the dimensionless frequency $\tilde{\omega} = \omega/(k\sqrt{gn/m})$. Right panels: corresponding Fourier transform (3.51), as a function of the dimensionless time $\tilde{t} = kt\sqrt{2k_BT/m}$. The blue solid and green dashed lines correspond to the interacting and ideal gas, respectively. The red dotted line is the fit based on Eq. (3.53). From top to bottom: $T = 0.7T_{\rm BKT}, 1.2T_{\rm BKT}$ and $1.8T_{\rm BKT}$.

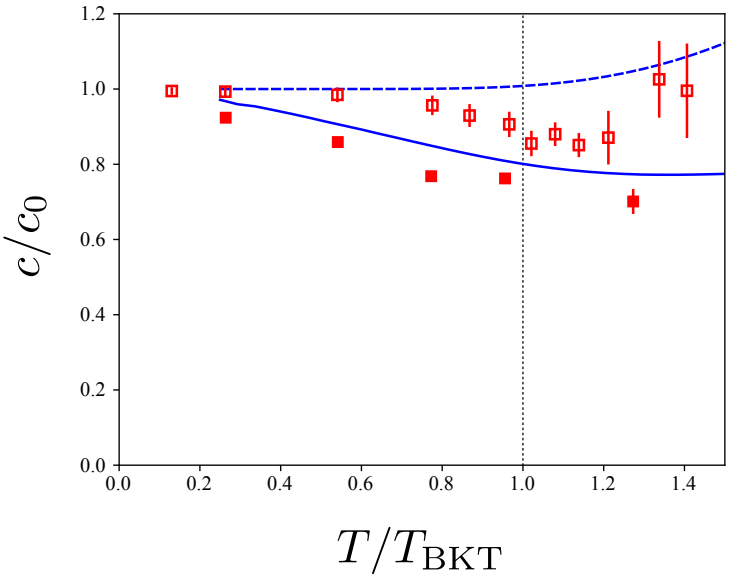

Figure 3.13: Sound velocity in units of $c_0 = \sqrt{gn/m}$, calculated for $g = 0.1\hbar^2/m$. The blue solid line is the sound velocity $c = \tilde{\omega}/k$ extracted from the Fourier transform Eq. (3.51) of χ''/ω calculated in RPA, while the blue dashed line is the isothermal sound velocity $c_T = \sqrt{1/(mn\kappa_T)}$, within the same theory. Solid and open squares represent the sound speed extracted from real time simulations and the isothermal sound velocity, respectively, both obtained with SPGPE [21].

Results

The velocity c extracted from $\mathcal{F}(t)$ is shown in Fig. 3.13 (solid line) as a function of T, in units of the zero temperature Bogoliubov sound velocity $c_0 = \sqrt{gn/m}$. We compare the extracted sound velocity with the prediction for the isothermal sound velocity $c_T = \sqrt{1/(mn\kappa_T)}$ determined by the isothermal compressibility (dashed line). The two curves are found to be close to each other, while the adiabatic sound velocity $c_S = \sqrt{1/(mn\kappa_T)}$, which describes the propagation of sound in the collisional regime, is not shown in the figure, lying well above c_T ($c_S/c_T \sim 2$ near T_{BKT}). This behavior can be understood by using sum rule arguments. In fact, the ratio between the energy weighted and inverse energy weighted moments of the dynamic structure factor provides an estimate for the mean excitation energy [7]:

$$c \simeq \frac{1}{\hbar q}\sqrt{\frac{m_1}{m_{-1}}} = \sqrt{\frac{1}{mn\kappa_T}}\,, \tag{3.54}$$

which is found to be the isothermal sound velocity c_T. This sum rule prediction is expected to be accurate in the collisionless regime but not in the collisional

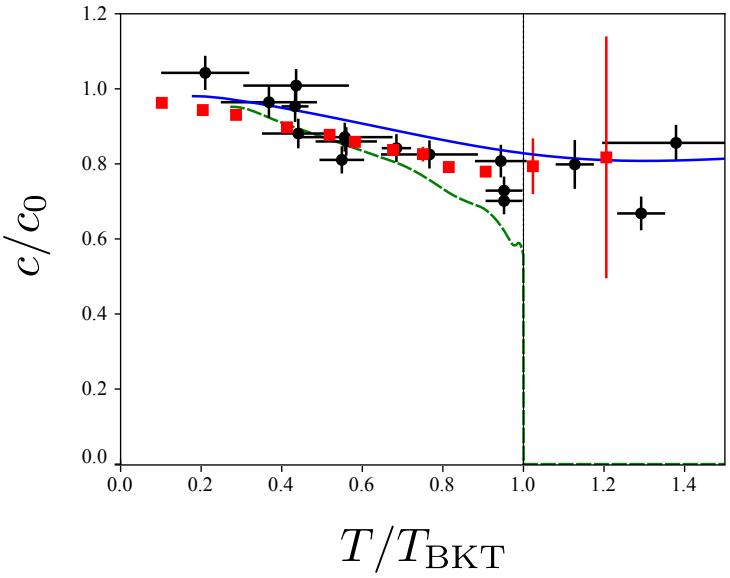

Figure 3.14: Sound velocity calculated for $g = 0.16\hbar^2/m$. Blue solid line: RPA; red squares: SGPE; The green dashed line is the second sound velocity predicted by Landau's two-fluid hydrodynamics of Sec. 3.3 and the black circles are the experimental data of Ref. [17].

regime, where the adiabatic sound does not exhaust the inverse energy weighted (compressibility) sum rule [88].

The propagation of sound can be also investigated using SPGPE. In SPGPE, the propagation of density waves has been simulated in [21] following the experimental procedure. Namely, an initial equilibrium state in presence of a static external perturbation is prepared, and then the real-time simulation is performed by removing suddenly the static perturbation and letting the system evolve [113]. The sound velocity is then extracted from the amplitude of the observed density oscillations, using Eq. (3.53) as a fitting function. We show the extracted sound speed as solid squares in Fig. 3.13. For the SPGPE too, the sound velocity is found to lie close to the isothermal compressibility sound (red open square), obtained from the equilibrium solution of SPGPE; Fig. 3.10.

In Fig. 3.14 we compare our results with the experimental observations of Ref. [17], and the predictions of SPGPE [21]. Below T_{BKT}, our predictions for the velocity of the collisionless sound are close to the ones for second sound based on Landau's two-fluid hydrodynamics (dashed green line). This is not surprising since, for a weakly interacting Bose gas at temperatures larger than gn/k_B, the velocity of second sound is well approximated by the expression (3.27) $\sqrt{(n_s/n)/(mn\kappa_T)}$

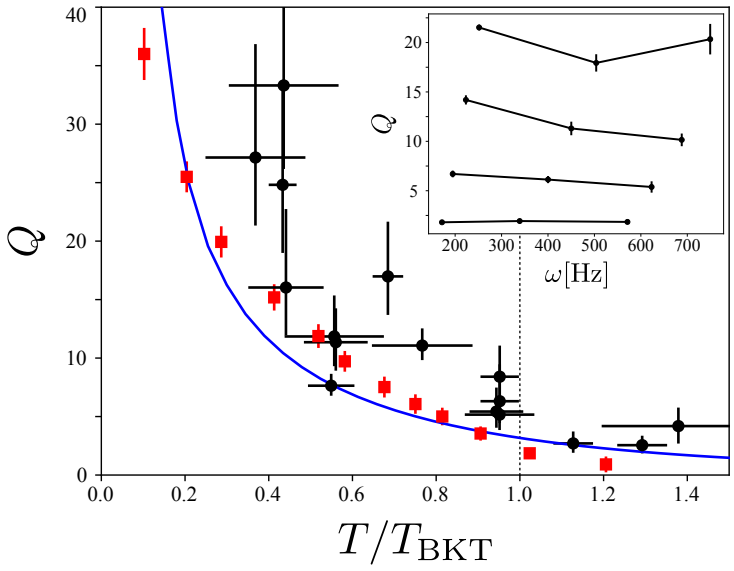

Figure 3.15: Quality factor $Q = 2\tilde{\omega}/\Gamma$. The blue solid line is Q evaluated from the Fourier transform $\mathcal{F}$ in RPA; black circles are experimental data [17]; red squares are the results of SGPE simulations. The inset shows Q as a function of frequency at different values of T from SGPE [21]; from top to bottom: $T/T_{\mathrm{BKT}} = 0.29,\ 0.52,\ 0.75,\ 1.02$. The error bars of the SGPE data in both panels represent the statistical deviations due to different noise realizations.

and differs from the isothermal velocity only by the multiplicative factor $\sqrt{n_s/n}$, which is fixed by the superfluid fraction and is ~ 0.7 near T_{BKT}. Conversely, neither our theoretical sound velocity nor the experimental one exhibit the jump to zero at T_{BKT}, which would be predicted by two-fluid hydrodynamics in the collisional regime.

Fig. 3.15 shows the quality factor $Q = 2\tilde{\omega}/\Gamma$. By increasing the temperature, Q decreases as the damping rate becomes quickly large. Above T_{BKT}, damping becomes so strong that the oscillatory behavior is hardly visible (see lowest panels Fig. 3.12). Again, there is an overall good agreement between theory and experiments. In RPA, the behavior of Q is the consequence of Landau damping, as we have alredady discussed for the 3D gas in Sec. 2.3.3. It corresponds to the coupling between the collective sound oscillation and the (thermally populated) single-particle excited states included in the ideal Bose gas response (3.35) [116]. The reason for which the quality factor in the experimental measurement is better than the theoretical prediction, can be understood as the experimental system being slightly hydrodynamic and thus reducing Landau damping. This is confirmed by the independence of Q on frequency, as shown in the inset of Fig. 3.15, cal-

culated in Ref. [21] using SPGPE. In fact, if damping were collisional, it would exhibit a quadratic increase with ω and hence a pronounced frequency dependence of the quality factor.

We briefly note that we have checked that the evaluation of the pole of the RPA response function (3.35) leads essentially to the same results for the sound speed and the damping rate (see Appendix D.2).

3.5 Probing the BKT jump in the second sound

To summarize, in this chapter we have investigated the propagation of sound wave, in both the hydrodynamic and collisionless regime. With respect to the 3D Bose gas, where the hydrodynamic and collisionless sounds have practically the same velocity, the situation in 2D is particularly interesting, since the hydrodynamic mode is expected to vanish at the superfluid phase transition temperature, while the collisionless one not. Regarding the observation of the BKT jump in the sound velocity, we are in a delicate situation where we need to find an "intermediate" region, in which interactions are strong enough to ensure hydrodynamics, but not too large to ensure the excitation of second sound from a density probe. From this point of view, the most interesting region for the experimental investigation would be around $\tilde{g} \simeq 0.7$, where the predicted compressibility sum rule amplitude $W_2/W_1 \simeq 1$ (see Fig. 3.7) is still large and hydrodynamic regime should be ensured from small sound velocity. Such value for the coupling constant has been already achieved in Cesium gases, by means of Feshbach resonance [67]. This situation is illustrated in Fig. 3.16, where we have calculated the response to a static density perturbation $\mathcal{F}(t)$, using the hydrodynamic response function Eq. (2.19). For $\tilde{g} = 0.7$ at intermediate temperature, one indeed finds that both sound modes contribute equally to the inverse energy-weighted sum rule, giving rise to a beating effect in the experimentally relevant total response. The observation of such beating would allow for the simultaneous measurement of first and second sounds, and further detect the BKT jump by observing the sudden vanishing of beatings at the critical point.

Another promising system for the observation of the BKT jump in the second sound velocity is the strongly interacting Fermi gas. While the universal relations do not allow us to study the crossover region of a 2D Fermi gas, we can stress from our results that the system in this region would be highly incompressible. This means that a density probe of the second sound is hopeless in the crossover region, and one should rather use a thermal perturbation as in the 3D unitary Fermi gas [103]. This observation also involves that one can safely use Eq. (3.26) for the evaluation of both sound velocities. A detailed study using many-body theories would be useful to confirm these predictions, and to further study the

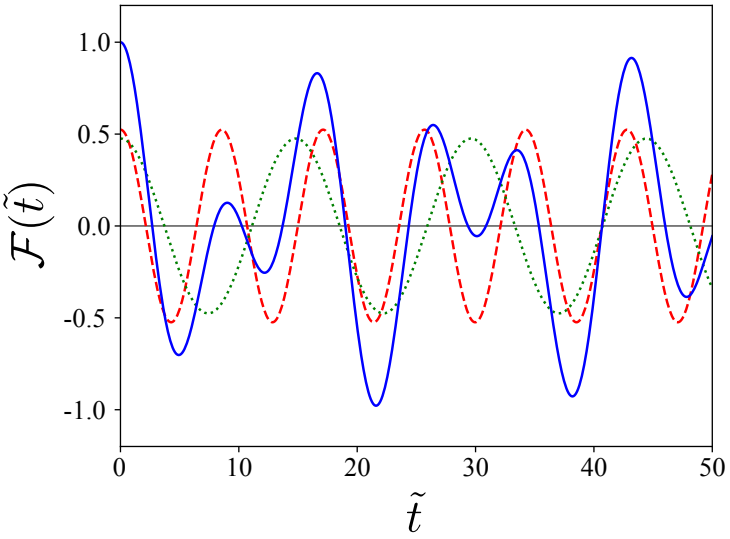

Figure 3.16: Density response $\mathcal{F}(t)$ of a strongly interacting Bose gas to a static perturbation, in the hydrodynamic regime, with $\tilde{g} = 0.7$ at $T = 0.8T_{\mathrm{BKT}}$. Blue solid line: total density response. Red dashed line: density response of the first sound mode. Green dotted line: density response of the second sound mode.

BCS region.

Chapter 4

Mixtures of 3D Bose gases at finite temperature

In this chapter, we investigate a mixture of two interacting superfluid Bose gases at finite-temperature, in 3D. We first develop the HF and Popov theories for the mixture, which are the generalizations of the single-component theories studied in Chap. 3. Although in the single-component gas the inclusion of the anomalous average in the Popov theory has no drastic effects in the behavior of thermodynamic quantities, one shall see that in the case of binary BECs, their inclusion is crucial. In particular, we study the miscibility of the mixture, and assess what are the conditions to observe the phase-separation of the two components at finite temperature.

4.1 Theory of Binary Bose-Einstein condensates

4.1.1 Binary BECs at zero temperature

The miscibility of liquids and gases, and in particular its temperature dependence, is a topic of high relevance in the study of classical fluids [117]. For quantum mixtures, this question was addressed long time ago in the context of ^{3}He-^{4}He liquids [118], and more recently for mixtures of quantum gases [7,27]. In particular, weakly interacting binary Bose gases occupying two different hyperfine states are the simplest, yet interesting example of quantum mixtures, for which the problem of miscibility has been intensively investigated, both experimentally [18, 119–122] and theoretically [123–134].

At zero-temperature, the miscibility criterion is obtained starting from the Gross-Pitaevskii energy functional of Sec. 1.2.4, adapted to the mixtures: [7, 123–

126, 128]

$$E = \int d^3\mathbf{r} \left[\frac{\hbar^2}{2m_1}|\nabla\Psi_1|^2 + \frac{\hbar^2}{2m_2}|\nabla\Psi_2|^2 + V_{1,\mathrm{ext}}|\Psi_1|^2 + V_{2,\mathrm{ext}}|\Psi_2|^2 + \frac{1}{2}g_{11}|\Psi_1|^2 + \frac{1}{2}g_{22}|\Psi_2|^2 + g_{12}|\Psi_1|^2|\Psi_2|^2 \right] , \tag{4.1}$$

where $\Psi_1(\mathbf{r})$ and $\Psi_2(\mathbf{r})$ are the order parameters for the respective component of the mixture, with mass m_1 and m_2, each of them being under an external potential $V_{1,\mathrm{ext}}(\mathbf{r})$ and $V_{2,\mathrm{ext}}(\mathbf{r})$. The interaction between identical atoms is modeled through the intra-atomic couping constant $g_{11} = 4\pi\hbar^2 a_{11}/m_1$ and $g_{22} = 4\pi\hbar^2 a_{22}/m_2$, whereas the interaction between different atomic species is given by the inter-atomic coupling constant $g_{12} = 4\pi\hbar^2 a_{11}/m_R$, with $m_R = 2m_1m_2/(m_1+m_2)$ the relative mass. In the simplest case where the atoms are confined in a box, one can calculate the energy in the miscible and phase-separated configurations straightforwardly. In the miscible case where all the atoms occupy the volume V of the box, one finds,

$$E_{\mathrm{mis}} = \frac{g_{11}}{2V}N_1^2 + \frac{g_{11}}{2V}N_2^2 + \frac{g_{12}}{V}N_1N_2 \, , \tag{4.2}$$

with N_1 and N_2 the number of atoms in the component 1 and 2, respectively. For the phase-separated case one instead finds,

$$E_{\mathrm{ps}} = \frac{g_{11}}{2V_1}N_1^2 + \frac{g_{22}}{2V_2}N_2^2 \, , \tag{4.3}$$

with V_1 and V_2 the volume occupied by the respective component. In the phase-separated state, the pressure between the two gases has to be the same (mechanical equilibrium), $\partial E_{\mathrm{ps}}/\partial V_1 = \partial E_{\mathrm{ps}}/\partial V_2$ implying the relationship $g_{11}(N_1/V_1)^2 = g_{22}(N_2/V_2)^2$. Consequently,

$$E_{\mathrm{ps}} = \frac{g_{11}}{2V}N_1^2 + \frac{g_{11}}{2V}N_2^2 + \frac{\sqrt{g_{11}g_{22}}}{V}N_1N_2 \, . \tag{4.4}$$

Thus, comparing Eqs. (4.2) and (4.3), the miscible state is energetically stable with respect to the phase-separated state as long as the following inequality holds:

$$g_{12} \leq \sqrt{g_{11}g_{22}} \, . \tag{4.5}$$

This criterion has been verified experimentally, for instance in the Rubidium mixtures, where the transition from the miscible to the phase-separated state has been observed by tuning the intra-atomic [119] or inter-atomic [121] coupling constant, using the Feshbach resonance.

4.1.2 Binary BECs at finite temperature

At finite temperature, theoretical studies have mainly focused on harmonically trapped systems, by means of the Hartree-Fock [127, 133, 134], Zaremba-Nikuni-Griffin [131] and Hartree-Fock-Bogoliubov [129, 130, 132] theories. Although they differ in the treatment of the intra-species interaction, all the above approaches treat the inter-species coupling at the mean-field level, thereby providing an inaccurate description of the thermal fluctuations associated with the spin degree of freedom. As one shall see, it is in fact crucial for the discussion of the miscibility to derive a finite-temperature theory, which properly includes the effects of thermal and quantum fluctuations in both the density and spin channels. In order to illustrate this point, we develop in this section two different approaches: the HF theory on one hand, and the Popov theory on the other hand.

In what follows, we consider the simplest symmetric configuration, in which the masses, as well as the intra-atomic coupling constants of the two components are the same: $m_1 = m_2 = M$ and $g_{11} = g_{22} = g$.

Hartree-Fock theory

The HF theory for the mixtures is obtained by starting from the two-components Hamiltonian:

$$\begin{aligned}\hat{H} = \sum_{i=1,2} \left\{ \sum_{\mathbf{k}} \varepsilon_{\mathbf{k}} \hat{a}^\dagger_{i,\mathbf{k}} \hat{a}_{i,\mathbf{k}} + \frac{g}{2V} \sum_{\mathbf{k},\mathbf{k}',\mathbf{q}} \hat{a}^\dagger_{i,\mathbf{k}} \hat{a}^\dagger_{i,\mathbf{k}'+\mathbf{q}} \hat{a}_{i,\mathbf{k}'} \hat{a}_{i,\mathbf{k}+\mathbf{q}} \right\} \\ + \frac{g_{12}}{V} \sum_{\mathbf{k},\mathbf{k}',\mathbf{q}} \hat{a}^\dagger_{1,\mathbf{k}} \hat{a}_{1,\mathbf{k}+\mathbf{q}} \hat{a}^\dagger_{2,\mathbf{k}'+\mathbf{q}} \hat{a}_{2,\mathbf{k}'} \,, \end{aligned} \tag{4.6}$$

and proceeding in the same way as the single-component case, Sec. 2.1.1. After the Bogoliubov ansatz of Sec. 1.2.3 followed by the mean-field assumption (2.1), one finds for the HF grand-canonical Hamiltonian

$$\hat{K}^{\mathrm{HF}} = \Omega_0^{\mathrm{HF}} + \sum_{i=1,2} \sum_{\mathbf{k}\neq 0} \left(\varepsilon_{\mathbf{k}} + 2gn_i + g_{12} n_{3-i} - \mu_i^{\mathrm{HF}} \right) \hat{a}^\dagger_{i,\mathbf{k}} \hat{a}_{i,\mathbf{k}} \,, \tag{4.7}$$

with Ω_0^{HF} given by

$$\Omega_0^{\mathrm{HF}} = \sum_{i=1,2} \left\{ \frac{g}{2V} N_{i,0}^2 - \frac{g}{V} \tilde{N}_i^2 - \mu_i^{\mathrm{HF}} N_{i,0} + \frac{g_{12}}{V} N_{1,0} N_{2,0} - \frac{g_{12}}{V} \tilde{N}_1 \tilde{N}_2 \right\} \,, \tag{4.8}$$

where $N_{i,0}$ and $\tilde{N}_i$ are the number of atoms in the condensed and normal phase for the i^{th} component, respectively. The grand-canonical energy is found by taking

the trace of the grand partition function:

$$\Omega^{\mathrm{HF}} = \Omega_0^{\mathrm{HF}} + \frac{1}{\beta}\sum_{i=1,2} \ln\left(1 - e^{-\beta(\varepsilon_{\mathbf{k}} + 2gn_i + g_{12}n_j - \mu_i^{\mathrm{HF}})}\right) . \tag{4.9}$$

As for the chemical potential in the condensed phase, it is given by the saddle-point equation $\partial\Omega/\partial n_{i,0} = 0$:

$$\mu_i^{\mathrm{HF}} = g(n_i + \tilde{n}_i^{\mathrm{HF}}) + g_{12}n_{3-i} \tag{4.10}$$

where the thermal atoms density is given by the Bose special function, $\tilde{n}_i^{\mathrm{HF}} = g_{3/2}(z_i)/\lambda_T^3$, with the fugacity $z_i = e^{-\beta g n_{i,0}}$. When a given component is in the normal phase, one instead has $\mu_i^{\mathrm{HF}} = \mu_i^{\mathrm{IBG}} + 2gn_i + g_{12}n_{3-i}$, with μ_i^{IBG} the ideal gas chemical potential. Finally, we verify that when taking the derivative of Ω^{HF} (4.9) with respect to μ_i^{HF}, one correctly finds the number density n_i.

Popov theory

As explicitly shown in Eq. (4.9), the HF theory accounts for the inter-species interaction only to the lowest order, linear in g_{12}. Indeed, Ω^{HF} is simply given by the sum of the single-component thermodynamic potential in each component Eq. (2.3), with additional mean-field terms $g_{12}(N_{1,0}N_{2,0} + \tilde{N}_1\tilde{N}_2)/V$, linear in g_{12} (the fugacity, as well as the thermal atoms density depend only on the intra-atomic coupling constant g). In order to include the effects of spin fluctuations, we develop the Popov theory for the mixtures of two condensates, starting from a model Hamiltonian which treats in a consistent way both inter and intra-species interactions. The associated grand-canonical Hamiltonian $\hat{K}$ can be diagonalized by means of Bogoliubov transformations, as well as proper renormalizations of the coupling constants [135]. The derivation follows closely the one of the HF theory, and is given in Appendix A.2. The grand-canonical Hamiltonian is found to be:

$$\hat{K} = \Omega_0 + \sum_{\mathrm{k}\neq 0}\left(E_{\mathbf{k}}^{+}\hat{\alpha}_{\mathbf{k}}^{\dagger}\hat{\alpha}_{\mathbf{k}} + E_{\mathbf{k}}^{-}\hat{\beta}_{\mathbf{k}}^{\dagger}\hat{\beta}_{\mathbf{k}}\right) , \tag{4.11}$$

where $\hat{\alpha}_{\mathbf{k}}^{\dagger}$ and $\hat{\beta}_{\mathbf{k}}^{\dagger}$ are, respectively, the creation operators for the quasiparticles in the density and spin channels obeying Bose statistics, and Ω_0 is the thermodynamic potential of the vacuum of these quasiparticles (see Eq. (A.37) in the Appendix). The excitation spectrum of the system reads $E_{\mathbf{k}}^{\pm} = \sqrt{\varepsilon_{\mathbf{k}}^2 + 2\Lambda_{\pm}\varepsilon_{\mathbf{k}}}$ where,

$$\Lambda_{\pm} = \frac{1}{2}\left(gn_0 \pm \sqrt{(g^2 - g_{12}^2)m_0^2 + g_{12}^2 n_0^2}\right) , \tag{4.12}$$

are the Bogoliubov sound velocities, with $n_0 = n_{1,0}^0 + n_{2,0}^0$ and $m_0 = n_{1,0}^0 - n_{2,0}^0$, where $n_{i,0}^0 = n_i - n_T^0$ is the condensate density evaluated to the lowest order

in the interaction. The thermodynamic potential is therefore given by $\Omega = \beta^{-1} \ln\left(\mathrm{Tr} e^{-\beta \hat{K}}\right)$:

$$\Omega = \Omega_0 + \frac{1}{\beta} \sum_{\pm} \sum_{\mathbf{k}} \ln\left(1 - e^{-\beta E^{\pm}_{\mathbf{k}}}\right) \tag{4.13}$$

In this expression, the thermal contribution of single-particles in the HF theory (4.9) has been replaced by that of quasiparticles. The chemical potential is evaluated from the saddle point equation $\partial\Omega/\partial n_{i,0}$ in a perturbative way, and is found to be (see Appendix A.2)

$$\mu_1 = g(n_1 + n_T^0) + g_{12} n_2 + g \sum_{\pm} \left(\frac{M\Lambda_{\pm}}{2\pi\hbar^2}\right)^{3/2} H_{\pm}(\tau_{\pm}, l) \quad (1 \leftrightarrow 2) \tag{4.14}$$

where the dimensionless function on the reduced temperature $\tau_{\pm} = k_B T/\Lambda_{\pm}$ and parameter $l = n^0_{2,0}/n^0_{1,0}$ is given by

$$\begin{aligned} H_{\pm}(\tau_{\pm}, l) = & \frac{1}{\sqrt{\pi}} \left\{ \frac{4\sqrt{2}}{3} \left(1 \pm \frac{1 + (2\bar{g}^2 - 1)l}{\sqrt{(1-l)^2 + 4\bar{g}^2 l}}\right) \right. \\ & \left. + \tau_{\pm} \int_0^{\infty} dx f(x) \left[\frac{(u_{\pm} - 1)^{3/2}}{u_{\pm}} \left(1 \pm \frac{1 + (2\bar{g}^2 - 1)l}{\sqrt{(1-l)^2 + 4\bar{g}^2 l}}\right) - \sqrt{\tau_{\pm} x} \right] \right\}, \end{aligned} \tag{4.15}$$

with $\bar{g} = g_{12}/g$.

4.2 Magnetic phase transition in binary BECs

We now investigate the miscibility of a uniform bosonic mixture at finite temperature, and consider the situation in which the inter-species interaction is close to, but still smaller than the intra-species value ($0 < \delta g = g - g_{12} \ll g$). Such configuration is found for instance in mixtures of ^{23}Na atoms occupying the hyperfine states $|F = 1, m_F = \pm 1\rangle$, where one has $\delta g/g = 0.07$ [136, 137].

4.2.1 Dynamical instability

The onset of a phase separation induced by a dynamical instability can be conveniently assessed if one calculates the susceptibilities of the system. Indeed, the miscible state is found to be dynamically stable against density and spin fluctua-

tions if the compressibility matrix is positive [84, 138]:

$$\frac{\partial \mu_1}{\partial n_1} \geq 0\,, \quad \frac{\partial \mu_2}{\partial n_2} \geq 0\,, \tag{4.16}$$

$$\frac{\partial \mu_1}{\partial n_1}\frac{\partial \mu_2}{\partial n_2} - \frac{\partial \mu_1}{\partial n_2}\frac{\partial \mu_2}{\partial n_1} \geq 0\,. \tag{4.17}$$

The first equation defines the positiveness of the single-component compressibility. In fact, it is sufficient for only one of the two conditions in Eq. (4.16) to be satisfied, since the other one is automatically verified when the inequality in Eq. (4.17) holds. In the situation where the atomic density in each component is equal ($n_1 = n_2$), these two conditions are equivalent to the following inequalities:

$$n^2 \kappa_T = \left(\frac{\partial \mu}{\partial n}\right)_T^{-1} \geq 0\,, \tag{4.18}$$

$$n^2 \sigma_T = \left(\frac{\partial h}{\partial m}\right)_T^{-1} \geq 0\,, \tag{4.19}$$

where we have introduced the total chemical potential $\mu = (\mu_1 + \mu_2)/2$ and total atoms density $n = n_1 + n_2$, as well as the chemical potential imbalance $h = (\mu_1 - \mu_2)/2$ and the magnetization density $m = n_1 - n_2$. Equation (4.18) defines the isothermal compressibility $\kappa_T = [\partial^2(F/V)/\partial n^2|_T]^{-1}$ of the mixture, while Eq. (4.19) the isothermal spin susceptibility $\sigma_T = [\partial^2(F/V)/\partial m^2|_{T,m=0}]^{-1}$.

At zero temperature, $\mu_1 = g n_1 + g_{12} n_2$ at the mean-field level (4.10), and one verifies that Eqs. (4.18) and (4.19) yield $n^2 \kappa_T(\sigma_T) = 2/(g \pm g_{12})$, so that phase separation occurs for $g \leq g_{12}$, as discussed in Sec. 4.1.1. For example, in the case of a mixture of ^{23}Na atoms, one has $\delta g/g = 0.07$ yielding an increase of a factor ~ 14 of the $T = 0$ value of the spin polarizability with respect to the value obtained in the absence of interspecies interactions. The huge increase of the spin susceptibility has been recently demonstrated experimentally in the case of a harmonically trapped mixture of sodium atoms [136, 137].

In Fig. 4.1 we report the HF and Popov calculations for the isothermal compressibility and the spin susceptibility, in the case of the sodium mixture discussed above, in the unpolarized configuration $n_1 = n_2 = n/2$. In that case, both components condense at the same critical temperature $k_B T_{\rm BEC} = 2\pi\hbar^2/M[n/2\zeta(3/2)]^{2/3}$. Comparing the compressibility of the mixture in panel (a) together with Fig. 2.5 for that of a single-component gas, one can see that both have a similar trend, without a significant difference between the HF and Popov theory. However as shown in panel (b), we find that the spin susceptibility predicted by the Popov theory deviates strongly from the HF calculation. Remarkably, the susceptibility predicted by the HF theory shown in panel (b) exhibits a divergent behavior

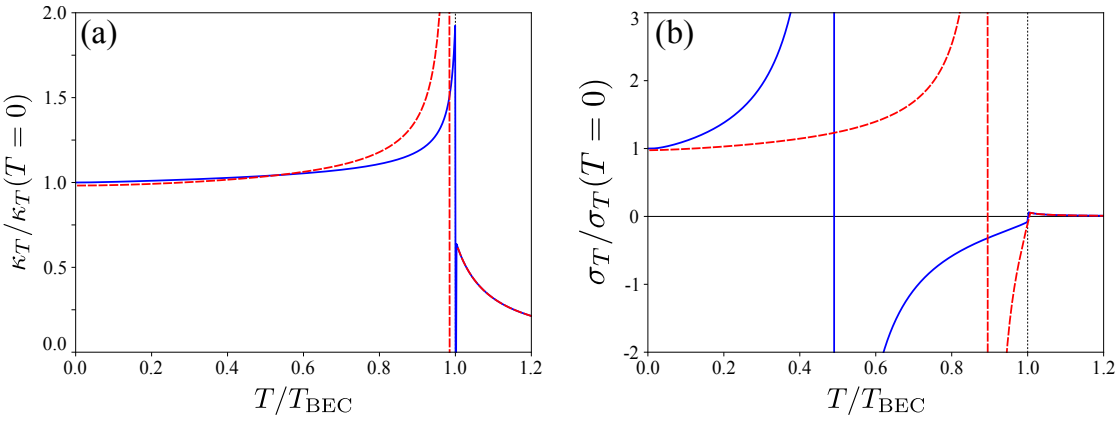

Figure 4.1: (a) Isothermal compressibility (4.18) and (b) spin susceptibility (4.19) for a binary mixture of Bose gases, with interaction parameters $gn/(k_B T_{\rm BEC}) = 0.1$ and $\delta g/g = 0.07$. The blue solid and the red dashed lines are the predictions of HF theory (Eq. (4.10)) and Popov theory (Eq. (4.14)), respectively. Both quantities are normalized to the mean-field $T = 0$ values, $\kappa_T(\sigma_T)(T = 0) = 2/(g \pm g_{12})$.

at $T \simeq 0.5 T_{\rm BEC}$, therefore signaling the onset of a magnetic dynamic instability. The origin of this instability can be understood if one writes the analytical expression for the spin susceptibility, obtained from Eq. (4.19) together with the high-temperature approximation for the HF chemical potential (see Eq. (2.8)):

$$2\left(\sigma_T^{\rm HF}\right)^{-1} \simeq \delta g - g^{3/2}\frac{\sqrt{\pi}}{\lambda_T^3}\sqrt{\frac{\beta}{n_0^0}}\,. \tag{4.20}$$

The onset of the dynamical instability in the HF description is due to the last $g^{3/2}$-term in Eq. (4.20), arising from interaction driven thermal fluctuations. As the temperature increases, beyond mean-field effects are enhanced, eventually leading to a divergent behavior of $\sigma_T^{\rm HF}$ at finite temperature. It is worth noticing that the spin susceptibility in the HF theory can also be written in the form [1]:

$$\sigma_T^{\rm HF} = \frac{2\kappa_T^{\rm sc}}{1 - g_{12}\kappa_T^{\rm sc}}\,, \tag{4.21}$$

with $\kappa_T^{\rm sc}$ the isothermal compressibility for a single-component HF gas, given by Eq. (2.46). The above expression explicitly indicates that the temperature dependence of the spin susceptibility is fully contained in the single-component property $\kappa_T^{\rm sc}$. Thus, one concludes that the divergent behavior of the susceptibility

[1] This is easily verified if one notices that the chemical potential difference in the HF theory can be written as $\mu_1 - \mu_2 = \mu_1^{\rm sc} - \mu_2^{\rm sc} - g_{12}(n_1 - n_2)$, with $\mu_i^{\rm sc}$ the chemical potential in a single-component gas.

in the HF framework arises from the enhancement of the single-component compressibility with the temperature, which in turn comes from both exchange effect and interaction-induced thermal fluctuations (see the discussion made after Eq. (2.46)). The situation is somewhat analogous to that of quantum droplets, where the Lee-Huang-Yang correction to the zero-temperature chemical potential is responsible for the stabilization of collapsing Bose mixtures [139]. While the LHY term originates from quantum fluctuations, the last term in Eq. (4.20) arises from interaction driven thermal fluctuations.

This last analogy motivates us to properly evaluate the interplay between thermal and quantum fluctuations in the mixture. Both fluctuations are properly taken into account in the Popov theory, and the analytical expression for the spin susceptibility can be calculated in a similar fashion to the HF approach (see Eq. (A.25)). We find:

$$2\left(\sigma_T\right)^{-1} \simeq \delta g - g^{3/2}\frac{\delta g}{g_{12}}\frac{2\sqrt{\pi}}{\lambda_T^3}\sqrt{\frac{\beta}{n_0}}\left[\left(1+\frac{g_{12}}{g}\right)^{3/2} - \left(1+\frac{g_{12}}{g}\right)\sqrt{\frac{\delta g}{g}}\right] . \quad (4.22)$$

In contrast to the HF prediction Eq. (4.20), the Popov approach gives rise to terms proportional to δg also for the beyond mean-field terms (second term in the right-hand side of Eq. (4.22)). A careful analysis of the grand-canonical Hamiltonian in Eq. (4.11) reveals that the emergence of such beyond mean-field terms in g_{12} is due to the correct treatment of the two-component anomalous densities $\langle \hat{a}_i^\dagger \hat{a}_j \rangle_{i\neq j}$ and $\langle \hat{a}_i \hat{a}_j \rangle_{i\neq j}$. These anomalous averages are natural extensions of the single component anomalous density $\langle \hat{a}_i \hat{a}_i \rangle$ of Bogoliubov theory [135], and are the consequences of the presence of Bose-Eistein condensation in both components (see Appendix A.2). The inclusion of such terms in the grand-canonical Hamiltonian Eq. (4.11) is crucial to provide a proper description of both spin and density fluctuations. It is worth noticing that besides the well-known solution $\delta g = 0$, Eq. (4.22) possesses a second root, leading to a dynamical instability at finite temperature even if $\delta g > 0$. In Fig. 4.1(b) the divergence of σ_T is found to occur at $T \sim 0.9 T_{\mathrm{BEC}}$. However at this temperature the system is already phase-separated, as we discuss in the next section.

4.2.2 Energetic instability

In the previous section, we have established the region where the mixed binary configuration is dynamically stable. We now turn to the investigation of a possible energetic instability, associated with the emergence of an energetically favorable phase separated state. Let us consider an unpolarized Bose mixture, miscible at zero temperature ($\delta g > 0$). Since we consider a uniform system, the mixture is prone to separate into two domains $(\mathcal{A}, \mathcal{B})$ of equal volume $V/2$, conserving the

total density $n^{\mathcal{A}} = n^{\mathcal{B}} = n$, but with opposite magnetization $m^{\mathcal{A}} = -m^{\mathcal{B}} = m$. For the investigation of energetic instability, one needs therefore to calculate the free energy, as a function of the magnetization m. This is achieved by evaluating the free energy using the thermodynamic relation $F = \Omega + \sum_i \mu_i N_i$, together with the Popov expression for Ω (4.13). At a given temperature $T \leq T_{\mathrm{BEC}}$, two situations emerge, depending on the value of m:

1. $m \leq n - 2\frac{\zeta(3/2)}{\lambda_T^3}$

   Both components are in the condensed phase. The free energy is therefore given by:

$$\begin{aligned}\frac{F}{V} =& \frac{g}{2}\left(n_1^2 + n_2^2\right) + g_{12} n_1 n_2 + \left(\frac{M}{2\pi\hbar^2}\right)^{3/2} \frac{4}{15\sqrt{\pi}} \sum_{\pm} \left(2\Lambda_{\pm}\right)^{5/2} \\ &+ g\frac{\zeta(3/2)^2}{\lambda_T^6} + \frac{1}{\beta V} \sum_{\pm} \sum_{\mathbf{k}} \ln\left(1 - e^{-\beta E_{\mathbf{k}}^{\pm}}\right) . \end{aligned} \tag{4.23}$$

2. $m > n - 2\frac{\zeta(3/2)}{\lambda_T^3}$

   In that case, the density of the minority component is smaller than the critical density for the BEC to occur. Consequently, only the majority component has a condensate component and one finds:

$$\begin{aligned}\frac{F}{V} =& \frac{g}{2}\left(n_1^2 + 2n_2^2 + \frac{\zeta(3/2)^2}{\lambda_T^6}\right) + g_{12} n_1 n_2 + \mu_2^{\mathrm{IBG}} n_2 \\ &+ \left(\frac{M}{2\pi\hbar^2}\right)^{3/2} \frac{4}{15\sqrt{\pi}} \left(2g n_{1,0}^0\right)^{5/2} + \frac{1}{\beta V} \sum_{\mathbf{k}} \ln\left(1 - e^{-\beta E_{\mathbf{k}}}\right) \\ &+ \frac{1}{\beta V} \sum_{\mathbf{k}} \ln\left(1 - e^{-\beta(\varepsilon_{\mathbf{k}} - \mu_2^{\mathrm{IBG}})}\right) , \end{aligned} \tag{4.24}$$

   where we chose n_2 to be the minority component in the normal phase. The ideal Bose gas chemical potential μ_2^{IBG} is defined through the relationship $n_2 = g_{3/2}(e^{\beta\mu_2^{\mathrm{IBG}}})/\lambda_T^3$, with $g_p(z)$ the Bose special function. As for the majority component in the condensed phase, it is now described by the quasi-particle energy $E_{\mathbf{k}} = \sqrt{\varepsilon_{\mathbf{k}}^2 + 2\varepsilon_{\mathbf{k}} g n_{1,0}^0}$.

Actually, the two phase-separated domains are in equilibrium when both the pressure ($P^{\mathcal{A}} = P^{\mathcal{B}}$) and the chemical potential ($\mu_i^{\mathcal{A}} = \mu_i^{\mathcal{B}}$) equilibrium conditions are satisfied. While the equilibrium condition for the pressure is automatically satisfied for the symmetric configuration considered here, the chemical potential

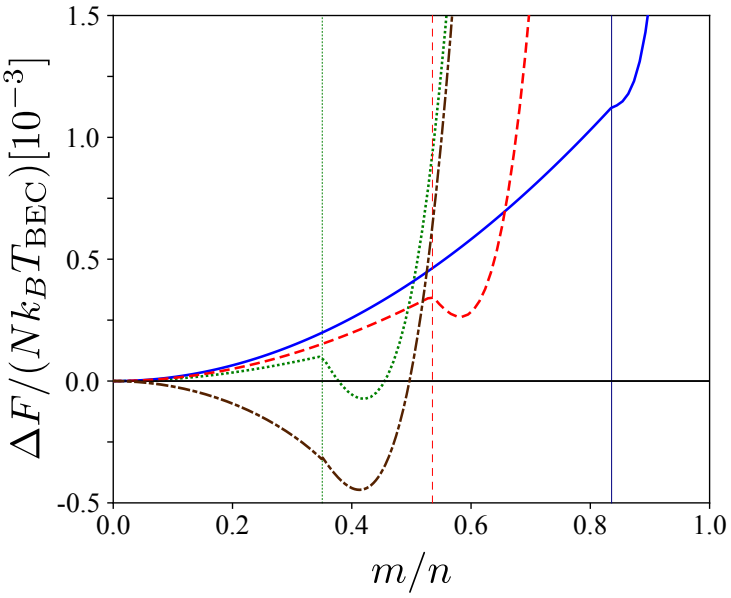

Figure 4.2: Difference of free energies between the miscible state ($m = 0$) and the phase-separated state described in the main text, calculated within the Popov theory for $gn/(k_BT_{\rm BEC}) = 0.1$ and $\delta g/g = 0.07$. Blue solid line: $T < T^*$, red dashed line: $T^* < T < T_M$, green dotted line $T > T_M$. The brown dotted-dashed line is the HF theory result for $T > T_M$. The vertical lines indicate the critical magnetization $m = n - 2\zeta(3/2)/\lambda_T^3$ above which the minority component is purely thermal.

equilibrium is found to be fulfilled only if, in each domain one of the two components is in the normal phase, therefore corresponding to the case 2 discussed above.

Figure 4.2 shows the calculated free energy as a function of the magnetization density, for different values of temperature. At low temperature, the free energy is a monotonously increasing function (see blue solid line), with a unique minimum at zero magnetization, corresponding to the mixed state. At a given temperature hereafter called T^*, a second minimum starts to develop in the region where the minority component is purely thermal, $m > n - 2\zeta(3/2)/\lambda_T^3$ (red dashed line). As already stressed, the emergence of such metastable state corresponds to the fulfillment of the chemical potential equilibrium between the two domains. An analytical expression for the temperature T^* can be obtained from Eq. (4.24), by employing the high temperature $k_BT \gg gn$ expansion for the Bose distribution

function (see Appendix A.2):

$$\frac{T^*}{T_{\rm BEC}} \simeq \frac{\delta g}{g}\frac{\zeta(3/2)}{\sqrt{2\pi}}\sqrt{\frac{T_{\rm BEC}}{gn}}\,. \tag{4.25}$$

By further increasing the temperature, the energy of the metastable state decreases, eventually reaching the same energy as the unpolarized state, therefore signaling the onset of a first order phase transition. Hereafter we use the notation T_M to denote this magnetic phase transition temperature, above which the mixed state is energetically unstable with respect to the phase separated state (green dotted line in Fig. 4.2). The new equilibrium phase predicted by Popov theory is hence characterized by a full space separation of the Bose-Einstein condensed components of the two atomic species, their thermal components remaining instead mixed, with a finite magnetization. The phase-separation is sketched in Fig. 4.3. We briefly note that HF theory predicts a similar behavior for the free energy, but with a dynamical instability, associated to the divergence of the spin susceptibility (4.20). This is shown as the brown dashed-dotted line in Fig. 4.2, where the curvature of the free energy becomes negative at high enough temperature.

So far, we have restricted our discussion to mixtures satisfying the miscibility criterion at zero-temperature: $g_{12} \leq g$. However, the above free energy analysis suggests that a similar phase-separation mechanism can take place even when the gas is initially phase-separated. Indeed, let us consider the situation in which $g_{12} > g$. Then, the spin susceptibility Eq. (4.22) as well as the square of the spin sound speed Eq. (4.12) is negative, implying a complex Bogoliubov excitation spectrum in the long wave-length limit. These are signatures of dynamical instability, with the occurrence of a phase-separation. Now, in the particular case discussed so far, where the two condensates are phase-separated, the spin channel in the Bogoliubov excitation (4.12) vanishes, and the system is well described by Eq. (4.24), regardless the values of g and g_{12}. In Fig. 4.4 we show the behavior of the free energy as a function of the magnetization density, for $\delta g/g = -0.07$, at $T = 0.6T_{\rm BEC}$. We find that for any small but finite temperature, a minimum of the free energy appears at $m < n$. Although one can not evaluate the energy in the region where $m < n - 2\zeta(3/2)/\lambda_T^3$ (shaded region in Fig. 4.4) because of the complex excitation spectrum, we expect that a complete phase-separation of the two gases ($m = n$) is made possible only at zero-temperature, and any small but finite temperature is responsible for the mixing of the non-condensed parts.

To summarize, we show in Fig. 4.5 the phase diagram of the two-component Bose mixture, by plotting the characteristic temperature T^*, providing the onset of a minimum in the free energy with $m \neq 0$, and the phase transition temperature T_M, as a function of $\delta g/g$. For the sodium mixture where $\delta g/g = 0.07$, we find that the phase-separated state appears as a metastable state at $T^* = 0.36T_{\rm BEC}$, while

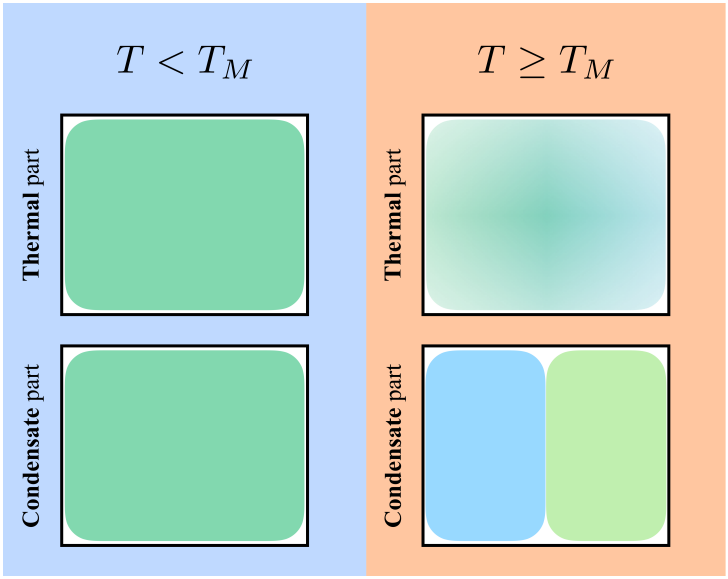

Figure 4.3: Sketch of the temperature driven phase-separation. Below the magnetic transition temperature $T < T_M$ (left panels), the mixture is perfectly miscible. As one crosses the transition point, $T \geq T_M$ (right panel), the thermal atoms have a finite magnetization ($m \neq 0$), whereas the condensate parts are fully separated.

the phase transition occurs at $T_M = 0.71 T_{\mathrm{BEC}}$. We briefly note that as $\delta g/g \to 0$, T^* tends to a finite value ($\simeq 0.1 T_{\mathrm{BEC}}$), as a consequence of quantum fluctuations, in contrast to Eq. (4.25) which only holds if $T^* \gg gn/k_B$. We also find that the phase separated state disappears slightly above the critical temperature T_{BEC}. At this temperature, the mixture becomes again miscible with both components in the normal phase. In the regime where $\delta g < 0$, we have verified that the mixture might be phase-separated in the absence of T_{BEC} too, provided that $g_{12} \gg g$.

4.2.3 Effects of spatial inhomogeneity in trapped BECs

So far, we have always been considering the homogeneous mixture in a uniform potential. However, for the experimental purpose, it is important to assess how the physics of phase-separation is modified in the presence of a confining trap. This can be conveniently assessed if we work in the grand-canonical ensemble, and recall the local density approximation (LDA) [4, 63]. For fixed chemical potentials (μ_1, μ_2), four possible configurations arise, according to our previous discussion:

1. BEC1-BEC2: both components are in the BEC phase.

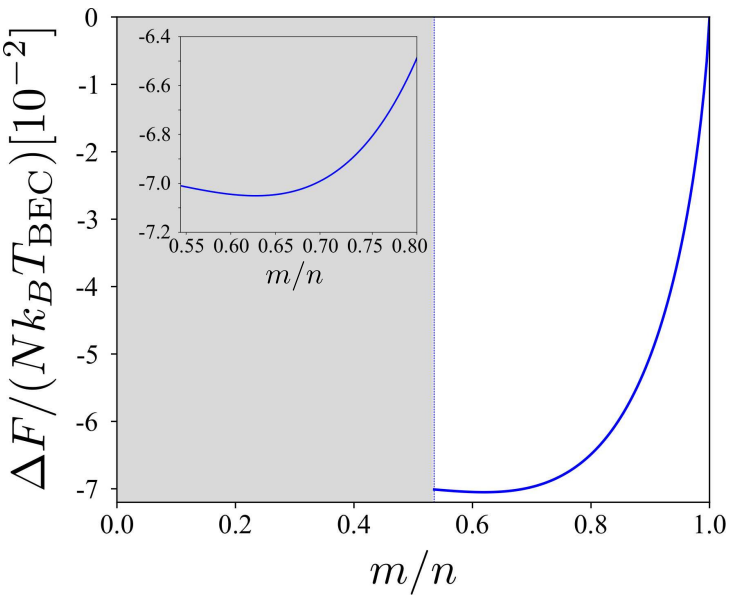

Figure 4.4: Difference of free energies between the immiscible state ($m = n$) and the phase-separated state described in the main text, for $gn/(k_BT_{\rm BEC}) = 0.1$ and $\delta g/g = -0.07$, calculated at $T = 0.6T_{\rm BEC}$. The gray shaded region $m < n - 2\zeta(3/2)/\lambda_T^3$ corresponds to the region in which the system is dynamically instable, with a complex single-particle spectrum. Inset: emphasis on the minimum of free energy.

2. N1-N2: both components are in the normal phase.

3. BEC1-N2: component 1 is in the majority and in the BEC phase, while component 2 is in the minority and in the normal phase.

4. BEC2-N1: component 2 is in the majority and in the BEC phase, while component 1 is in the minority and in the normal phase.

In Fig. 4.6, we show the grand-canonical phase diagram for the symmetric mixture, as a function of the chemical potentials, obtained by comparing the thermodynamic energy Ω/V of these four configurations, and looking for the energetically favorable state. The diagram is calculated using the Popov theory, for a fixed value of temperature $gn_T^0/(k_BT) = 0.05$ and $\delta g/g = 0.07$.

Within the LDA, the inhomogeneous gas is described as a set of locally homogeneous subsystems, with local chemical potential [140]:

$$\mu_i(\mathbf{r}) = \mu_i - V_{{\rm ext},i}(\mathbf{r}) \tag{4.26}$$

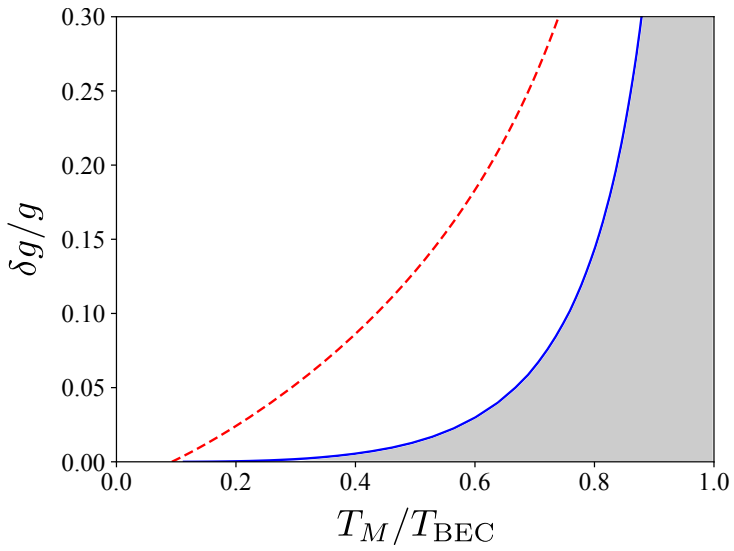

Figure 4.5: Phase diagram for binary condensates with $gn/(k_B T_{\mathrm{BEC}}) = 0.1$. The blue solid and the red dashed lines are the phase transition temperature T_M, and characteristic temperature T^*, respectively. The gray area corresponds to the regime of phase-separation.

For a harmonic trap, $V_{\mathrm{ext},i}(\mathbf{r}) = m_i\omega_i^2 r^2/2$, and in the symmetric case where both components feel the same external potential, the density profile in the trap will follow the linear curve $\mu_1 = \mu_2 - (\mu_1^0 - \mu_2^0)$ in the phase diagram, with $\mu_i^0 = \mu_i(r = 0)$. Looking closely to Fig. 4.6, one finds that the mixture is miscible at every position of the trap for $\mu_1^0 = \mu_2^0$ only, and an imbalance in the chemical potentials leads inevitably to the appearance of a region in which the two BECs do not coexist. We briefly note that a similar phase diagram has been obtained within the HF framework in Ref. [134], although predicting the existence of a tricritical point, arising from the divergence of the magnetic susceptibility.

4.3 Sound propagation in binary BECs

The propagation of sound waves in a mixture can be investigated in a similar way to the single-component gas. For the hydrodynamic sounds, we need to generalize the two-fluid equation (1.82) to the case of mixtures, by considering the normal fluid and the superfluid in each atomic component. Such derivation has been achieved for the particular case of liquid He in Ref. [141], and symmetric Bose-Bose mixtures in Ref. [130]. The development of a more general hydrodynamic equation for the binary superfluid mixture is under progress, and will be discussed

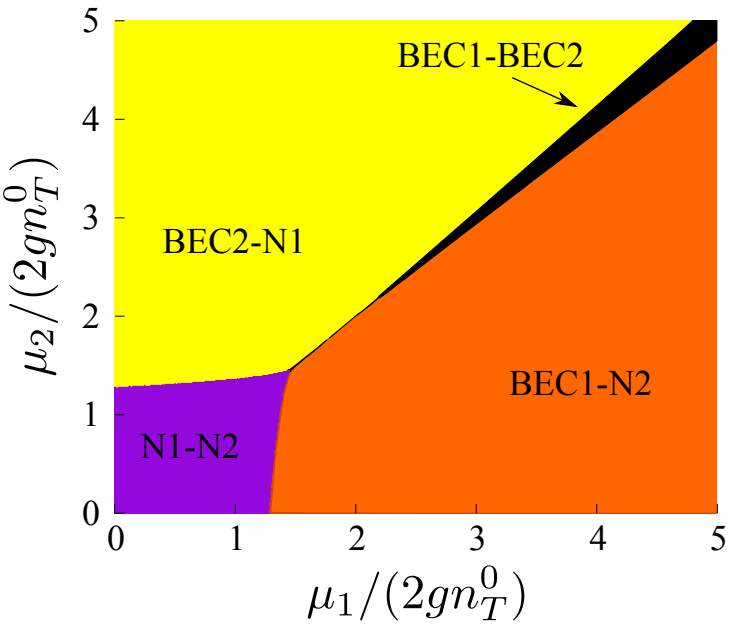

Figure 4.6: Grand-canonical phase diagram for binary condensates, with $gn_T^0/(k_BT) = 0.05$ and $\delta g/g = 0.07$. For the description of the different phases, see main text.

in a future publication.

In the collisionless regime instead, the RPA formalism we have been using so far is not applicable, since this approach is equivalent to the HF theory, which predicts an erroneous divergence of the spin susceptibility. For instance, from the study made in Sec. 3.4.3, one expects for the collisionless sounds in the mixture to be well described by the sum-rule result Eq. (3.54). In particular, the spin sound velocity is expected to be directly related to the magnetic susceptibility as

$$c_s \simeq \sqrt{\frac{1}{mn\sigma_T}}\,. \tag{4.27}$$

The proper description of spin fluctuations through the inclusion of the anomalous densities is therefore crucial, and one needs to develop a beyond-HF dynamic approach [5, 77].

Conclusion

In this thesis, we investigated the propagation of sound waves in dilute Bose gases, in a variety of configurations. In particular, we worked on the three-dimensional Bose gas (Chap. 2), and the two-dimensional Bose gas (Chap. 3). We further discussed the finite-temperature properties of the three-dimensional Bose-Bose mixtures (Chap. 4).

In the first chapter, we showed that the physics of sound wave is closely related to the phenomenon of superfluidity, this connection being the central motivation in investigating sound dynamics in ultracold atomic systems. After introducing some basic concepts about Bose-Einstein condensation, we reviewed the theoretical frameworks needed for the calculation of sound waves velocities. These concern the two-fluid hydrodynamic theory of Landau, which gives rise to the phenomenon of second sound, and the linear response theory, suitable for describing collisionless sound.

These theories were used in Chap. 2, to investigate sound waves in a weakly interacting 3D Bose gas, both in the hydrodynamic and the collisionless regimes. For this purpose, we derived the Hartree-Fock theory for the dilute Bose gas at finite temperature. Although the problem of sound propagation in 3D is well-known in the literature, this case-study permitted us to have an insight on the nature of the sound waves. In particular, we showed that the second sound and the collisionless mode have similar temperature dependence of their velocity, and correspond essentially to an oscillation of the condensate component.

The Chap. 3 is devoted to the propagation of sound waves in 2D. After briefly reviewing the general physics of Berezinskii-Kosterlitz-Thouless phase transition, we have introduced the universal thermodynamics for the critical region near the phase transition. Although low-dimensional systems are known to exhibit strong thermal fluctuations, quasi-condensate mean-field theories were found to give qualitatively correct results for the interested thermodynamic quantities in the superfluid regime, when compared to the universal description of Prokof'ev and Svistunov [82]. Combining the mean-field theory together with the universal approach, we provided a systematic investigation of the behavior of the second sound in a 2D interacting Bose gas, exploring the transition from the weakly interacting limit to

the regime characterized by larger values of the 2D coupling constant. We pointed out the crucial role played by the thermal expansion coefficient, which not only governs the density or entropy nature of the sound waves, but also characterize the BKT jump of sound speeds.

Motivated by the recent experiment by the group of Collège de France in Paris [17], we further studied the propagation of sound wave in a uniform 2D Bose gas, in the absence of collisions. While hydrodynamic (second) sound and collisionless sound velocities do not exhibit major difference in the 3D case, our study revealed that the collisionless sound in 2D differs drastically from the hydrodynamic one, possessing a finite velocity both below and above the BKT transition. Our result is in close agreement with the measurement of Paris, and we further interpreted the observed damping of the sound mode as arising from Landau damping mechanism.

In the final chapter of this thesis, we studied the binary mixture of weakly interacting Bose gases. We developed a beyond mean-field Popov theory for the binary condensates, which properly include the effects of thermal and quantum fluctuations in both the density and spin channels. We underlined the important role played by the two-component anomalous densities, which give rise to a profound change in the thermodynamic properties of the mixtures. In particular, we found that the inclusion of spin fluctuations enables to cure the divergent behavior of the spin susceptibility, predicted by Hartree-Fock theory. Detailed analysis of the free energy further showed the existence of a first-order phase transition from a miscible state to a polarized state, driven by interaction induced thermal fluctuations.

Future perspectives

We conclude this thesis by making some remarks about the possible future perspectives. First, for the problem of sound propagation, the experiment by the group of Collège de France [17], and our complementary theoretical work, have shed light on the physics of collisionless sound. An important issue is the crossover between the collisionless and collisional regimes. For instance, it is not clear how the observed collisionless mode would evolve to the hydrodynamic sounds as one increases the collisional rate. The RPA analysis made in Sec. 2.3.3 indicates that the response function (2.48) possesses in fact two poles, the second one arising from the response of thermal atoms. Clarifying this point might allow for a better understanding about the evolution of the sound modes in the crossover. On the other hand, it seems that reaching the hydrodynamic regime in dilute Bose gases is experimentally challenging, thus motivating the investigation of strongly interacting systems.

As for the mixtures, the magnetic phase transition we have discussed has revealed the important interplay between thermal and beyond mean-field effects.

The methodology we have developed for the derivation of the Popov theory in App. A can be applied to other systems, such as the coherently coupled BECs [142,143], or dipolar Bose gases [31,144]. Recently, these systems have been realized experimentally, and have gathered much attraction from the community, for the richness of their phase diagrams, presenting exotic phases [145–147]. However, few works have been devoted to the finite temperature description [148,149], and a better understanding about the role played by the thermal fluctuations is needed. Finally, the magnetic phase transition discussed in this thesis has never been observed experimentally, the main reason being the inhomogeneity of the trapped systems. Recently, box-like potentials providing uniform trapping have become available for both Bose [58] and Fermi [150] gases. Thus, the experimental possibility of observing the predicted magnetic phase transition is a realistic option. Important open issues concern the propagation of sound in these polarized domains, the possible emergence of a similar magnetic phase transition in two dimensions, and the structure of the interface between different domains.

Appendix A

Popov theory for 3D dilute Bose gases

We develop in this appendix the Popov theory [102, §6], a finite-temperature generalization of the Bogoliubov theory discussed in Sec. 1.2.3. This approach is based on a perturbative treatment of the grand canonical potential to second order in the interaction coupling constant, and properly includes beyond mean-field quantum and thermal fluctuations.

A.1 Single-component Bose gas

A.1.1 Formalism

Grand canonical Hamiltonian

For the derivation of the Popov theory, we essentially follow the same procedure as the HF theory, developed in Sec. 2.1.1, by applying the mean-field approximation (2.1) to the single-component Hamiltonian (1.48). However, different from the HF approach, we keep in the Popov theory the terms in the Hamiltonian in which the creation and annihilations operators appear by pairs ("Bogoliubov" terms). Thus, applying the Bogoliubov prescription and the mean-field approximation, one obtains for the grand canonical Hamiltonian $\hat{K} = \hat{H} - \mu\hat{N}$:

$$\begin{aligned}\hat{K} =& \frac{g}{2V}N_0^2 - \frac{g}{V}\tilde{N}^2 - \mu N_0 + \sum_{\mathbf{k}\neq 0}\left(\varepsilon_{\mathbf{k}} + 2gn - \mu\right)\hat{a}_{\mathbf{k}}^\dagger\hat{a}_{\mathbf{k}} \\ &+ \frac{g}{2V}N_0\sum_{\mathbf{k}\neq 0}\left(\hat{a}_{\mathbf{k}}^\dagger\hat{a}_{-\mathbf{k}}^\dagger + \hat{a}_{\mathbf{k}}\hat{a}_{-\mathbf{k}}\right), \end{aligned} \tag{A.1}$$

with $\tilde{N} = \sum_{\mathbf{k}\neq 0} n_{\mathbf{k}}$ the number of non-condensed atoms. In obtaining Eq. (A.1), we have further neglected the cubic products of non-condensate operators, as well

as terms like $g\tilde{m}\hat{a}^\dagger_{\mathbf{k}}\hat{a}^\dagger_{-\mathbf{k}}$ and $g\tilde{m}^2$, where $\tilde{m} = V^{-1}\sum_{\mathbf{k}}\langle\hat{a}_{\mathbf{k}}\hat{a}_{-\mathbf{k}}\rangle$ is the anomalous density. As one shall see below, the leading order of the anomalous density is of order g, and these terms correspond therefore to beyond-second order contributions. We briefly note that these terms are included in the Hartree-Fock-Bogoliubov (HFB) theory [77, 135], making a key difference with the actual approach. Like for the Bogoliubov theory at zero temperature in Sec. 1.2.3, the last term of Eq. (A.1) is of order g^2, leading to the problem of ultraviolet divergence. This issue arising from the approximated treatment of inter-atomic interactions is again solved by a renormalization of the coupling constant: $g \to g(1 + g/V\sum_{\mathbf{k}} m/(\hbar k)^2)$.

Equation (A.1) has the same structure as the Bogoliubov Hamiltonian (1.48) and can be diagonalized in exactly the same way, by means of Bogoliubov transformation Eq. (1.52). Then, one finds that the off-diagonal terms vanish for the following values of coefficients $u_{\mathbf{k}}$ and $v_{\mathbf{k}}$:

$$u_{\mathbf{k}}, v_{-\mathbf{k}} = \pm\left(\frac{\varepsilon_{\mathbf{k}} + \Lambda}{2\tilde{E}_{\mathbf{k}}} \pm \frac{1}{2}\right)^{1/2}, \tag{A.2}$$

where we have introduced the effective chemical potential $\Lambda = |\mu - 2gn|$ for future convenience [151], and $\tilde{E}_{\mathbf{k}} = \sqrt{(\varepsilon_{\mathbf{k}} + \Lambda)^2 - (gn_0)^2}$ is the Bogoliubov quasi-particle spectrum. By means of Eq. (A.2), the Hamiltonian (A.1) reduces to an effective Hamiltonian describing a gas of non-interacting quasi-particles:

$$\hat{K} = \Omega_0 + \sum_{\mathbf{k}\neq 0}\tilde{E}_{\mathbf{k}}\hat{\alpha}^\dagger_{\mathbf{k}}\hat{\alpha}_{\mathbf{k}}\,, \tag{A.3}$$

with Ω_0 the thermodynamic potential of the vacuum of quasi-particles:

$$\Omega_0 = g\frac{N_0^2}{2V} - g\frac{\tilde{N}^2}{V} - \mu N_0 + \frac{1}{2}\sum_{\mathbf{k}\neq 0}\left(\tilde{E}_{\mathbf{k}} - \varepsilon_{\mathbf{k}} - \Lambda + \frac{m}{\hbar^2}\frac{(gn_0)^2}{k^2}\right). \tag{A.4}$$

The thermodynamic potential is obtained according to $\Omega = \frac{1}{\beta}\ln Z$, where $Z = \mathrm{Tr}(e^{-\beta\hat{K}})$ is the grand partition function. The trace is taken over all the quasi-particles states and one finds:

$$\Omega = \Omega_0 + \frac{1}{\beta}\sum_{\mathbf{k}}\ln\left(1 - e^{-\beta\tilde{E}_{\mathbf{k}}}\right). \tag{A.5}$$

Finally, it is worth noticing that in terms of $u_{\mathbf{k}}$ and $v_{\mathbf{k}}$, the non-condensate and anomalous densities are expressed as:

$$\tilde{n} = \frac{1}{V}\sum_{\mathbf{k}}(u^2_{\mathbf{k}} + v^2_{-\mathbf{k}})f(\tilde{E}_{\mathbf{k}}) + v^2_{-\mathbf{k}}\,, \tag{A.6}$$

$$\tilde{m} = \frac{1}{V}\sum_{\mathbf{k}} 2u_{\mathbf{k}}v^*_{-\mathbf{k}}f(\tilde{E}_{\mathbf{k}}) + u_{\mathbf{k}}v^*_{-\mathbf{k}}\,, \tag{A.7}$$

where $f(E) = (e^{\beta E} - 1)^{-1}$ is the Bose distribution function.

Chemical potential

Let us now calculate the chemical potential. This is achieved from the saddle point equation $\partial\Omega/\partial n_0|_{\tilde{n},T,\mu} = 0$, which provides the following result:

$$\mu = gn_0 + \frac{1}{2}\sum_{\mathbf{k}} \left\{ \frac{1}{\tilde{E}_{\mathbf{k}}} \left[2g(\varepsilon_{\mathbf{k}} + \Lambda) - g^2 n_0\right] (2f(\tilde{E}_{\mathbf{k}}) + 1) - 2g + \frac{g^2 n_0}{\varepsilon_{\mathbf{k}}} \right\} . \quad \text{(A.8)}$$

In principle, the above equation has to be solved self-consistently together with Eq. (A.6) for the non-condensed density. However, such procedure is known to exhibit an unphysical gap in the quasi-particle energy [135]. In this work, we follow the methodology of Ref. [5] and solve perturbatively the coupled equations. This allows us to avoid the problem of the gap and provides the correct chemical potential to order g^2. To the lowest order in the interaction ($\mathcal{O}(1)$), Eq. (A.6) yields for the non-condensate density the ideal Bose gas thermal atoms density, $n_T^0 = \zeta(3/2)/\lambda_T^3$. As for the chemical potential, the leading contribution is instead linear in g, and one finds from Eq. (A.8) that $\mu^0 = gn_0 + 2gn_T^0 = gn + gn_T^0$. Consequently, $\Lambda^0 = gn_0^0 = g(n - n_T^0)$, and one finds that the Bogoliubov spectrum is gapless to the lowest order:

$$E_{\mathbf{k}} = \sqrt{\varepsilon_{\mathbf{k}}^2 + 2\Lambda\varepsilon_{\mathbf{k}}} . \quad \text{(A.9)}$$

In the above equation, as well as in what follows, we omit the superscript 0. Inserting this expression in Eq. (A.6), one finds the subleading order correction for the non-condensed density to be

$$\tilde{n} = n_T^0 + \left(\frac{m\Lambda}{2\pi\hbar^2}\right)^{3/2} G(\tau) \quad \text{(A.10)}$$

with $G(\tau)$ a dimensionless function, depending on the reduced temperature $\tau = k_B T/\Lambda$, according to

$$G(\tau) = \frac{2}{\sqrt{\pi}} \left\{ \frac{\sqrt{2}}{3} + \tau \int_0^\infty dx f(x) \left(\sqrt{u-1} - \sqrt{\tau x}\right) \right\} . \quad \text{(A.11)}$$

with $u = \sqrt{1 + (\tau x)^2}$. The subleading order term in μ is calculated from Eq. (A.8) by replacing $\tilde{E}_{\mathbf{k}} \to E_{\mathbf{k}}$ and $gn_0 \to \Lambda$ in the beyond mean-field terms:

$$\mu = gn + gn_T^0 + g\left(\frac{m\Lambda}{2\pi\hbar^2}\right)^{3/2} H(\tau) , \quad \text{(A.12)}$$

with the dimensionless function defined as:

$$H(\tau) = \frac{2}{\sqrt{\pi}} \left\{ \frac{4\sqrt{2}}{3} + \tau \int_0^\infty dx f(x) \left(\frac{(u-1)^{3/2}}{u} - \sqrt{\tau x} \right) \right\} , \quad \text{(A.13)}$$

where we have used Eq. (A.10) to express n_0 as a function of Λ. These equations give the exact second order expression for the chemical potential, as a function of the total density n and temperature T, when one uses $\Lambda^0 = g(n - n_T^0)$. This result was first derived by Popov [102, §6] in the high-temperature regime (Eq. (A.25) below), and the same expression (A.12) was derived in Refs. [152] and [133] within the finite-temperature extension of the Beliaev diagrammatic techniques, as well as in Ref. [5] starting from the time-dependent HFB equations. In this thesis, we therefore refer this approach to the Popov theory.

As we have already noticed, the quasi-particle spectrum of Eq. (A.9) is gapless in the long wavelength limit, therefore fulfilling the Goldstone theorem, stating that the spontaneous breaking of continuous symmetry must be associated to the existence of a long wave-length gapless mode [153]. This is in sharp contrast with the HFB approach, which is known to exhibit an unphysical gap due to an inconsistency in second order. As a matter of fact, the HFB Hamiltonian contains additional terms, given by

$$\hat{K}^{\mathrm{HFB}} = \hat{K}^{\mathrm{Popov}} - \frac{g}{2} V \tilde{m}^2 + \frac{g}{2} \tilde{m} \sum_{\mathbf{k} \neq 0} \left(\hat{a}_{\mathbf{k}}^\dagger \hat{a}_{-\mathbf{k}}^\dagger + \hat{a}_{\mathbf{k}} \hat{a}_{-\mathbf{k}} \right) . \tag{A.14}$$

Clearly, the last term of Eq. (A.14) will be responsible for the modification of the Bogolibov spectrum according to

$$E^{\mathrm{HFB}} = \sqrt{(\varepsilon_{\mathbf{k}} + \Lambda) - g(n_0 + \tilde{m})} \,, \tag{A.15}$$

making it gapped in the long wavelength limit, and that even when the densities are evaluated to the lowest order. An improvement of the Bogoliubov spectrum can therefore be obtained only if one properly considers all the second-order diagrams in the self-energy [133]. We also stress that though the anomalous density does not explicitly appear in the Hamiltonian Eq. (A.1), our theory is formally different from the HFB-Popov approximation [133,135]. The key point in our approach is to take the derivative of the thermodynamic potential with respect to the condensate density, *before* assuming the gapless spectrum (Hugenholtz-Pines theorem [154]). The difference between the two approaches will be clarified hereafter.

Equation (A.12) can also be solved self-consistently by using $\Lambda = |\mu - 2gn|$ in the beyond mean-field terms. Although such procedure would allow for the calculation of higher order corrections, the validity of these new terms are questionable. Indeed, Eq. (A.9) assumes $\Lambda = gn_0$ to hold, which is formally true only when Λ and gn_0 are evaluated to the lowest order, while it is an approximation when next order contributions are included. Solving Eq. (A.12) self-consistently is therefore an *ad-hoc* procedure in which we have assumed a gapless spectrum (A.9) [135]. In the following, we will refer to the *second-order* Popov theory, when the lowest-order expression Λ^0 is used, and to the *self-consistent* Popov theory, if Eq. (A.12)

is solved with $\Lambda = |\mu - 2gn|$. From this point of view, choosing Λ or gn_0 as the perturbation parameter is only a matter of convenience, since it gives the same second order results and their difference arises only for (*a priori* non-reliable) higher order terms [151]. In this work, we have chosen Λ since, by construction, it has the same beyond linear order corrections as the chemical potential (for $\mu = \mu^0 + \delta\mu$, then, $\Lambda = \Lambda^0 - \delta\mu$). As we shall see below, this correspondence provides the correct low-temperature expansion of the chemical potential and the correct lowest order expression for the free energy. The beyond mean-field theory developed in this thesis is therefore valid as far as the following inequalities are satisfied:

$$1 \gg \frac{\Lambda}{k_B T_{\mathrm{BEC}}} \gg (na^3)^{2/3}\,, \tag{A.16}$$

with $k_B T_{\mathrm{BEC}} = 2\pi\hbar^2/m\,[n/\zeta(3/2)]^{2/3}$ the BEC critical temperature for a non-interacting Bose gas. The first inequality in Eq. (A.16) involves the smallness of the perturbation parameter, whereas the second inequality arises from perturbation theory, and ensures the corrections to thermodynamics due to critical fluctuations occurring around the phase transition to be small [7]. We verify that our approach fails in describing the region in the close vicinity of the BEC transition, where $\Lambda \to 0$.

Finally, the anomalous density can be evaluated from Eq. (A.7) using the gapless spectrum:

$$\tilde{m} = -\frac{1}{V}\sum_{\mathbf{k}} \frac{\Lambda}{E}\left(f(E_{\mathbf{k}}) + \frac{1}{2}\right)\,. \tag{A.17}$$

One can immediatly notice that the anomalous density is of order g ($\propto \Lambda$). As we have already mentioned previously, the second term in the right-hand side of Eq. (A.17) is ultraviolet divergent. Using the two densities Eqs. (A.10) and (A.17), the chemical potential can now be rewritten as:

$$\mu = gn_0 + 2g\tilde{n} + g\tilde{m}\,. \tag{A.18}$$

One can verify that the above expression coincides with Eq. (A.12), when applying the proper renormalization of the coupling constant, $gn_0 + g\tilde{m} \to gn_0(1 + g/V\sum_{\mathbf{k}} m/(\hbar k)^2) + g\tilde{m}$. We also note that the aforementioned Popov approximation of the HFB theory is recovered when putting $\tilde{m} = 0$ in Eq. (A.18).

A.1.2 Discussion

Analytical expression

We now discuss the behavior of the chemical potential in different temperature regimes. First at zero temperature, $H(\tau) = 8\sqrt{2}/(3\sqrt{\pi})$, and one obtains to order

g^2:

$$\mu(T=0) = gn\left(1 + \frac{32}{3\sqrt{\pi}}\sqrt{na^3}\right), \tag{A.19}$$

retrieving correctly the chemical potential calculated by Lee, Huang and Yang (see Eq. (1.59) with $\mu = \partial E_0/\partial n$).

At low temperature $\tau \ll 1$, one can expand the dimensionless function $H(\tau)$ in Eq. (A.13) as:

$$H(\tau) \simeq \sqrt{\frac{2}{\pi}}\left(\frac{8}{3} - \sqrt{\frac{\pi}{2}}\zeta(3/2)\tau^{3/2} + \frac{\pi^4}{30}\tau^4\right). \tag{A.20}$$

Inserting this expression in Eq. (A.12), one gets the low-temperature behavior of the chemical potential:

$$\mu \simeq gn + g\left(\frac{m\Lambda}{2\pi\hbar^2}\right)^{3/2}\sqrt{\frac{2}{\pi}}\left(\frac{8}{3} + \frac{\pi^4}{60}\tau^4\right). \tag{A.21}$$

The above expression coincides with the result obtained when considering the thermodynamics of a Bose gas with phonon quasi-particles [7, §4]. It is worth noticing that Eq. (A.21) is valid for any temperatures $\tau \ll 1$, whereas the use of gn_0 for the perturbation parameter would restrict the validity of expression (A.21) in a narrower temperature region. Actually, in the same temperature regime Eq. (A.10) provides the result

$$n_0 = n - \left(\frac{m\Lambda}{2\pi\hbar^2}\right)^{3/2}\frac{2}{\sqrt{\pi}}\left[\frac{\sqrt{2}}{3} + \frac{\pi^2}{6\sqrt{2}}\tau^2 - \frac{\pi^4}{120\sqrt{2}}\tau^4\right]. \tag{A.22}$$

The presence of the τ^2-term will be at the origin of a lower bound ($k_BT/gn \gg (na^3)^{1/4}$) on the validity range of Eq. (A.21) when Λ is replaced by gn_0.

At high temperature $\tau \gg 1$ instead, one can neglect the $T = 0$ quantum fluctuations contribution in Eq. (A.12):

$$\mu = \simeq gn_0 + \frac{g}{V}\sum_{\mathbf{k}}\frac{2\varepsilon_{\mathbf{k}} + \Lambda}{E_{\mathbf{k}}}f(E_{\mathbf{k}}). \tag{A.23}$$

In order to evaluate the above integral, one can separate the integration domain into two parts, and approximate the Bose distribution function in the long wavelength domain ($\beta E_{\mathbf{k}} \ll 1$) by the Rayleigh-Jeans one, $f(E) \simeq 1/(\beta E)$, while in the short wavelength domain ($\varepsilon_{\mathbf{k}} \gg \Lambda$) it can be replaced by the non-interacting atoms

distribution. Equivalently, one can add and subtract the ideal gas contribution:

$$\begin{aligned}\mu &= gn_0 + 2gn_T^0 + 2g\frac{m\sqrt{2m}}{2\pi^2\hbar^3}\int_0^\infty d\varepsilon\sqrt{\varepsilon}\left(\frac{\varepsilon+\Lambda}{E}f(E) - f(\varepsilon)\right)\\ &\simeq gn_0 + 2gn_T^0 + 2g\frac{m\sqrt{2m}}{2\pi^2\hbar^3}\int_0^\infty d\varepsilon\sqrt{\varepsilon}\left(\frac{\varepsilon+\Lambda}{E}\frac{1}{\beta E} - \frac{1}{\beta\varepsilon}\right)\\ &= gn_0 + 2gn_T^0 - g\frac{3\sqrt{2\pi}}{\lambda_T^3}\sqrt{\beta\Lambda}\,. \end{aligned} \tag{A.24}$$

Proceeding in the same way for the condensate density (A.10), one finally arrives at [102, 152]:

$$\mu \simeq gn + gn_T^0 - g\frac{2\sqrt{2\pi}}{\lambda_T^3}\sqrt{\Lambda}\,. \tag{A.25}$$

It is insightful to compare the above result with the prediction of HF theory Eq. (2.8). Comparing the two equations, we find that both give similar result, though the HF theory underestimates the effects of thermal fluctuations by a factor $\sqrt{2}$. This rather good agreement is justified by the fact that at high temperature, large momentum modes $\hbar k \sim \sqrt{2mk_BT}$ contribute the most to the excitations and one can therefore approximate the Bogoliubov excitation spectrum Eq. (A.9) by the mean-field expression $E \simeq \varepsilon_{\mathbf{k}} + \Lambda$. We briefly note that the Popov approximation of the HFB theory also leads to a similar result in the high-temperature regime.

Finally, in the absence of a condensate ($n_0 = 0$), the Popov approach reduces to the HF theory, in which $\mu = \mu^{\rm IBG} + 2gn$, with $\mu^{\rm IBG}$ the ideal Bose gas chemical potential. Consequently, the BEC phase transition is predicted to occur at the ideal gas phase transition temperature, $T_{\rm BEC} = 2\pi\hbar^2/m\,[n/\zeta(3/2)]^{2/3}$.

Free energy

In view of developing the Popov theory for the mixtures in the next section, let us evaluate the free energy for the dilute Bose gas to order g^2. The free energy $F = E - TS$ is given from Eq. (A.5) according to $F = \Omega + \mu N$:

$$\frac{F}{V} = \frac{g}{2}n_0^2 - g\tilde{n}^2 + \mu\tilde{n} + \frac{1}{\beta}\sum_{\mathbf{k}}\ln\left(1 - e^{-\beta E_{\mathbf{k}}}\right) + \frac{\Omega_{\rm QF}}{V} \tag{A.26}$$

where $\Omega_{\rm QF}$ is the contribution from quantum fluctuations, corresponding to the last term of Eq. (A.4). In order to derive the second order expression, let us decompose the key quantities into a sum of the lowest order term (^{0}) and subleading terms (δ): $\mu = \mu^0 + \delta\mu$, $\tilde{n} = n_T^0 + \delta\tilde{n}$ and $\Lambda = \Lambda^0 - \delta\mu$, where $\delta\tilde{n}$ is of order $g^{1/2}$ whereas $\delta\mu$ of order $g^{3/2}$. Then, expanding the first mean-field contributions to order g^2,

$$\frac{F}{V} = \frac{g}{2}(n^2 + {n_T^0}^2) + n_T^0\delta\mu + \frac{1}{\beta}\sum_{\mathbf{k}}\ln\left(1 - e^{-\beta E_{\mathbf{k}}}\right) + \frac{\Omega_{\rm QF}}{V}\,. \tag{A.27}$$

In order to find the second-order contribution of the logarithmic term, let us suppose for simplicity the high temperature limit $k_B T \gg gn$. Following the same calculations as Eq. (A.24), the sum over the momentum in Eq. (A.27) can be evaluated analytically, and one finds

$$\frac{1}{\beta}\sum_{\mathbf{k}} \ln\left(1 - e^{-\beta E_{\mathbf{k}}}\right) \simeq -\frac{\zeta(5/2)}{\beta\lambda_T^3} + n_T^0(\Lambda^0 - \delta\mu) - \frac{4\sqrt{2\pi}}{3\lambda_T^3}(\beta\Lambda^0)^{3/2}\,. \tag{A.28}$$

Inserting Eq. (A.28) into (A.27), the $n_T^0\delta\mu$ terms are found to cancel with each others. It is worth stressing that such cancellation would not happen if one would choose gn_0 instead of Λ for the perturbation parameter. The above argument remains true for any temperatures, and one finally finds to order g^2:

$$\frac{F}{V} = \frac{g}{2}(n^2 + {n_T^0}^2) + \frac{1}{\beta}\sum_{\mathbf{k}} \ln\left(1 - e^{-\beta E_{\mathbf{k}}^0}\right) + \frac{\Omega_{\mathrm{QF}}}{V}\,, \tag{A.29}$$

with $E_{\mathbf{k}}^0 = \sqrt{\varepsilon_{\mathbf{k}}^2 + 2gn_0^0\varepsilon_{\mathbf{k}}}$. One can verify that taking the derivative of the free energy with respect to n, we recover the chemical potential Eq. (A.12).

A.1.3 Results

We now show the numerical results for the key thermodynamic quantities, for the interaction parameter $\eta = 0.05$. The left panel of Fig. A.1 shows the condensate density, evaluated from the Popov theory Eq. (A.10), together with the predictions from the HF and UR approaches. The Popov theory agrees well with the UR prediction in the high-temperature region. In the right panel, we compare the results of the Popov theory in different limits. We see that the second order Popov result, in which we have used the lowest order expression for the effective chemical potential $\Lambda^0 = g(n - n_T^0)$ in the subleading terms of Eq. (A.10), agrees with the self-consistent calculation in a wide range of temperature. In particular, Popov theory predicts correctly the depletion of the condensate at zero temperature.

In figure A.2 we make a similar comparison for the chemical potential. In a mean-field description, the chemical potential is predicted to evolve monotonically from gn at zero temperature to $2gn$ at the critical temperature. The Popov theory confirms this picture, although capturing quantum corrections at $T = 0$ and exhibiting an unphysical jump at T_{BEC} (see Sec. 2.1.2).

Figure A.3 shows the isothermal compressibility of the gas, $\kappa_T = n^{-1}\partial n/\partial P|_T$. For an ideal Bose gas, the compressibility is predicted to diverge in the BEC phase, and therefore the quantity is expected to be sensitive to the way interaction is treated in the theory [155]. This is shown in Fig. A.3, where one finds that all approaches predict an enhancement of the compressibility in the BEC phase,

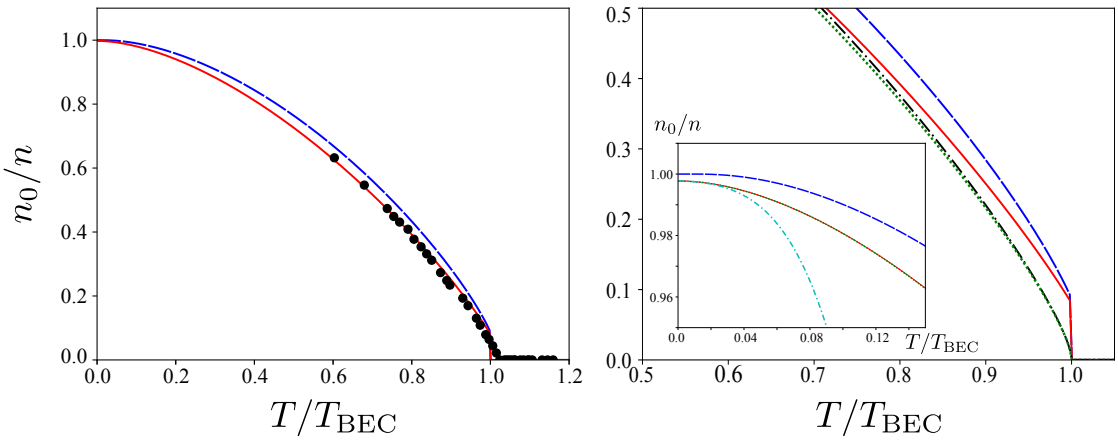

Figure A.1: Condensate density $n_0 = n - \tilde{n}$ as a function of temperature, for interaction parameter $gn/(k_B T_{\mathrm{BEC}}) = 0.05$. Left panel: comparison of different theories. The red line is the Popov theory prediction in which Eqs. (A.10) and (A.12) have been solved self-consistently. The blue dashed line shows the result of the HF theory and the black dots are the universal relations prediction, from Ref. [83]. Right panel: comparison of Popov theory in different limits. Red and blue lines: same as left panel. Green dashed line: Popov theory calculated up to the second order (by putting $\Lambda = g(n - n_T^0)$ in Eq. (A.10)). Cyan dotted-dashed and black dotted lines: low-temperature expression (A.22) and high-temperature expression (A.10), respectively.

increasing with the temperature. In particular, one finds that the Popov theory limited to the lowest order (green dashed line) shows a worse agreement to the universal relations prediction, in comparison to the self-consistent theories. This is understood from the fact that in the vicinity of T_{BEC}, thermal fluctuations become important and beyond second order terms have non-negligible contributions to the thermodynamic quantities. Although the correctness of self-consistent theories is questionable in this regime, its solution automatically includes higher order terms, and thus some of the qualitative physics.

A.2 Binary Bose mixtures

A.2.1 General case

We consider a uniform mixture of two component Bose gases, and extend the Popov theory of Sec. A.1.1 using the same methodology [156]. The Hamiltonian

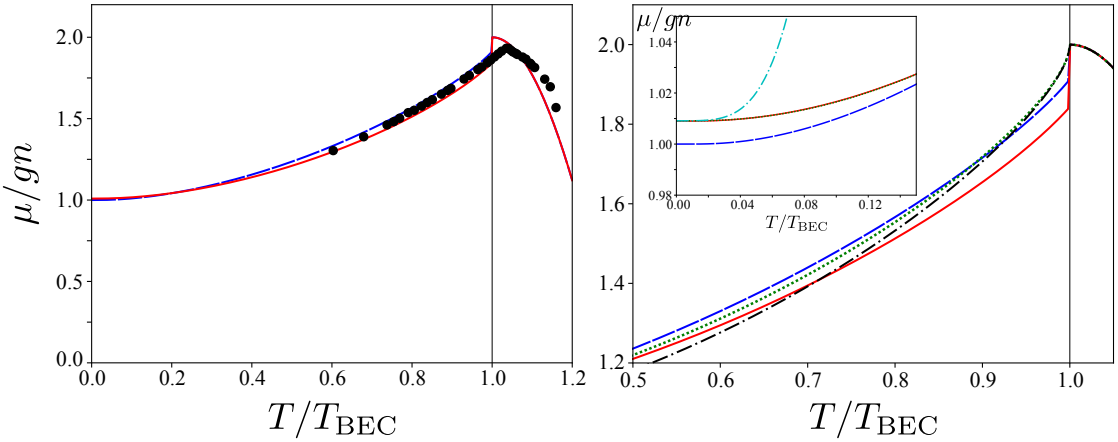

Figure A.2: Chemical potential as a function of temperature. Left panel: comparison of different theories. Right panel: study of high and low temperature limits. Line guides are the same as in Fig. A.1.

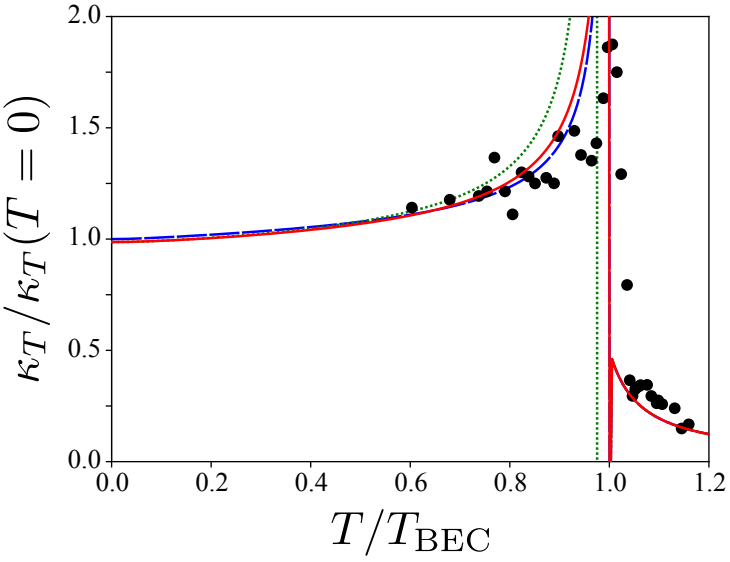

Figure A.3: Isothermal compressibility as a function of temperature. Red line: self-consistent Popov theory. Blue dashed line: HF theory. Green dashed line: Popov theory calculated up to the second order.

including all the possible point-like interaction takes the form,

$$H = \sum_{i=1,2} \left\{ \sum_{\mathbf{k}} \varepsilon_{i,\mathbf{k}} \hat{a}^{\dagger}_{i,\mathbf{k}} \hat{a}_{i,\mathbf{k}} + \frac{g_{ii}}{2V} \sum_{\mathbf{k},\mathbf{k}',\mathbf{q}} \hat{a}^{\dagger}_{i,\mathbf{k}} \hat{a}^{\dagger}_{i,\mathbf{k}'+\mathbf{q}} \hat{a}_{i,\mathbf{k}'} \hat{a}_{i,\mathbf{k}+\mathbf{q}} \right\} + \frac{g_{12}}{V} \sum_{\mathbf{k},\mathbf{k}',\mathbf{q}} \hat{a}^{\dagger}_{1,\mathbf{k}} \hat{a}_{1,\mathbf{k}+\mathbf{q}} \hat{a}^{\dagger}_{2,\mathbf{k}'+\mathbf{q}} \hat{a}_{2,\mathbf{k}'} \,, \tag{A.30}$$

where the subscript $i = \{1, 2\}$ refers to the i^{th} component of the gases. The interaction between identical atoms is modeled through the intra-atomic couping constant $g_{11} = 4\pi\hbar^2 a_{11}/m_1$ and $g_{22} = 4\pi\hbar^2 a_{22}/m_2$, whereas the interaction between different atomic species is given by the inter-atomic coupling constant $g_{12} = 4\pi\hbar^2 a_{11}/m_R$, with $m_R = 2m_1 m_2/(m_1 + m_2)$ the relative mass. Applying the Bogoliubov prescription and replacing $\hat{a}_{i,0}$ and $\hat{a}^\dagger_{i,0}$ with the number of particles in the condensate state $\sqrt{N_{i,0}}$, one obtains for the grand canonical Hamiltonian $K = H - \sum_i \mu_i N_i$:

$$\begin{aligned}\hat{K} = \sum_{i=1,2} \Bigg\{ & \frac{g_{ii}}{2V} N_{i,0}^2 - \frac{g_{ii}}{V} \tilde{N}_i^2 - \mu_i N_{i,0} + \sum_{\mathbf{k}\neq 0} \left(\varepsilon_{i,\mathbf{k}} + 2g_{ii} n_i + g_{12} n_j - \mu_i\right) \hat{a}^\dagger_{i,\mathbf{k}} \hat{a}_{i,\mathbf{k}} \\ & + \frac{g_{ii}}{2V} N_{i,0} \sum_{\mathbf{k}\neq 0} \left(\hat{a}^\dagger_{i,\mathbf{k}} \hat{a}^\dagger_{i,-\mathbf{k}} + \hat{a}_{i,\mathbf{k}} \hat{a}_{i,-\mathbf{k}} \right) \Bigg\} + \frac{g_{12}}{V} N_{1,0} N_{2,0} - \frac{g_{12}}{V} \tilde{N}_1 \tilde{N}_2 \\ & + \frac{g_{12}}{V} \sqrt{N_{1,0} N_{2,0}} \sum_{\mathbf{k}\neq 0} \left(\hat{a}^\dagger_{1,\mathbf{k}} + \hat{a}_{1,-\mathbf{k}} \right) \left(\hat{a}^\dagger_{2,-\mathbf{k}} + \hat{a}_{2,\mathbf{k}} \right) , \end{aligned} \tag{A.31}$$

where $\varepsilon_{i,\mathbf{k}} = \hbar^2 k^2/(2m_i)$, and $\tilde{N}_i = \sum_{\mathbf{k}\neq 0} \hat{a}^\dagger_{i,\mathbf{k}} \hat{a}_{i,\mathbf{k}}$. In the above equation, we have again kept the terms quadratic in $\hat{a}_{\mathbf{k}\neq 0}$, $\hat{a}^\dagger_{\mathbf{k}\neq 0}$ up to order g^2 (g_{12}^2), by neglecting the terms quadratic in the fluctuations of non-condensate density around its mean value, as well as the terms proportional to the anomalous densities. The terms in the bracket in Eq. (A.31) correspond to the single-species Hamiltonian (A.1) in each component, whereas the other terms represent the interspecies interaction contributions. Equation (A.31) can be diagonalized after applying the following canonical transformations:

$$\begin{aligned} \hat{a}'_{1,\mathbf{k}} &= \lambda_{\mathbf{k}} \hat{a}_{1,\mathbf{k}} + w_{\mathbf{k}} \hat{a}^\dagger_{2,-\mathbf{k}} + z_{\mathbf{k}} \hat{a}_{2,\mathbf{k}} , \\ \hat{a}'_{2,\mathbf{k}} &= \lambda_{\mathbf{k}} \hat{a}_{2,\mathbf{k}} + w_{\mathbf{k}} \hat{a}^\dagger_{1,-\mathbf{k}} - z_{\mathbf{k}} \hat{a}_{1,\mathbf{k}} . \end{aligned} \tag{A.32}$$

Then the last line of Eq. (A.31) involving the coupling of both components, in which the operators $\hat{a}'_1$ and $\hat{a}'_2$ appear by pairs, vanish if the weight functions take the expressions:

$$\begin{aligned} \lambda_{\mathbf{k}}^2 &= \frac{1}{2} \left[1 + \frac{\tilde{E}_{1,\mathbf{k}}^2 - \tilde{E}_{2,\mathbf{k}}^2}{\sqrt{(\tilde{E}_{1,\mathbf{k}}^2 - \tilde{E}_{2,\mathbf{k}}^2)^2 + 16 g_{12}^2 \tilde{\varepsilon}_{1,\mathbf{k}} \tilde{\varepsilon}_{2,\mathbf{k}} n_{1,0} n_{2,0}}} \right] \\ z_{\mathbf{k}}^2 (w_{\mathbf{k}}^2) &= \frac{(\tilde{\varepsilon}_{1,\mathbf{k}} \pm \tilde{\varepsilon}_{2,\mathbf{k}})^2}{8 \tilde{\varepsilon}_{1,\mathbf{k}} \tilde{\varepsilon}_{2,\mathbf{k}}} \left[1 - \frac{\tilde{E}_{1,\mathbf{k}}^2 - \tilde{E}_{2,\mathbf{k}}^2}{\sqrt{(\tilde{E}_{1,\mathbf{k}}^2 - \tilde{E}_{2,\mathbf{k}}^2)^2 + 16 g_{12}^2 \tilde{\varepsilon}_{1,\mathbf{k}} \tilde{\varepsilon}_{2,\mathbf{k}} n_{1,0} n_{2,0}}} \right] \end{aligned} \tag{A.33}$$

where we have introduced the "gapped" kinetic energy $\tilde{\varepsilon}_{i,\mathbf{k}} = \varepsilon_{i,\mathbf{k}} + \Lambda_i - g_{ii}n_{i,0}$ and single-component excitation spectrum $\tilde{E}_{i,\mathbf{k}} = \sqrt{(\varepsilon_{i,\mathbf{k}} + \Lambda_i)^2 - (g_{ii}n_{i,0})^2}$, with effective chemical potential,

$$\Lambda_i = |\mu_i - 2g_{ii}n_i - g_{12}n_{3-i}| \,. \tag{A.34}$$

Henceforth, Eq. (A.31) reduces to the sum of two uncoupled Hamiltonian, which can be diagonalized by means of the Bogoliubov transformation Eq. (1.52) applied to $(\hat{a}'^{\dagger}_{1,\mathbf{k}}, \hat{a}'_{1,\mathbf{k}})$ and $(\hat{a}'^{\dagger}_{2,\mathbf{k}}, \hat{a}'_{2,\mathbf{k}})$, respectively. Finally, the grand-canonical Hamiltonian in the diagonalized form is expressed as:

$$\hat{K} = \Omega_0 + \sum_{\mathrm{k}\neq 0} \left(\tilde{E}_{+,\mathbf{k}} \hat{\alpha}^{\dagger}_{\mathbf{k}} \hat{\alpha}_{\mathbf{k}} + \tilde{E}_{-,\mathbf{k}} \hat{\beta}^{\dagger}_{\mathbf{k}} \hat{\beta}_{\mathbf{k}} \right) \tag{A.35}$$

where $\hat{\alpha}^{\dagger}_{\mathbf{k}}$ (resp. $\hat{\beta}^{\dagger}_{\mathbf{k}}$) is the creation operator for the quasiparticles in the density (resp. spin) channel, obeying the Bose statistics. The excitation spectrum of the system reads

$$\tilde{E}_{\pm} = \sqrt{\frac{1}{2}\left[(\tilde{E}^2_{1,\mathbf{k}} + \tilde{E}^2_{2,\mathbf{k}})^2 \pm \sqrt{(\tilde{E}^2_{1,\mathbf{k}} - \tilde{E}^2_{2,\mathbf{k}})^2 + 16 g^2_{12} \tilde{\varepsilon}_{1,\mathbf{k}} \tilde{\varepsilon}_{2,\mathbf{k}} n_{1,0} n_{2,0}} \right]} \,, \tag{A.36}$$

and the vacuum energy of Bogoliubov quasi-particles is given by

$$\begin{aligned} \Omega_0 = & \sum_{i=1,2} \left(\frac{g_{ii}}{2V} N^2_{i,0} - \frac{g_{ii}}{V} \tilde{N}^2_i - \mu_i N_{i,0} \right) + \frac{g_{12}}{V} N_{1,0} N_{2,0} \\ & + \frac{1}{2} \sum_{\mathbf{k}\neq\mathbf{0}} \Bigg\{ \left(\tilde{E}_{+,\mathbf{k}} - \varepsilon_{1,\mathbf{k}} - \Lambda_1 \right) + \left(\tilde{E}_{-,\mathbf{k}} - \varepsilon_{2,\mathbf{k}} - \Lambda_2 \right) \\ & + \frac{1}{\hbar^2 k^2} \left[m_1 (g_{11} n_{1,0})^2 + m_2 (g_{22} n_{2,0})^2 + 2 m_R g^2_{12} n_{1,0} n_{2,0} \right] \Bigg\} \,. \end{aligned} \tag{A.37}$$

In the above expression, the first line corresponds to the mean-field contribution, whereas the last two lines account for the quantum fluctuations. In particular, the last line arises from the normalization of the coupling constants $g_{ii} \to g_{ii}[1 + g_{ii}/V \sum_{\mathbf{k}} m_i/(\hbar k)^2]$ and $g_{12} \to g_{12}[1 + g_{12}/V \sum_{\mathbf{k}} m_R/(\hbar k)^2]$. [156, 157]

The chemical potential in each component can be calculated in a similar fashion to the single-component case, by evaluating the saddle point equation $\partial\Omega/\partial n_{i,0}|_{\tilde{n},T} = 0$ and solving it perturbatively. First, one finds that to the lowest order in the coupling constants, $n^0_{i,0} = n_i - n^0_{i,T}$ where $n^0_{i,T} = \zeta(3/2)/\lambda^3_{i,T}$ is the ideal gas thermal density in component i, with the species dependent thermal de Broglie wavelength $\lambda_{i,T} = \sqrt{2\pi\hbar^2/(m_i k_B T)}$. As for the chemical potential, one finds that

$\mu_i^0 = g_{ii}(n_i + n_{i,T}^0) + g_{12}n_{3-i}$, involving the equality $\Lambda_i^0 = g_{ii}n_{i,0}^0$. The gapless spectrum is therefore given by Eq. (A.36) with the replacement $g_{ii}n_{i,0} \to \Lambda_i$. We remind that such identification is *a priori* justified only when $n_{i,0}$ and Λ_i are evaluated to the lowest order. It follows that $\tilde{E}_{i,\mathbf{k}}$ has to be replaced by the single-particle Bogoliubov spectrum $E_{i,\mathbf{k}} = \sqrt{\varepsilon_{i,\mathbf{k}}^2 + 2\Lambda_i\varepsilon_{i,\mathbf{k}}}$ as well as $\tilde{\varepsilon}_{i,\mathbf{k}} \to \varepsilon_{i,\mathbf{k}}$ in Eq. (A.36). Equivalently, the excitation spectrum can also be written as

$$E_{\pm,\mathbf{k}} = \sqrt{\left(\frac{\nu_1^2 + \nu_2^2}{2}\right)\varepsilon_{\mathbf{k}}^2 + 2\varepsilon_{\mathbf{k}}\Lambda_{\pm,\mathbf{k}}}\,, \tag{A.38}$$

where we have introduced the relative kinetic energy $\varepsilon_{\mathbf{k}} = \hbar^2k^2/(2m_R)$ and the inverse mass ratios $\nu_i = m_R/m_i$. The effective chemical potential $\Lambda_\pm$ is therefore associated to the Bogoliubov density (+) and spin (−) sounds, and takes the following expression:

$$\Lambda_{\pm,\mathbf{k}} = \frac{1}{2}\left(\nu_1\Lambda_1 + \nu_2\Lambda_2 \pm \Gamma_{\mathbf{k}}\right) \tag{A.39}$$

$$\Gamma_{\mathbf{k}} = \sqrt{\left[\frac{(\nu_1^2 - \nu_2^2)}{2}\varepsilon_{\mathbf{k}} + (\nu_1\Lambda_1 - \nu_2\Lambda_2)\right]^2 + 4\bar{g}^2\nu_1\Lambda_1\nu_2\Lambda_2}\,. \tag{A.40}$$

where we have defined the reduced coupling constant $\bar{g} = g_{12}/\sqrt{g_{11}g_{22}}$. Finally, the condensate density $n_{i,0} = n_i - V^{-1}\sum_{\mathbf{k}\neq 0}\langle\hat{a}_{i,\mathbf{k}}^\dagger\hat{a}_{i,\mathbf{k}}\rangle$ is given by $(1 \leftrightarrow 2)$:

$$n_{1,0} = n_1 - \frac{1}{4V}\sum_{\mathbf{k}}\sum_{\pm}\left(1 \pm \frac{E_{1,\mathbf{k}}^2 - E_{2,\mathbf{k}}^2}{2\varepsilon_{\mathbf{k}}\Gamma_{\mathbf{k}}}\right)\left[\frac{\varepsilon_{1,\mathbf{k}}^2 + E_{\pm,\mathbf{k}}^2}{2\varepsilon_{1,\mathbf{k}}E_{\pm,\mathbf{k}}}\left(2f(E_{\pm,\mathbf{k}}) + 1\right) - 1\right] \tag{A.41}$$

and the chemical potential:

$$\begin{aligned}\mu_1 =& g_{11}n_1 + g_{12}n_2 \\ &+ \frac{g_{11}}{4V}\sum_{\mathbf{k}}\sum_{\pm}\left(1 \pm \frac{E_{1,\mathbf{k}}^2 - E_{2,\mathbf{k}}^2 + 4\bar{g}^2\Lambda_2\varepsilon_{2,\mathbf{k}}}{2\varepsilon_{\mathbf{k}}\Gamma_{\mathbf{k}}}\right)\left[\frac{\varepsilon_{1,\mathbf{k}}}{E_{\pm,\mathbf{k}}}\left(2f(E_{\pm,\mathbf{k}}) + 1\right) - 1\right] \\ &+ \frac{g_{11}}{2V}\sum_{\mathbf{k}}\frac{1}{\varepsilon_{\mathbf{k}}}\left[\frac{1}{\nu_1}\Lambda_1 + \bar{g}\Lambda_2\right]\,.\end{aligned} \tag{A.42}$$

In the absence of a condensate, the Popov theory reduces to the HF theory. Then, both approaches predict the BEC to occur at the ideal gas critical temperature $k_BT_{i,\mathrm{BEC}} = 2\pi\hbar^2/m_i\,[n_i/\zeta(3/2)]^{2/3}$. In the normal phase, the chemical potential is therefore given by

$$\mu_1 = \mu_1^{\mathrm{IBG}} + 2g_{11}n_1 + g_{12}n_2\,, \tag{A.43}$$

with μ_{IBG} the chemical potential of an ideal gas.

A.2.2 Equal mass case

In the case where the masses of the two components are equal $m_1 = m_2 = m$, the function Γ in Eq. (A.40) becomes independent of the wave-vector:

$$\Lambda_\pm = \frac{1}{2}\left[\Lambda_1 + \Lambda_2 \pm \sqrt{(\Lambda_1 - \Lambda_2)^2 + 4\bar{g}^2\Lambda_1\Lambda_2}\right], \tag{A.44}$$

and one can write down the chemical potential into a form close to the single-component case Eq. (A.12):

$$\mu_1 = g_{11}n_1 + g_{11}n_T^0 + g_{12}n_2 + g_{11}\sum_\pm \left(\frac{m\Lambda_\pm}{2\pi\hbar^2}\right)^{3/2} H_\pm(\tau_\pm, l) \tag{A.45}$$

where the dimensionless function on the reduced temperature $\tau_\pm = k_B T/\Lambda_\pm$ and parameter $l = \Lambda_2/\Lambda_1$ is given by

$$\begin{aligned} H_\pm(\tau_\pm, l) =& \frac{1}{\sqrt{\pi}}\left\{\frac{4\sqrt{2}}{3}\left(1 \pm \frac{1 + (2\bar{g}^2 - 1)l}{\sqrt{(1-l)^2 + 4\bar{g}^2 l}}\right)\right. \\ &\left. + \tau_\pm \int_0^\infty dx f(x)\left[\frac{(u_\pm - 1)^{3/2}}{u_\pm}\left(1 \pm \frac{1 + (2\bar{g}^2 - 1)l}{\sqrt{(1-l)^2 + 4\bar{g}^2 l}}\right) - \sqrt{\tau_\pm x}\right]\right\}, \end{aligned} \tag{A.46}$$

with $u_\pm = \sqrt{1 + \tau_\pm^2 x^2}$. The chemical potential μ_2 in the second component is instead obtained from Eq. (A.45), replacing l by $1/l = \Lambda_1/\Lambda_2$. We can easily verify that for $g_{12} = 0$ and $n_2 = 0$, the spin-channel vanishes and one retrieves the single-component result Eq. (A.12).

Finally, in analogy to the single component gas, one can define new anomalous densities involving two creation or annihilation operators. In particular, the binary system possesses two additional anomalous pair densities,

$$\tilde{n}_{12} = \frac{1}{V}\sum_{\mathbf{k}} \left\langle \hat{a}_{1,\mathbf{k}}^\dagger \hat{a}_{2,\mathbf{k}} \right\rangle, \quad \tilde{m}_{12} = \frac{1}{V}\sum_{\mathbf{k}} \langle \hat{a}_{1,\mathbf{k}} \hat{a}_{2,-\mathbf{k}} \rangle, \tag{A.47}$$

arising from the presence of Bose-Einstein condensates in both components. In the mass-balanced case, one finds from the quasi-particles amplitudes of Eqs. (A.33) and (A.2) that:

$$\tilde{n}_{12} = \frac{1}{4V}\sum_{\mathbf{k}}\sum_\pm (\pm)\frac{2\bar{g}\sqrt{\Lambda_1\Lambda_2}}{\Gamma}\left[\frac{\varepsilon_{\mathbf{k}} + \Lambda_\pm}{E_{\pm,\mathbf{k}}}\left(2f(E_{\pm,\mathbf{k}}) + 1\right) - 1\right] \tag{A.48}$$

$$\tilde{m}_{12} = \frac{-1}{4V}\sum_{\mathbf{k}}\sum_\pm (\pm)\frac{2\bar{g}\sqrt{\Lambda_1\Lambda_2}}{\Gamma}\frac{\Lambda_\pm}{E_{\pm,\mathbf{k}}}\left[2f(E_{\pm,\mathbf{k}}) + 1\right]. \tag{A.49}$$

Using the newly introduced densities, the chemical potential in the equal mass case can be conveniently written into the form

$$\mu_1 = g_{11}(n_1 + \tilde{n}_1 + \tilde{m}_1) + g_{12}n_2 + g_{12}\sqrt{\frac{g_{11}\Lambda_2}{g_{22}\Lambda_1}}\,(\tilde{n}_{12} + \tilde{m}_{12})\ . \tag{A.50}$$

As we discuss in the main text Sec. 4.2, the anomalous pair densities play a crucial role in describing the spin thermodynamics of the mixtures.

At zero temperature, one finds to order g^2 (g_{12}^2),

$$\begin{aligned}\mu_1(T=0) =& g_{11}n_1\Bigg\{1 + \frac{32}{3\sqrt{\pi}}\sqrt{n_1 a_{11}^3}\sum_{\pm}\frac{1}{2}\left(1 \pm \frac{1 + (2\bar{g}^2 - 1)l}{\sqrt{(1-l)^2 + 4\bar{g}l}}\right)\\ &\times\left[\frac{1}{2}\left(1 + l \pm \sqrt{(1-l)^2 + 4\bar{g}l}\right)\right]^{3/2}\Bigg\}\,.\end{aligned} \tag{A.51}$$

We have verified that (A.51) corresponds to the same expression as the chemical potential evaluated from the LHY energy functional of Ref. [139], which was derived in the canonical ensemble. This functional has been successfully used for the description of self-bound quantum droplets.

At temperature $k_B T \gg gn$ the Bose distribution function can be expanded in the same way as the single-component case (A.25), yielding the following analytical expression:

$$\mu_1 \simeq g_{11}n_1 + g_{11}n_T^0 + g_{12}n_2 - g_{11}\frac{2\sqrt{2\pi}}{\lambda_T^3}\sum_{\pm}\frac{1}{2}\left(1 \pm \frac{1 + (2\bar{g}^2 - 1)l}{\sqrt{(1-l)^2 + 4\bar{g}^2 l}}\right)\sqrt{\beta\Lambda_{\pm}}\,. \tag{A.52}$$

It is worth noticing that the HF theory in the same temperature regime predicts the chemical potential to behave like

$$\mu_1^{\mathrm{HF}} \simeq g_{11}n_1 + g_{11}n_T^0 + g_{12}n_2 - g_{11}\frac{2\sqrt{\pi}}{\lambda_T^3}\sqrt{\beta\Lambda_1^{\mathrm{HF}}}\,. \tag{A.53}$$

Since $\Lambda^{\mathrm{HF}} = gn_0^{\mathrm{HF}}$, the HF theory does not include any beyond-linear order corrections in g_{12}.

Appendix B

Interaction in two-dimensional Bose gases

B.1 Interaction in 2D

B.1.1 2D system

We start from the purely 2D scattering problem, which follows essentially the same procedure as the 3D case, carried in Sec. 1.2.3. Let us consider two atoms with identical mass colliding through a short-range interaction. We place ourself into a system of coordinate where the center-of-mass is at rest, to reduce the problem to a single particle scattering problem. Then, the asymptotic form of the colliding atoms wave-function is given by the sum between an incident plane-wave and an outgoing spheric-wave (see. Sec. 1.2.3)

$$\psi(\mathbf{r}) \simeq e^{i\mathbf{kr}} + e^{-i\mathbf{kr}} - 2f(k,\theta)\sqrt{\frac{i}{8\pi rk}}e^{ikr}, \tag{B.1}$$

where $f(k,\theta)$ is the scattering amplitude, depending on the relative momentum $\mathbf{k}$ and the scattering angle θ. In the above equation, the multiplicative factor of $f(k,\theta)$ has been chosen for future convenience, and we have considered the collision of two identical bosons, taking into account their symmetric nature [30].

As we have seen in Sec. 1.2.3, the main contribution for the scattering amplitude in a weakly interacting Bose gas comes from the s-wave scattering. However, while in 3D the scattering amplitude tends to a constant in the limit of low density $k \to 0$ (see Eq. (1.42)), this is no longer true in the 2D case, in which the scattering amplitude exhibits a logarithmic dependence on the relative momentum [94]:

$$\lim_{k\to 0} f(k,\theta) = -\frac{2\pi}{\ln(\eta k a_{2D})}, \tag{B.2}$$

with η some constant, and we have introduced the 2D s-wave scattering length a_{2D}. Within the Born approximation of Sec. 1.2.3, one finally finds that the weakly interacting 2D Bose gas can be modeled by a contact potential $V(\mathbf{r}) = g_{2D}\delta(\mathbf{r})$ yielding the same asymptotic behavior (B.2), when the 2D coupling constant g_{2D} is related to $f(k)$ according to $g_{2D} = \hbar^2 f(k)/m$:

$$g_{2D} = \frac{2\pi\hbar^2}{m}\frac{1}{\ln\left(1/(\eta k a_{2D})\right)}\,. \tag{B.3}$$

B.1.2 Confined 3D system

Although Eq. (B.3) gives a direct relationship between g_{2D} and a_{2D}, actual experiments are carried in tightly confined three-dimensional systems, where while the kinematics is effectively 2D, the inter-atomic interactions are described by the 3D scattering length a_s [12]. Thus, let us consider a 3D Bose gas harmonically confined in the z-direction, $V_z = m\omega_z z^2/4$, interacting through a central potential $V(r)$. The Shrödinger equation for the relative motion is given by

$$\left(-\frac{\hbar^2}{m}\Delta + V(r) + V_z(z)\right)\Psi(\mathbf{r}) = E\Psi(\mathbf{r})\,. \tag{B.4}$$

This scattering problem has been investigated by Petrov and Shlyapnikov [158]. In particular, they found that in the ultracold dilute limit, the scattering amplitude for the quasi-2D Bose gas can be expressed as

$$f_{Q2D} \simeq \frac{4\pi}{\sqrt{2\pi}l_z/a_s + \ln(B\hbar\omega_z/\pi\varepsilon)}, \tag{B.5}$$

where $l_z = \sqrt{\hbar/(m\omega_z)}$ is the harmonic length, $B \simeq 0.915$ a constant, and ε is the characteristic energy scale of colliding atoms.

An estimate for the contribution of the log-term in Eq. (B.5) is obtained by replacing the colliding atoms energy ε by the thermal energy of the gas $\sim k_B T_{\mathrm{BKT}}$ and using the experimental values of Ref. [17]:

$$\omega_z = 4.6\cdot 2\pi\,\mathrm{kHz}\,, \qquad a_s = 5.2\cdot 10^{-3}\,\mu\mathrm{m}\,. \tag{B.6}$$

We find:

$$\sqrt{2\pi}\frac{l_z}{a_s} \approx 77 \qquad \ln\left(\frac{B\hbar\omega_z}{\pi\varepsilon}\right) \approx -0.66. \tag{B.7}$$

One can see that in the experimental condition, the logarithmic term is negligible with respect to the l_z/a_s term. Finally,

$$f_{Q2D} \simeq \sqrt{8\pi}\frac{a_s}{l_z}\,, \tag{B.8}$$

and the 2D coupling constant is related to the 3D s-wave scattering length according to:

$$g_{2D} = \frac{\hbar^2}{m}\sqrt{8\pi}\frac{a_s}{l_z}\,. \tag{B.9}$$

B.2 Collisional time in 2D

Let us now evaluate the collisional time in a 2D Bose gas, in order to give an estimate for the hydrodynamicity in the experiment of Ref. [17]. For this purpose, we first need to evaluate the scattering cross section σ [30]. The probability per unit time that a particle will cross through a contour $C = 2\pi r$ is given by the flux of the scattered wave intensity through this contour

$$\alpha(k) = v\left(4|f(k)|^2\frac{1}{8\pi kr}\right)2\pi r = \frac{v|f(k)|^2}{k}, \tag{B.10}$$

where $v = \hbar k/(2m)$ is the relative velocity of colliding atoms. The elastic scattering cross-section is then obtained by dividing $\alpha(k)$ by the current density in the incident wave, which is given by

$$\mathbf{j} = \frac{\hbar}{im}\left[\psi_i^*\nabla\psi_i - \psi_i\nabla\psi_i^*\right] = 4\frac{\hbar\mathbf{k}}{m}\,, \tag{B.11}$$

where we have used $\psi_i = e^{i\mathbf{kr}} + e^{-i\mathbf{kr}}$ from Eq. (B.1). Using Eqs. (B.10) and (B.11) one finally obtains [158]

$$\sigma(k) = \frac{\alpha(k)}{|\mathbf{j}(\mathbf{k})|} = \frac{|f(k)|^2}{2k}. \tag{B.12}$$

In terms of the 2D coupling constant, one gets the expression

$$\sigma = \frac{\hbar}{m}\tilde{g}^2\frac{1}{v}, \tag{B.13}$$

where we have introduced the dimensionless coupling constant $\tilde{g} = mg_{2D}/\hbar^2$.

In the experiment of the Collège de France group, the system is excited through a static perturbation, so that the frequency of the excited mode is given by a sound wave $\omega \simeq ck$, where c and $k = 2\pi/L$ are, respectively, the sound velocity and the lowest mode wave vector defined from the box size L. One can give an estimate for the collisional time using the classical expression (1.107) adapted to the 2D gas,

$$\tau = \left(n\sigma v_{\rm th}\right)^{-1}\,, \tag{B.14}$$

where n is the 2D number density of atoms, and we have considered the particles moving at thermal velocity $v_{\rm th}$, given by the Maxwell-Boltzmann distribution.

Interestingly, one can see that when using expression (B.13) for the cross-section in Eq. (B.14), $v_{\rm th}$ cancels out and the collisional time does not depend on the temperature. Further approximating the sound velocity by the Bogoliubov zero-temperature sound $c \simeq c_0 = \hbar\sqrt{\tilde{g}n}/m$ in the expression for ω, one finally obtains the expression

$$\omega\tau \simeq \sqrt{\frac{1}{n\tilde{g}^3}}\frac{2\pi}{L}. \tag{B.15}$$

Inserting the experimental values of Ref. [17]

$$L = 38\,\mu m\,, \qquad n = 30\,\mu m^{-2}\,, \qquad \tilde{g} = 0.16\,, \tag{B.16}$$

one gets an estimate for the rate of collisions:

$$\omega\tau \simeq 0.47\,. \tag{B.17}$$

Appendix C

Quasi-condensate Popov theory for 2D dilute Bose gases

In this appendix, we generalize the Popov theory of Appendix A to the case of 2D Bose gas. For this purpose, we introduce the concept of *quasi*-condensate, which arises from the *quasi*-long range order of the 2D system. Although thermal fluctuations are enhanced in low-dimensional system, and therefore mean-field theories are not expected to be accurate, the introduction of such quasi-condensate allows for a good description of the 2D Bose gas thermodynamics.

C.1 Bogoliubov theory revisited

C.1.1 Formalism

Let us start from the zero-temperature case, by developing the Bogoliubov theory for the quasi-condensate [93, 94]. For this purpose, we consider a uniform system and write down the Bose field operator in the modulus-phase representation [159]:

$$\hat{\Psi}(\mathbf{r}) = \sqrt{\hat{n}(\mathbf{r})} e^{i\hat{\theta}(\mathbf{r})} \,. \tag{C.1}$$

As we discussed in Sec. 3.1.1, a condensate corresponding to the macroscopic occupation of a single-state mode is prohibited in 2D, and hence the Bogoliubov prescription we have used in App. A is not suitable. Instead, we use the fact that in 2D, density fluctuations are significantly suppressed (see Sec. 3.1.2), and write the field operator in terms of density and phase fluctuations as:

$$\hat{\Psi}(\mathbf{r}) = \sqrt{n_{qc} + \delta\hat{n}(\mathbf{r})} e^{i\hat{\theta}(\mathbf{r})} \,, \tag{C.2}$$

with $\delta\hat{n} \ll n_{qc}$. The physical meaning of n_{qc}, which has not to be confused with the condensate, will be clarified hereafter. By definition, $\delta\hat{n}$ and $\hat{\theta}$ are unitary

operators. Equivalently, Eq. (C.2) can be written in the form

$$\hat{\Psi}(\mathbf{r}) = \sqrt{n_{qc}} + \delta\hat{\Psi}(\mathbf{r})\,, \tag{C.3}$$

analogous to the 3D case, but now with $\delta\hat{\Psi}$ corresponding to the fluctuation term, including both density *and* phase fluctuations. Expanding Eq. (C.2) as $\hat{\Psi} = \sqrt{n_{qc}} + i\sqrt{n_{qc}}\delta\hat{\theta} + \delta\hat{n}/(2\sqrt{n_{qc}}) + \cdots$ one identifies

$$\begin{aligned} \delta\hat{n}(\mathbf{r}) &= \sqrt{n_{qc}}\left[\delta\hat{\Psi}^\dagger(\mathbf{r}) + \delta\hat{\Psi}(\mathbf{r})\right]\,, \\ \hat{\theta}(\mathbf{r}) &= \frac{i}{2\sqrt{n_{qc}}}\left[\delta\hat{\Psi}^\dagger(\mathbf{r}) - \delta\hat{\Psi}(\mathbf{r})\right]\,, \end{aligned} \tag{C.4}$$

valid to any order in $\delta\hat{\Psi}$. From the Bose commutation rule for the field operator $\hat{\Psi}$, one finds that the fluctuation fields are conjugated:

$$\left[\delta\hat{n}(\mathbf{r})\,, \hat{\theta}(\mathbf{r}')\right] = i\delta(\mathbf{r}-\mathbf{r}')\,. \tag{C.5}$$

Now, let us follow the usual Bogoliubov approach and expand the Hamiltonian Eq. (1.47), up to quadratic order in the fluctuation field $\delta\hat{\Psi}$. For the uniform system under consideration, we readily obtain

$$\hat{H} = \int d^2\mathbf{r}\left\{\frac{\hbar^2}{2m}\left[\frac{1}{4n_{qc}}\left(\nabla\delta\hat{n}(\mathbf{r})\right)^2 + n_{qc}\left(\nabla\hat{\theta}(\mathbf{r})\right)^2\right] + \frac{g}{2}\delta\left(\hat{n}(\mathbf{r})\right)^2\right\}\,. \tag{C.6}$$

Since we are considering the uniform gas, the field operators can be expressed in the plane-wave basis,

$$\delta\hat{n}(\mathbf{r}) = \sum_{\mathbf{k}}\delta\hat{n}_{\mathbf{k}}e^{i\mathbf{k}\mathbf{r}} \equiv \delta\hat{n}^\dagger(\mathbf{r}) = \sum_{\mathbf{k}}\delta\hat{n}^\dagger_{\mathbf{k}}e^{-i\mathbf{k}\mathbf{r}}\,, \tag{C.7}$$

where from the unitarity of the operators one has $\delta\hat{n}_{\mathbf{k}} = \delta\hat{n}^\dagger_{-\mathbf{k}}$, and the same identity holds for $\hat{\theta}$. We find

$$\hat{H} = E_{\mathrm{MF}} + \sum_{\mathbf{k}} n_{qc}\varepsilon_{\mathbf{k}}\hat{\theta}^\dagger_{\mathbf{k}}\hat{\theta}_{\mathbf{k}} + \frac{2gn_{qc}+\varepsilon_{\mathbf{k}}}{4n_{qc}}\delta\hat{n}^\dagger_{\mathbf{k}}\delta\hat{n}_{\mathbf{k}}\,, \tag{C.8}$$

with E_{MF} the constant mean-field energy. Although the actual Hamiltonian seems to be diagonal, it is not the case since the density and phase fluctuation fields are conjugated through Eq. (C.5). As usual, the Hamiltonian is diagonalized by applying the Bogoliubov transformation

$$\begin{aligned} \hat{\gamma}_{\mathbf{k}} &= \lambda_{\mathbf{k}}\delta\hat{n}_{\mathbf{k}} + w_{\mathbf{k}}\hat{\theta}_{\mathbf{k}}\,, \\ \hat{\gamma}^\dagger_{-\mathbf{k}} &= \lambda^*_{-\mathbf{k}}\delta\hat{n}_{\mathbf{k}} + w^*_{-\mathbf{k}}\hat{\theta}_{\mathbf{k}}\,, \end{aligned} \tag{C.9}$$

where we have used the unitary property of the operators. The new creation and annihilation operators must obey the Bose commutation rule. It follows that this is satisfied for the following choice of the quasi-particles amplitudes:

$$\lambda_{\mathbf{k}} \in \mathbb{R}\,, \qquad w_{\mathbf{k}} = \frac{i}{2\lambda_{\mathbf{k}}}\,. \tag{C.10}$$

Applying the Bogoliubov transformation in the Hamiltonian (C.8), we find that the off-diagonal terms vanish if

$$\lambda_{\mathbf{k}}^2 = \frac{1}{4n_{qc}}\frac{E_{\mathbf{k}}}{\varepsilon_{\mathbf{k}}}\,, \tag{C.11}$$

where $E_{\mathbf{k}} = \sqrt{\varepsilon_{\mathbf{k}}(\varepsilon_{\mathbf{k}} + 2gn_{qc})}$ is the Bogoliubov spectrum. Finally,

$$\hat{H} = E_0 + \sum_{\mathbf{k}} E_{\mathbf{k}}\hat{\gamma}_{\mathbf{k}}^{\dagger}\hat{\gamma}_{\mathbf{k}}\,, \tag{C.12}$$

with E_0 the ground-state energy.

C.1.2 Effects of fluctuations

We turn to the interpretation of the obtained results. First of all, the finding of Bogoliubov spectrum implies that according to the Landau's criterion (1.62), there is a superfluid with non zero critical velocity. Next, let us look at the fluctuations in the density and phase channels. From the definition of the quasi-particle amplitudes (C.9) we obtain

$$\Delta n = \sum_{\mathbf{k}} \langle \delta\hat{n}_{\mathbf{k}}^{\dagger}\delta\hat{n}_{\mathbf{k}}\rangle = \sum_{\mathbf{k}} \frac{n_{qc}\varepsilon_{\mathbf{k}}}{E_{\mathbf{k}}}\left(2f(E_{\mathbf{k}}) - 1\right)\,, \tag{C.13}$$

$$\Delta\theta = \sum_{\mathbf{k}} \langle \hat{\theta}_{\mathbf{k}}^{\dagger}\hat{\theta}_{\mathbf{k}}\rangle = \sum_{\mathbf{k}} \frac{E_{\mathbf{k}}}{4n_{qc}\varepsilon_{\mathbf{k}}}\left(2f(E_{\mathbf{k}}) - 1\right)\,. \tag{C.14}$$

The relative weight of the fluctuations for a given wave vector can be estimated as [12]

$$\frac{\Delta n_{\mathbf{k}}}{\Delta\theta_{\mathbf{k}}} \propto \frac{k^2}{k^2 + 4\tilde{g}n_{qc}}\,. \tag{C.15}$$

The above result shows that the long-wavelength phonon excitation ($k \to 0$) of the system involves mainly phase fluctuations, since $\Delta n_{\mathbf{k}}/\Delta\theta_{\mathbf{k}}$ becomes small. Although this is also true in the 3D Bose gas, in 2D it has the important implication that the number equation will exhibits an infrared divergence. On the other hand, for the short-wavelength particle-like excitations ($k \to \infty$), the ratio tends to 1 and both phase and density fluctuations contribute equally.

One can give an estimate for the density fluctuations, if in Eq. (C.13) we neglect the quantum fluctuations contribution and we approximate the Bose distribution function by $f(E) \simeq k_B T/E$. It is needed to add some remarks about this approximation, since we will use it all along this appendix. In fact, although such procedure allows for the simplification of the momentum sum, it implies a logarithmic divergence in the limit of $k \to \infty$, that was not present in the exact expression. However, we have to keep in mind that approximating the Bose distribution function by the Rayleigh-Jeans one is only valid in the temperature regime where $k_B T \gg E_{\mathbf{k}}$. This last condition sets therefore a natural upper cut-off in the sum of Eq. (C.13), and also avoids the problem of ultraviolet divergence. From a more physical point of view, this approximation consists to retain the universal long-range behavior of the system (see Eq. (3.15) in main text and following discussion).

Finally, using the approximated distribution function, the density fluctuations Eq. (C.13) with respect to the mean value reads (we put $n_{qc} \simeq n$)

$$\frac{\Delta n}{n^2} \simeq \frac{2}{D} \ln\left(\frac{k_B T}{2gn}\right) . \tag{C.16}$$

This expression confirms our preliminary discussion made in Sec. 3.1.2: the density fluctuations in 2D Bose gas are small, as far as $D \gg 1$.

C.1.3 Algebraic decay of one-body density matrix

We can now study the behavior of the one-body density matrix, in the long-range limit. As we have already discussed, the long-range physics is only governed by phase fluctuations, so that one can neglect the effects of density fluctuations in calculating the one-body density matrix:

$$n^{(1)}(s) \simeq n_{qc} \langle e^{-i\hat{\theta}(\mathbf{s})+i\hat{\theta}(0)} \rangle = n_{qc} e^{-\frac{1}{2}\langle \left[\hat{\theta}(\mathbf{s})-\hat{\theta}(0)\right]^2 \rangle} , \tag{C.17}$$

where we have used in the last equality the fact that the probability distribution for the fluctuations of phase are Gaussian. Then, expanding the field operators in the plane-wave basis and by means of Eq. (C.14), one finds [160]

$$\begin{aligned} \langle \left[\hat{\theta}(\mathbf{s}) - \hat{\theta}(0)\right]^2 \rangle &= \sum_{\mathbf{k}} \frac{E_{\mathbf{k}}}{2n_{qc}\varepsilon_{\mathbf{k}}} \left(2f(E_{\mathbf{k}}) + 1\right) \left(1 - \cos(\mathbf{ks})\right) \\ &\simeq \frac{2mk_B T}{(2\pi\hbar)^2} \frac{1}{n_{qc}} \int_{|\mathbf{k}| \leq k_c} d^2\mathbf{k} \frac{1 - \cos(\mathbf{ks})}{k^2} , \end{aligned} \tag{C.18}$$

where in the last line we have assumed the thermodynamic limit, and replaced the sum by an integral. Further, we have performed the same classical field approximation for the distribution function as before, introducing a wave vector cut-off given

by $\hbar k_c = k_B T/\sqrt{g n_{qc}/m}$. The integral takes its main contribution in the regime where $k \gg 1/s$, and one can therefore approximate $1 - \cos(\mathbf{kr}) \simeq 1$. Finally, one finds the off-diagonal long-range behavior of the density matrix to be

$$n^{(1)}(s) = n_{qc} \left(\frac{R_c}{s} \right)^{1/(n_{qc}\lambda_T^2)} , \tag{C.19}$$

with $R_c = 1/k_c$. This result shows the peculiarity of interacting 2D systems, namely, the algebraic decay of the off-diagonal one-body density matrix. The 2D gas is said to exhibit a *quasi*-long-range order. In practice, one needs to properly take into account short distance physics, including the contributions to the correlation function from the density fluctuations, as well as the effects of vortex pairs, essential to describe the BKT physics. This can be heuristically achieved by replacing the quasi-condensate density n_{qc} in Eq. (C.19) by the superfluid density n_s [12]. This is motivated from the fact that, in absence of density fluctuations, the Hamiltonian Eq. (C.6) reads:

$$\hat{H} \simeq \frac{\hbar^2 n_{qc}}{2m} \int d^2\mathbf{r} \left(\nabla \hat{\theta}(\mathbf{r}) \right)^2 . \tag{C.20}$$

The above expression corresponds to a kinetic energy with local velocity $v_s = \hbar/m\nabla\theta$, which one can identify with the superfluid component velocity Eq. (1.72). We may expect only the superfluid component to flow under a variation of θ, motivating therefore the replacement of n_{qc} by n_s. In this way, Eq. (3.9) in the main text has been obtained. We briefly note that the same expression involving the superfluid density can be obtained from a hydrodynamic approach [7, §6.7].

It is now time to give an interpretation on the physical meaning of n_{qc}. For this purpose, it is insightful to notice that the field operator Eq. (C.2) can be written as

$$\hat{\Psi}(\mathbf{r}) = \hat{\Psi}_0(\mathbf{r}) + \hat{\tilde{\Psi}}(\mathbf{r}) \tag{C.21}$$

$$\simeq \sqrt{n_{qc}} e^{i\hat{\theta}(\mathbf{r})} + \hat{\tilde{\Psi}}(\mathbf{r}) . \tag{C.22}$$

Under this definition, $\hat{\Psi}_0$ corresponds to the *quasi*-condensate field, i.e. a condensate with a fluctuating field [104, 105]. This definition directly implies that

$$n_{qc} = \sqrt{2\langle |\hat{\Psi}|^2 \rangle^2 - \langle |\hat{\Psi}|^4 \rangle} , \tag{C.23}$$

since $\hat{\tilde{\Psi}}$ is a Gaussian field. Comparing the above expression with Eq. (1.35) for the two-body density matrix of an ideal gas, the analogy between the quasi-condensate and the genuine condensate is clear. Both characterize the suppression

of the Gaussian density fluctuations. Formally, the quasi-condensate can be defined in any dimensions and it is related to the condensate through the relationship [83]:

$$n_0 = \lim_{s\to\infty} n_{qc} e^{-\chi(s)} , \tag{C.24}$$

with $\chi(s) = \frac{1}{2}\langle[\hat{\theta}(\mathbf{s}) - \hat{\theta}(0)]^2\rangle$. We verify that in 2D, the above definition yields a zero condensate. Therefore, the quasi-condensate can be considered to act as a well-defined condensate as far as the system size L is much smaller than the correlation length of the algebraic decay,

$$L \ll R_C e^{n_{qc}\lambda_T^2} . \tag{C.25}$$

C.2 Quasi-condensate Popov theory

The modified Popov theory for the 2D Bose gas was introduced independently by Svistunov [104, 105] and Anderson et al. [160, 161], as a modification of the Popov theory to include the effects of phase fluctuations and thus, the description of the quasi-condensate.

C.2.1 Formalism

We here follow the derivation of Anderson et al., and start from the field operator Eq. (C.3). This is just the Bogoliubov ansatz in which the condensate density has been replaced by the quasi-condensate density. Therefore, by applying the same perturbative approach as in Sec. A.1.1, we naturally find the same expressions (A.6) and (A.8) for the the non-(quasi)condensate density and the chemical potential:

$$\tilde{n} = \frac{1}{V}\sum_{\mathbf{k}} \left[\left(\frac{\varepsilon_{\mathbf{k}} + gn_{qc}}{2E_{\mathbf{k}}} - \frac{1}{2} \right) + \frac{\varepsilon_{\mathbf{k}} + gn_{qc}}{E_{\mathbf{k}}} f(E_{\mathbf{k}}) \right] , \tag{C.26}$$

$$\mu = gn_{qc} + \frac{g}{V}\sum_{\mathbf{k}} \left[\left(\frac{2\varepsilon_{\mathbf{k}} + gn_{qc}}{2E_{\mathbf{k}}} - 1 \right) + \frac{2\varepsilon_{\mathbf{k}} + gn_{qc}}{E_{\mathbf{k}}} f(E_{\mathbf{k}}) \right] . \tag{C.27}$$

where following the notation of Ref. [160], we have replaced Λ by gn_{qc} in order to obtain a gapless Bogoliubov spectrum.

In the above expressions, the momentum sums exhibit an infrared divergent behavior, in accordance with the Hohenberg-Mermin-Wagner theorem [13, 73]. To overcome this problem, we can resort to two methods. The first one, is to consider that we are in the temperature regime where the HF approximation $E_{\mathbf{k}} \simeq \varepsilon_{\mathbf{k}} +$

gn_{qc} can be performed. Such approximation clearly removes the soft mode of the spectrum and one immediately obtains

$$\mu^{\rm HF} = gn_{qc}^{\rm HF} + 2g\tilde{n}^{\rm HF}\,, \tag{C.28}$$

$$\tilde{n}^{\rm HF} = -\frac{1}{\lambda_T^2}\ln\left(1 - e^{-\beta g n_{qc}^{\rm HF}}\right)\,. \tag{C.29}$$

In the temperature region where $k_BT \gg gn$, one can further simplify the thermal density as

$$\tilde{n}^{\rm HF} \simeq -\frac{1}{\lambda_T^2}\ln\left(\frac{gn_{qc}^{\rm HF}}{k_BT}\right)\,. \tag{C.30}$$

The second approach, adopted in the original work by Anderson et al., is to notice that in the quasi-condensate formalism, the infrared divergence is in fact artificial, arising from a wrong treatment of the phase fluctuations. Indeed, in deriving Eqs. (C.26) and (C.27), we have used the Bogoliubov ansatz and applied the perturbative scheme. The resulting quadratic terms in the fluctuations are (see Eqs. (C.2) and (C.3)):

$$\delta\hat{\Psi}^\dagger(\mathbf{r})\delta\hat{\Psi}(\mathbf{r}) \simeq n_{qc}\hat{\theta}(\mathbf{r})\hat{\theta}(\mathbf{r}) + \frac{1}{4n_{qc}}\delta\hat{n}^\dagger(\mathbf{r})\delta\hat{n}(\mathbf{r})\,, \tag{C.31}$$

with quadratic terms in both the density and phase fluctuations. However, it is clear that in an exact approach, $n = \langle\hat{\Psi}^\dagger(\mathbf{r})\hat{\Psi}(\mathbf{r})\rangle$ and

$$\langle e^{-i\hat{\theta}(\mathbf{r})}e^{i\hat{\theta}(\mathbf{r})}\rangle = 1 + \langle\hat{\theta}(\mathbf{r})\hat{\theta}(\mathbf{r})\rangle + \cdots = 1\,, \tag{C.32}$$

so that phase fluctuations will not contribute to any local quantities. Therefore, one needs to subtract the quadratic contributions of phase fluctuations from Eqs. (C.26) and (C.27). We have already calculated this quantity in the previous section, and from Eq. (C.14) we find that one needs to subtract

$$n_{qc}\langle\hat{\theta}(\mathbf{r})\hat{\theta}(\mathbf{r})\rangle = \sum_{\mathbf{k}}\frac{gn_{qc}}{2E_{\mathbf{k}}}\left(2f(E_{\mathbf{k}}) + 1\right)\,. \tag{C.33}$$

Then, the chemical potential and the condensate depletion within the modified Popov theory are found to be [160]

$$\mu = gn_{qc} + 2g\tilde{n}\,, \tag{C.34}$$

$$\tilde{n} = \frac{1}{V}\sum_{\mathbf{k}}\left[\left(\frac{\varepsilon_{\mathbf{k}}}{2E_{\mathbf{k}}} - \frac{1}{2}\right) + \frac{\varepsilon_{\mathbf{k}}}{E_{\mathbf{k}}}f(E_{\mathbf{k}})\right]\,. \tag{C.35}$$

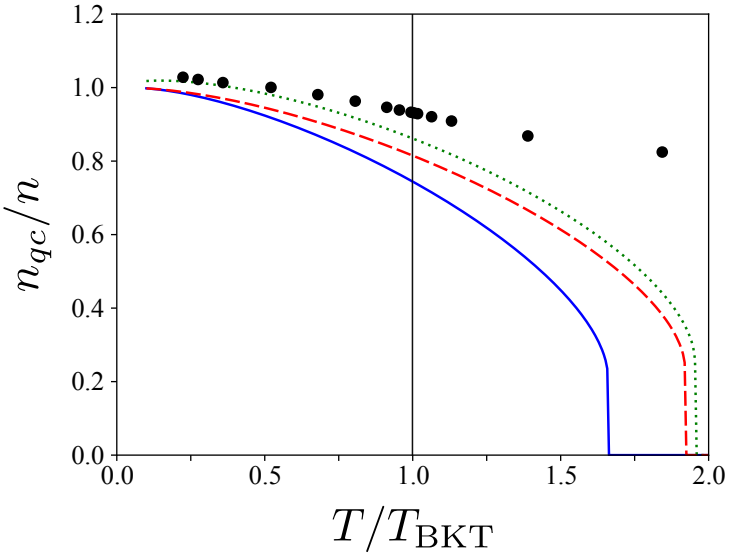

Figure C.1: Quasi-condensate density n_{qc}/n, evaluated for $\tilde{g} = 0.16$. The blue solid line is the Hartree-Fock theory result Eq. (C.29), the red dashed and green dotted lines are the predictions of Popov theory, using Eq. (C.35) and Eq. (C.36), respectively. the black dots are universal relations result from Ref. [83].

Like in 3D, quantum fluctuations lead to an ultraviolet divergence of $\tilde{n}$, which has to be removed by a proper renormalization of the coupling constant. For simplicity, we will not consider its contribution in what follows.

Equation (C.35) in the absence of quantum fluctuations can be solved straightforwardly if we recall the classical field approximation for the distribution function. Then, one finds:

$$\tilde{n} \simeq -\frac{1}{\lambda_T^2} \ln\left(\frac{2gn_{qc}}{k_B T}\right) . \tag{C.36}$$

The above expression, together with Eq. (C.34), constitute the equation of state, used in Sec. 3.2 for the description of the universal thermodynamics in a 2D Bose gas. We note that Eq. (C.36) is very similar to the HF prediction (C.30). These expressions for the non-condensate density suggest that the concept of quasi-condensate is meaningful in an interacting gas only. Similarly, we anticipate that mean-field based approaches will fail in the region where the quasi-condensate vanishes, since the thermal atoms density diverges for $n_{\mathrm{qc}} \to 0$.

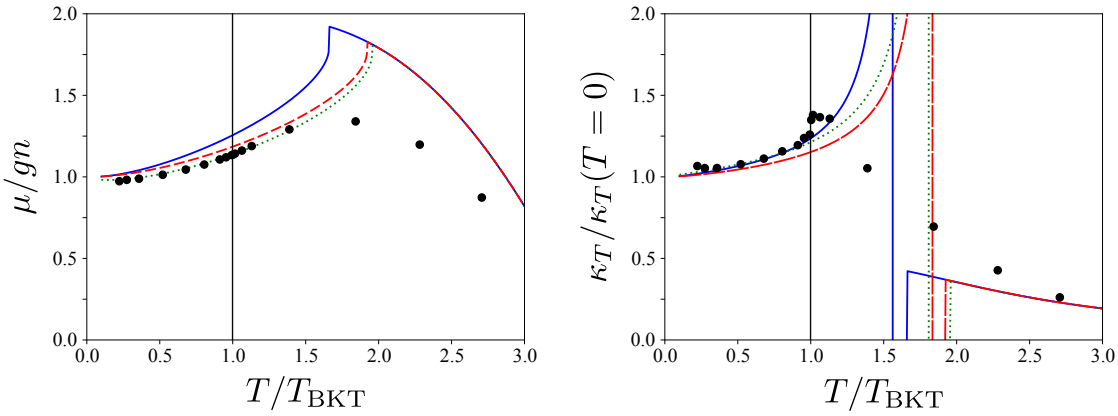

Figure C.2: Left panel: chemical potential of 2D Bose gas evaluated for $\tilde{g} = 0.16$. Right panel: isothermal compressibility. The blue solid line is the Hartree-Fock theory result. The red dashed line is the Popov theory prediction, and the green dotted line its universal part. The black dots are universal relations result from Ref. [83].

C.2.2 Comparative study of different theories

We show in Fig. C.1 the quasi-condensate density as a function of temperature, for the weakly interacting 2D Bose gas, with the dimensionless coupling constant $\tilde{g} = 0.16$. Interestingly, the quasi-condensate is found to be close to unity for a wide region of temperature, including the normal region above T_{BKT}. Both the HF (C.30) and modified Popov theory (C.35) predictions lie close to the universal relations result of [82] in the superfluid regime, however the mean-field based theories decrease rapidly as one increases the temperature. Eventually, Eqs. (C.30) and (C.35) do not provide any solutions around $T \sim 2T_{\mathrm{BKT}}$, leading to an unphysical jump of n_{qc}.

Figure C.2 shows the chemical potential and the isothermal compressibility. Again, the similitude between the three approaches are remarkable below the critical temperature. However, the chemical potential calculated in the mean-field theories is predicted to increase up to $\mu = 2gn$, in an analogous way to the 3D case, while for the UR, $\mu \leq 1.25gn$. More drastic is the compressibility, which in the UR description, exhibits a continuous evolution at the critical point and smoothly decreases above T_{BKT}, whereas the mean-field methods predict an erroneous divergence. This behavior is again identical to the 3D result (see Fig. 2.5) and comes from the vanishing quasi-condensate. Indeed, for the HF and Popov

theories, a simple expression for the compressibility can be obtained:

$$\frac{\kappa_T}{\kappa_T(T=0)} = 1 + \frac{1}{\lambda_T^2 n_{qc} - 2}\,. \tag{C.37}$$

The above expression is model-independent, reflecting the universal nature of the system. We have verified that also the universal relations satisfies this relationship, at least below T_{BKT} where the quasi-condensate is well-defined.

The above analysis suggests that the analogy between quasi-condensate and genuine condensate is valid for $T < T_{\mathrm{BKT}}$ only. This was expected since, in the normal regime, free vortices destroying phase-fluctuations appear, spoiling the quasi-condensate picture (see Sec. 3.1.2).

Appendix D

Study of the 2D RPA response function

In this appendix, we sketch the development of the theoretical tools used for the investigation of the collisionless sound waves in the 2D Bose gas, discussed in Chap. 3. We start from the study of the response of a damped harmonic oscillator, which is used to fit the RPA response in order to extract the sound velocity in Sec. 3.4.3. Then, we analyze the pole of the 2D RPA response function and evaluate the analytical expression for the complex pole.

D.1 Response of a harmonic oscillator

The equation of motion for a damped harmonic oscillator in presence of an external force $F(t)$ is given by,

$$\ddot{x} + \omega_0^2 x + \gamma \dot{x} = \frac{F(t)}{m}, \tag{D.1}$$

with ω_0 the natural frequency and γ the damping constant. Looking for plane-wave solution in the form $x = x_0 + \delta x e^{-i\omega t}$, the equation of motion gives,

$$\delta x(t) = \frac{F(t)/m}{\omega_0^2 - \omega^2 - i\omega\gamma}, \tag{D.2}$$

from which one can extract the response function defined as $\delta x = F(t)\chi(\omega)/m$ [1],

$$\chi(\omega) = \frac{1}{\omega_0^2 - \omega^2 - i\omega\gamma}. \tag{D.3}$$

[1] We adopt the same sign convention as the study of the two-dimensional Bose gas, both for the plane-wave solution and the response function.

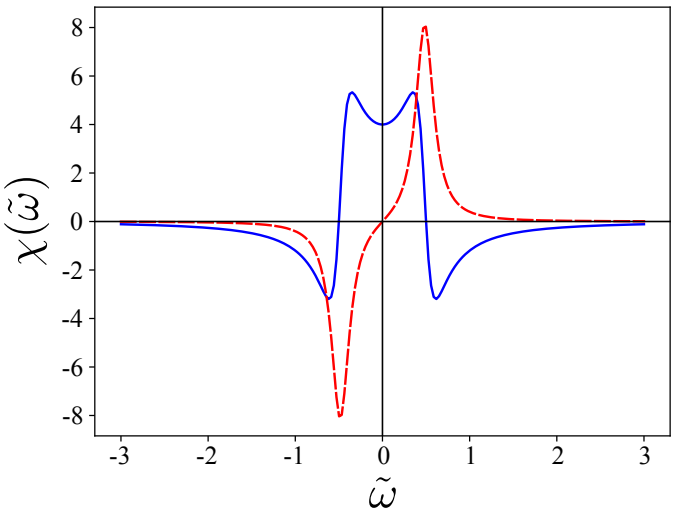

Figure D.1: Real and imaginary part of the damped harmonic oscillator response function (D.1), in blue and red lines, respectively. The oscillator parameters are $\omega_0 = 0.5$ and $\gamma = 0.25$ (arbitrary units).

The poles of the response function are:

$$\omega_{1,2} = -i\frac{\gamma}{2} \pm \sqrt{\omega_0^2 - \frac{\gamma^2}{4}}. \tag{D.4}$$

For a direct comparison with the 2D Bose gas, we will only consider the situation where the inequality $\omega_0 > \gamma/2$ holds. This situation corresponds to the under-damped harmonic oscillator. The real and imaginary parts of Eq. (D.3) are given by,

$$\chi'(\omega) = \frac{\omega_0^2 - \omega^2}{(\omega^2 - \omega_0^2)^2 + \omega^2\gamma^2}, \tag{D.5}$$

$$\chi''(\omega) = \frac{\omega\gamma}{(\omega^2 - \omega_0^2)^2 + \omega^2\gamma^2}. \tag{D.6}$$

Figure D.1 shows the numerical results for the real and imaginary part of the response function, for an arbitrary set of oscillator parameters.

As we have seen in Sec. 3.4.3, the quantity reliable for the investigation of the experiment of Ref. [17], corresponds to the imaginary part of the inverse weighted response function. From Eq. (D.6), it is given by

$$\frac{\chi''(\omega)}{\omega} = \frac{\gamma}{(\omega^2 - \omega_0^2)^2 + \omega^2\gamma^2}. \tag{D.7}$$

Let us calculate its Fourier transform:

$$\mathcal{F}^{-1}\left[\chi''(\omega)/\omega\right](t) = \frac{1}{2\pi}\int_{-\infty}^{\infty} \frac{\gamma}{(\omega^2-\omega_0^2)^2+\omega^2\gamma^2} e^{i\omega t} d\omega. \tag{D.8}$$

First, the denominator can be factorized as,

$$(\omega^2-\omega_0^2)^2+\omega^2\gamma^2 = (\omega-\omega_1)(\omega+\omega_1)(\omega-\omega_2)(\omega+\omega_2), \tag{D.9}$$

where $\omega_{1,2}$ are the poles of χ defined in Eq. (D.4). Then one can decompose the denominator as a sum over these factors,

$$\begin{aligned}\frac{1}{(\omega^2-\omega_0^2)^2+\omega^2\gamma^2} = \frac{1}{2}\frac{1}{\omega_1^2-\omega_2^2}\Bigg[&\frac{1}{\omega_1}\left(\frac{1}{\omega-\omega_1}-\frac{1}{\omega+\omega_1}\right)\\ &-\frac{1}{\omega_2}\left(\frac{1}{\omega-\omega_2}-\frac{1}{\omega+\omega_2}\right)\Bigg].\end{aligned} \tag{D.10}$$

We note that $\omega_2 = -\omega_1^*$, where * denotes the complex conjugate, and we introduce the following new variables,

$$\tilde{\omega} = \sqrt{\omega_0^2 - \frac{\gamma^2}{4}}, \qquad \Gamma = \gamma/2, \tag{D.11}$$

so that $\omega_1 = \tilde{\omega} - i\Gamma$. Equation (D.8) is rewritten as,

$$\begin{aligned}\mathcal{F}^{-1}\left[\chi''(\omega)/\omega\right](t) = \frac{i}{4\tilde{\omega}}\Bigg\{&\frac{1}{\omega_1}\left[\mathcal{F}^{-1}\left(\frac{1}{\omega-\omega_1}\right)-\mathcal{F}^{-1}\left(\frac{1}{\omega+\omega_1}\right)\right]\\ &+\frac{1}{\omega_1^*}\left[\mathcal{F}^{-1}\left(\frac{1}{\omega+\omega_1^*}\right)-\mathcal{F}^{-1}\left(\frac{1}{\omega-\omega_1^*}\right)\right]\Bigg\}.\end{aligned} \tag{D.12}$$

We can now evaluate easily each Fourier transform, using Cauchy's integral formula,

$$\begin{aligned}\mathcal{F}^{-1}\left(\frac{1}{\omega-\omega_1}\right)-\mathcal{F}^{-1}\left(\frac{1}{\omega+\omega_1}\right) &= \frac{1}{2\pi}\left(\oint_C - \int_{\text{arc}}\right)\left(\frac{e^{i\omega t}}{\omega-\omega_1}-\frac{e^{i\omega t}}{\omega+\omega_1}\right)\\ &= -ie^{-i\omega_1 t} - \frac{\omega_1}{\pi}\int_{\text{arc}}\frac{e^{i\omega t}}{\omega^2-\omega_1^2}\\ &= -ie^{-i\omega_1 t}\end{aligned} \tag{D.13}$$

where the contour integrals have been evaluated using the residue theorem, assuming positive time ($t \geq 0$) to restrict the contour to the upper-half complex plane.

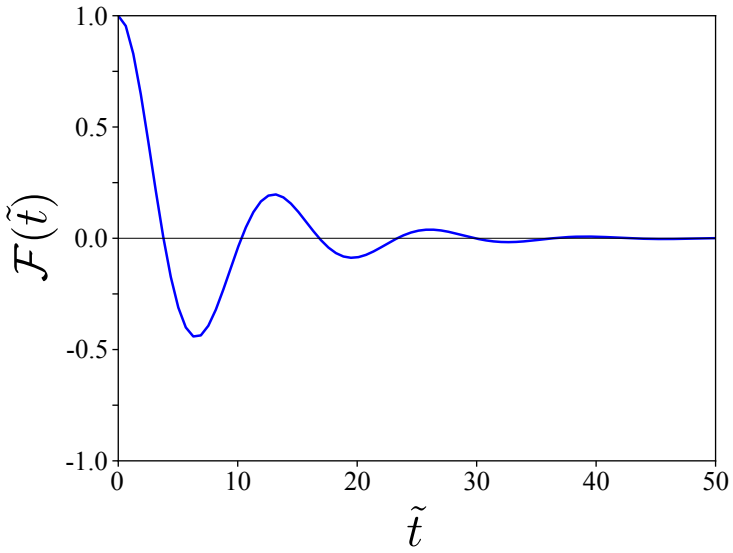

Figure D.2: Fourier transform of inverse-weighted response function, $\mathcal{F}^{-1}(\chi''/\omega)(t)$, for the damped harmonic oscillator (D.15). The oscillator parameters are $\omega_0 = 0.5$ and $\gamma = 0.25$.

As for the last line, we used the estimation lemma. By doing the same for the second line of Eq. (D.12), one obtains,

$$\begin{aligned}\mathcal{F}^{-1}\left[\frac{\chi''(\omega)}{\omega}\right](t) &= \frac{1}{4\tilde{\omega}}\frac{1}{\omega_1\omega_1^*}\left(\omega_1^* e^{-i\omega_1 t} + \omega_1 e^{i\omega_1^* t}\right) \\ &= \frac{1}{4\tilde{\omega}}\frac{1}{\tilde{\omega}^2+\Gamma^2}\left[(\tilde{\omega}+i\Gamma)e^{-i(\tilde{\omega}-i\Gamma)t} + (\tilde{\omega}-i\Gamma)e^{i(\tilde{\omega}+i\Gamma)t}\right]. \quad \text{(D.14)}\end{aligned}$$

Finally, using trigonometric relation,

$$\mathcal{F}^{-1}\left[\frac{\chi''(\omega)}{\omega}\right](t) = \frac{1}{2\tilde{\omega}}\frac{1}{\tilde{\omega}^2+\Gamma^2}e^{-\Gamma t}\left[\tilde{\omega}\cos(\tilde{\omega}t) + \Gamma\sin(\tilde{\omega}t)\right]. \quad \text{(D.15)}$$

Figure D.2 shows the obtained Fourier transform. It is worth noticing that Eq. (D.15) contains a sine-function, for which its relative contribution becomes greater as the damping becomes important. For our analysis of the sound wave in the 2D Bose gas, this means that we have to avoid the fitting of the Fourier transform of the RPA response function to the simplest $e^{-\Gamma t}\cos(\omega t)$ model, and use a function which takes into account this sine-function contribution.

It is interesting to observe that the Fourier transform of χ''/ω oscillates at the same frequency as the real part of the poles of the response function, $\tilde{\omega} = \sqrt{\omega_0^2 - \gamma^2/4}$. On the other hand, the position of the peaks of χ'' and χ''/ω are

given respectively by,

$$\omega_{\mathrm{Peaks},\chi''} = \pm\left[\frac{1}{6}\left(2\omega_0^2 - \gamma^2 + \sqrt{(2\omega_0^2-\gamma^2)^2 + 12\omega_0^4}\right)\right]^{1/2}, \tag{D.16}$$

$$\omega_{\mathrm{Peaks},\chi''/\omega} = \pm\sqrt{\omega_0^2 - \frac{\gamma^2}{2}}, \tag{D.17}$$

which are both different from $\tilde{\omega}$. This analysis confirms that in order to study the poles of the response function (and hence the sound velocity), looking at the peak position of χ'' or χ''/ω is not sufficient, and one needs to go to the Fourier analysis.

D.2 Poles study

We now calulcate the pole of the 2D Bose RPA response function (3.35), by means of the classical field approximation introduced in App. C. The idea is to calculate the pole of the RPA response function by approximating the Bose distribution function by:

$$f(w) = \frac{1}{e^{w^2+\eta}-1} \simeq \frac{1}{w^2+\eta}\,, \tag{D.18}$$

where $\mathbf{w} = \mathbf{p}/\sqrt{2mk_BT}$ and $\eta = \beta\Lambda$.

The expression for the RPA response function reads (dimensionless form)

$$\chi = \frac{\chi_0}{1+\tilde{g}\chi_0} \tag{D.19}$$

where the response function for the non-interacting system is given by using the approximation (D.18) into the expression (3.39):

$$\chi_0\left(u = \frac{\omega}{k}\sqrt{\frac{m}{2k_BT}}\right) \simeq \frac{1}{(2\pi)^2}\left(\int_0^\infty \frac{\mathrm{d}w_x}{w_x-u}\frac{\pi w_x}{(w_x^2+\eta)} + i\pi^2\frac{u}{(u^2+\eta)^{3/2}}\right) \tag{D.20}$$

Then, introducing the variables $z = \sqrt{\eta}w_x$ and $\epsilon = \sqrt{\eta}/u$, the real part of (D.20) reads

$$\begin{aligned}
\chi_0'(u) &= \frac{1}{(2\pi)^2}\frac{\pi}{u\sqrt{\eta}}\int_{-\infty}^{\infty}\frac{zdz}{(z^2+1)^{3/2}}\frac{1}{z\epsilon-1} \\
&= \frac{1}{(2\pi)^2}\frac{\pi}{u\sqrt{\eta}}\int_0^\infty \frac{z}{(z^2+1)^{3/2}}\left[\frac{1}{1+z\epsilon} - \frac{1}{1-z\epsilon}\right]dz \qquad \text{(D.21)} \\
&= \frac{1}{(2\pi)^2}\frac{\pi}{u\sqrt{\eta}}I_0 \qquad \text{(D.22)}
\end{aligned}$$

We now separate the integration into two parts,

$$I_0 = \int_0^{z_1} ... + \int_{z_1}^{\infty} ... = I_1 + I_2, \qquad 1 \ll z_1 \ll 1/\epsilon.$$

The first integral gives

$$\begin{aligned} I_1 &= \int_0^{z_1} \frac{z}{(z^2+1)^{3/2}} \left[\frac{1}{1+z\epsilon} - \frac{1}{1-z\epsilon}\right] dz \\ &\approx -2\epsilon \int_0^{z_1} \frac{z^2 dz}{(z^2+1)^{3/2}}. \end{aligned} \tag{D.23}$$

This integral can be solved by part and in the limit of $z_1 \gg 1$ one gets

$$I_1 \simeq 2\epsilon \left[1 - \ln(2z_1)\right]. \tag{D.24}$$

As for the second integral

$$\begin{aligned} I_2 &= \int_{z_1}^{\infty} \frac{z}{(z^2+1)^{3/2}} \left[\frac{1}{1+z\epsilon} - \frac{1}{1-z\epsilon}\right] dz \\ &\approx \int_{z_1}^{\infty} \frac{dz}{z^2} \left[\frac{1}{1+z\epsilon} - \frac{1}{1-z\epsilon}\right]. \end{aligned} \tag{D.25}$$

The integral can be solved from a change of variables (putting $u = 1/(z\epsilon)$), and gives

$$\begin{aligned} I_2 &= \epsilon \left[\frac{1}{z_1\epsilon} - \ln\left(\frac{1}{z_1\epsilon}+1\right) - \frac{1}{z_1\epsilon} - \ln\left(\frac{1}{z_1\epsilon}-1\right)\right] \\ &= \epsilon \left[2\ln(z_1\epsilon) - \ln(1+z_1\epsilon) - \ln(1-z_1\epsilon)\right] \\ &\approx 2\epsilon \ln(z_1\epsilon) \end{aligned} \tag{D.26}$$

where we have used $z_1\epsilon \ll 1$ in the last line. From Eqs. (D.24) and (D.26) one has

$$I_0 = I_1 + I_2 = 2\epsilon \left[1 - \ln\left(\frac{2}{\epsilon}\right)\right]. \tag{D.27}$$

Using this result, one finally has the following pole equation:

$$1 + \tilde{g}\left\{\frac{1}{2\pi u^2}\left[1 - \ln(2u) + \frac{1}{2}\ln\eta\right] + i\frac{1}{4}\frac{u}{(u^2+\eta)^{3/2}}\right\} = 0. \tag{D.28}$$

Assuming a complex pole in the form $u_{\text{pole}} = u - i\gamma$, one obtains the following set of equations

$$\begin{cases} u^2 - \gamma^2 + \frac{\tilde{g}}{2\pi}\left[1 - \frac{1}{2}\ln((2u)^2 + (2\gamma)^2) + \frac{1}{2}\ln\eta\right] &= 0, \\ -2u\gamma - \frac{\tilde{g}}{2\pi}\arctan\left(\frac{-\gamma}{u}\right) + \frac{\tilde{g}}{4} &= 0. \end{cases} \tag{D.29}$$

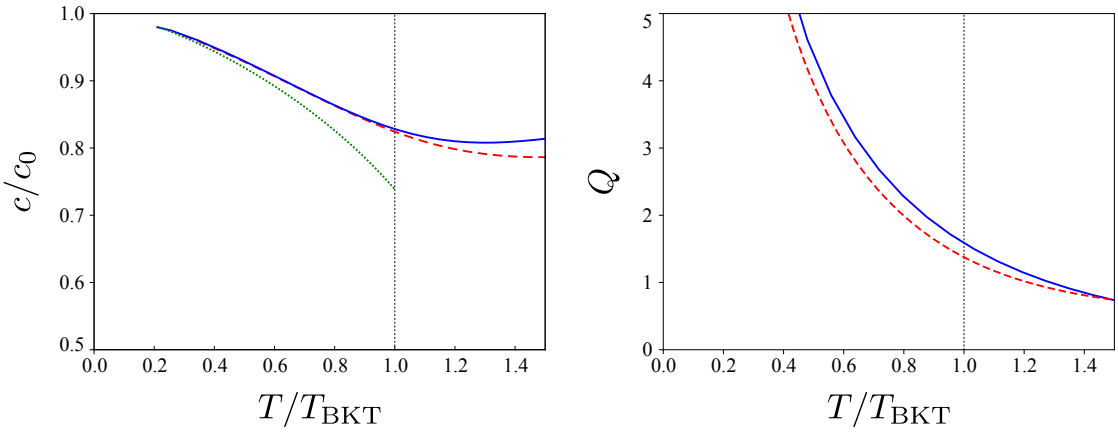

Figure D.3: Left panel: sound velocity evaluated from the response function. The red dashed line is the real part of the pole evaluated from Eq. (D.29), the blue solid line the sound velocity extracted from the Fourier transform of the response function (see Sec. 3.4.3). The green dotted-line corresponds to the $T \to 0$ asymptotic expression Eq. (D.30). Right panel: quality factor evaluated from the response function. The red dashed line is the prediction from Eq. (D.29), the blue solid line the one extracted from the Fourier transform of the RPA response function.

In Fig. D.3 we show the results for the sound velocity, normalized to the zero-temperature Bogoliubov sound, c/c_0 and the quality factor $Q = u/\gamma$, evaluated by solving Eq. (D.29), for $\tilde{g} = 0.16$. Comparing them with the results obtained in Sec. 3.4.3, from the Fourier transform of the inverse-weighted RPA response function, we see that both approaches are consistent, giving almost the same sound velocity and the same behaviour for the quality factor.

We note that in the very low-temperature region where the quality factor is large (see right panel Fig. D.3), one can neglect the imaginary part γ in the first line of Eq. (D.29), yielding the result

$$u^2 + \frac{\tilde{g}}{2\pi}\left[1 - \ln(2u) + \frac{1}{2}\ln\eta\right] = 0\,. \tag{D.30}$$

Solution of Eq. (D.30) is plotted as a green dotted line in Fig. D.3 [2]. In the limit of $T \to 0$, this equation is further simplified to $u^2 = -\frac{\tilde{g}}{4\pi}\ln\eta$. Then, from the

[2]We briefly note that a solution for Eq. (D.30) exists only if the minimum of the function (which possesses a positive concavity) is larger than zero. The derivative gives the position of this minimum to be at $u_{\mathrm{min}} = \sqrt{\tilde{g}/(2\pi)}$, and it follows that Eq. (D.30) possesses a solution only

number equation evaluated using Eq. (D.18),

$$n = \frac{mk_BT}{2\pi\hbar^2}\int f_0(w)\mathrm{d}^2w \approx -\frac{mk_BT}{2\pi\hbar^2}\ln\eta\,, \tag{D.32}$$

one finally recovers the Bogoliubov speed of sound

$$mc^2 = g_{2D}n\,, \tag{D.33}$$

where we have used that $u = c\sqrt{m/(2k_BT)}$ and $g_{2D} = \tilde{g}\hbar^2/m$.

---

if

$$\eta \leq \frac{\tilde{g}}{\pi}\frac{1}{e^3}\,. \tag{D.31}$$

Bibliography

[1] L. D. Landau and E. M. Lifshitz, *Fluid Mechanics* (Pergamon Press, Oxford, 1987).

[2] M. H. Anderson, J. R. Ensher, M. R. Matthews, C. E. Wieman, and E. A. Cornell, Science **269**, 198 (1995).

[3] K. B. Davis, M. O. Mewes, M. R. Andrews, N. J. van Druten, D. S. Durfee, D. M. Kurn, and W. Ketterle, Physical Review Letters **75**, 3969 (1995).

[4] F. Dalfovo, S. Giorgini, L. P. Pitaevskii, and S. Stringari, Reviews of Modern Physics **71**, 463 (1999).

[5] S. Giorgini, Physical Review A **61**, 063615 (2000).

[6] I. Bloch, J. Dalibard, and W. Zwerger, Reviews of Modern Physics **80**, 885 (2008).

[7] L. P. Pitaevskii and S. Stringari, *Bose-Einstein Condensation and Superfluidity* (Oxford University Press, Oxford, 2016).

[8] L. D. Landau, Physical Review **60**, 356 (1941).

[9] L. P. Pitaevskii and S. Stringari, in *Universal Themes of Bose-Einstein Condensation*, edited by D. W. Snoke, N. P. Proukakis, and P. B. Littlewood, chap. 16, pp. 322–347, Cambridge University Press, Cambridge, 2017.

[10] R. J. Donnelly, Physics Today **62**, 34 (2009).

[11] L. a. Sidorenkov, M. K. Tey, R. Grimm, Y.-H. Hou, L. P. Pitaevskii, and S. Stringari, Nature **498**, 78 (2013).

[12] Z. Hadzibabic and J. Dalibard, Rivista del Nuovo Cimento **34**, 389 (2011).

[13] N. D. Mermin and H. Wagner, Physical Review Letters **17**, 1133 (1966).

[14] V. . L. Berezinskii, Journal of Experimental and Theoretical Physics **34**, 610 (1972).

[15] J. M. Kosterlitz and D. J. Thouless, Journal of Physics C: Solid State Physics **6**, 1181 (1973).

[16] T. Ozawa and S. Stringari, Physical Review Letters **112**, 025302 (2014).

[17] J. L. Ville, R. Saint-Jalm, É. Le Cerf, M. Aidelsburger, S. Nascimbène, J. Dalibard, and J. Beugnon, Physical Review Letters **121**, 145301 (2018).

[18] D. S. Hall, M. R. Matthews, J. R. Ensher, C. E. Wieman, and E. A. Cornell, Physical Review Letters **81**, 1539 (1998).

[19] J. Stenger, S. Inouye, D. M. Stamper-Kurn, H.-J. Miesner, A. P. Chikkatur, and W. Ketterle, Nature **396**, 345 (1998).

[20] M. Ota and S. Stringari, Physical Review A **97**, 033604 (2018).

[21] M. Ota, F. Larcher, F. Dalfovo, L. P. Pitaevskii, N. P. Proukakis, and S. Stringari, Physical Review Letters **121**, 145302 (2018).

[22] M. Ota, S. Giorgini, and S. Stringari, Physical Review Letters **123**, 075301 (2019).

[23] K. Huang, *Statistical Mechanics* (Wiley, New York, 1963).

[24] L. P. Kadanoff and G. Baym, *Quantum Statisical Mechanics* (W.A. Benjamin, New York, 1962).

[25] D. Tong, Lectures on Kinetic Theory, University of Cambridge Lecture Notes, 2012.

[26] L. D. Landau and E. M. Lifshitz, *Physical Kinetics* (Pergamon Press, Oxford, 1981).

[27] C. J. Pethick and H. Smith, *Bose-Einstein Condensation in Dilute Gases* (Cambridge University Press, Cambridge, 2008).

[28] A. L. Fetter and J. D. Walecka, *Quantum Theory of Many-Paricles Systems* (McGraw-Hill, San Francisco, 1971).

[29] M. Naraschewski and R. J. Glauber, Physical Review A **59**, 4595 (1999).

[30] L. D. Landau and E. M. Lifshitz, *Quantum Mechanics* (Pergamon Press, Oxford, 1965).

[31] M. A. Baranov, M. Dalmonte, G. Pupillo, and P. Zoller, Chemical Reviews **112**, 5012 (2012).

[32] C. C. Tannoudji, Condensation de Bose-Einstein des gas atomiques ultra froids: effet des interactions, Collège de France Lecture Notes, 1998.

[33] E. M. Lifshitz and L. P. Pitaevskii, *Statistical Physics Part 2* (Pergamon Press, Oxford, 1981).

[34] N. N. Bogoliubov, J. Phys. USSR **11**, 23 (1947).

[35] T. D. Lee, K. Huang, and C. N. Yang, Physical Review **106**, 1135 (1957).

[36] P. Kapitza, Nature **141**, 74 (1938).

[37] J. F. Allen and A. D. Misener, Nature **141**, 75 (1938).

[38] F. London, Nature **141**, 643 (1938).

[39] L. Tisza, Nature **141**, 913 (1938).

[40] S. Balibar, Journal of Low Temperature Physics **146**, 441 (2007).

[41] E. P. Gross, Il Nuovo Cimento **20**, 454 (1961).

[42] L. P. Pitaevskii, Journal of Experimental and Theoretical Physics **13**, 451 (1961).

[43] V. I. Yukalov, Laser Physics Letters **4**, 632 (2007).

[44] G. Rickayzen, *Green's Functions and Condensed Matter* (Academic Press, London, 1991).

[45] P. Nozières and D. Pines, *Theory of Quantum Liquids Vol. 1* (Addison-Wesley, California, 1990).

[46] A. Griffin, T. Nikuni, and E. Zaremba, *Bose-Condensed Gases at Finite Temperatures* (Cambridge University Press, Cambridge, 2009).

[47] E. A. Uehling and G. E. Uhlenbeck, Physical Review **43**, 552 (1933).

[48] T. Nikuni, E. Zaremba, and A. Griffin, Physical Review Letters **83**, 10 (1999).

[49] E. Zaremba, Physical Review A **57**, 518 (1998).

[50] E. Zaremba, T. Nikuni, and A. Griffin, Journal of Low Temperature Physics Nos **1164** (1999).

[51] T. Nikuni and A. Griffin, Journal of Low Temperature Physics **111** (1998).

[52] S. J. Rooney, P. B. Blakie, and A. S. Bradley, Physical Review A **86**, 053634 (2012).

[53] R. N. Bisset, M. J. Davis, T. P. Simula, and P. B. Blakie, Physical Review A **79**, 033626 (2009).

[54] P. B. Blakie, A. S. Bradley, M. J. Davis, R. J. Ballagh, and C. W. Gardiner, Advances in Physics **57**, 363 (2008).

[55] M. R. Andrews, D. M. Kurn, H.-J. Miesner, D. S. Durfee, C. G. Townsend, S. Inouye, and W. Ketterle, Physical Review Letters **79**, 553 (1997).

[56] R. Meppelink, S. B. Koller, and P. van der Straten, Physical Review A **80**, 043605 (2009).

[57] A. L. Gaunt, T. F. Schmidutz, I. Gotlibovych, R. P. Smith, and Z. Hadzibabic, Physical Review Letters **110**, 200406 (2013).

[58] R. Lopes, C. Eigen, N. Navon, D. Clément, R. P. Smith, and Z. Hadzibabic, Physical Review Letters **119**, 190404 (2017).

[59] S. J. Garratt, C. Eigen, J. Zhang, P. Turzák, R. Lopes, R. P. Smith, Z. Hadzibabic, and N. Navon, Physical Review A **99**, 021601 (2019).

[60] W. Ketterle and M. W. Zwierlein, Rivista del Nuovo Cimento **31**, 247 (2008).

[61] S. Nascimbène, N. Navon, K. J. Jiang, F. Chevy, and C. Salomon, Nature **463**, 1057 (2010).

[62] N. Navon, S. Nascimbène, F. Chevy, and C. Salomon, Science **328**, 729 (2010).

[63] M. J. H. Ku, A. T. Sommer, L. W. Cheuk, and M. W. Zwierlein, Science **335**, 563 (2012).

[64] Y.-H. Hou, L. P. Pitaevskii, and S. Stringari, Physical Review A **88**, 043630 (2013).

[65] Z. Hadzibabic, P. Krüger, M. Cheneau, B. Battelier, and J. Dalibard, Nature **441**, 1118 (2006).

[66] R. Desbuquois, L. Chomaz, T. Yefsah, J. Léonard, J. Beugnon, C. Weitenberg, and J. Dalibard, Nature Physics **8**, 645 (2012).

[67] L.-C. Ha, C.-L. Hung, X. Zhang, U. Eismann, S.-K. Tung, and C. Chin, Physical Review Letters **110**, 145302 (2013).

[68] R. Desbuquois, T. Yefsah, L. Chomaz, C. Weitenberg, L. Corman, S. Nascimbène, and J. Dalibard, Physical Review Letters **113**, 020404 (2014).

[69] V. Makhalov, K. Martiyanov, and A. Turlapov, Physical Review Letters **112**, 045301 (2014).

[70] P. A. Murthy et al., Physical Review Letters **115**, 010401 (2015).

[71] K. Hueck, N. Luick, L. Sobirey, J. Siegl, T. Lompe, and H. Moritz, Physical Review Letters **120**, 060402 (2018).

[72] P. Dyke et al., Physical Review A **93**, 011603 (2016).

[73] P. C. Hohenberg, Physical Review **158**, 383 (1967).

[74] V. N. Popov, Theoretical and Mathematical Physics **11**, 565 (1972).

[75] D. S. Fisher and P. C. Hohenberg, Physical Review B **37**, 4936 (1988).

[76] J. Levinsen and M. M. Parish, Annual Review of Cold Atoms and Molecules **3**, 71 (2015).

[77] N. P. Proukakis and B. Jackson, Journal of Physics B **41**, 203002 (2008).

[78] G. Baym, J.-P. Blaizot, M. Holzmann, F. Laloë, and D. Vautherin, Physical Review Letters **83**, 1703 (1999).

[79] P. Arnold and G. Moore, Physical Review Letters **87**, 120401 (2001).

[80] S. Pilati, S. Giorgini, and N. Prokof'ev, Physical Review Letters **100**, 140405 (2008).

[81] N. Prokof'ev, O. Ruebenacker, and B. Svistunov, Physical Review Letters **87**, 270402 (2001).

[82] N. Prokof'ev and B. Svistunov, Physical Review A **66**, 043608 (2002).

[83] N. Prokof'ev, O. Ruebenacker, and B. Svistunov, Physical Review A **69**, 053625 (2004).

[84] L. D. Landau, E. M. Lifshitz, and L. P. Pitaevskii, *Statistical Physics Part 1* (Pergamon Press, Oxford, 1980).

[85] L. Verney, L. P. Pitaevskii, and S. Stringari, Europhysics Letters **111**, 40005 (2015).

[86] H. Hu, E. Taylor, X.-J. Liu, S. Stringari, and A. Griffin, New Journal of Physics **12**, 043040 (2010).

[87] A. Minguzzi and M. P. Tosi, Journal of Physics: Condensed Matter **9**, 10211 (1997).

[88] P. Nozières and D. Pines, *Theory of Quantum Liquids Vol. 2* (Addison-Wesley, California, 1990).

[89] A. Griffin, *Excitations in a Bose-Condensed Liquid* (Cambridge University Press, Cambridge, 1993).

[90] L. P. Pitaevskii and S. Stringari, Physics Letters A **235**, 398 (1997).

[91] V. Pastukhov, Journal of Physics A **48**, 405002 (2015).

[92] A. Griffin and E. Zaremba, Physical Review A **56**, 4839 (1997).

[93] C. Mora and Y. Castin, Physical Review A **67**, 053615 (2003).

[94] J. Dalibard, Fluides quantiques de basse dimension et transition de Kosterlitz-Thouless, Collège de France Lecture Notes, 2016.

[95] K. W. Madison, F. Chevy, W. Wohlleben, and J. Dalibard, Physical Review Letters **84**, 806 (2000).

[96] M. R. Matthews, B. P. Anderson, P. C. Haljan, D. S. Hall, C. E. Wieman, and E. A. Cornell, Physical Review Letters **83**, 2498 (1999).

[97] M. W. Zwierlein, J. R. Abo-Shaeer, A. Schirotzek, C. H. Schunck, and W. Ketterle, Nature **435**, 1047 (2005).

[98] D. R. Nelson and J. M. Kosterlitz, Physical Review Letters **39**, 1201 (1977).

[99] D. J. Bishop and J. D. Reppy, Physical Review Letters **40**, 1727 (1978).

[100] A. I. Safonov, S. A. Vasilyev, I. S. Yasnikov, I. I. Lukashevich, and S. Jaakkola, Physical Review Letters **81**, 4545 (1998).

[101] J. M. Kosterlitz, Journal of Physics C **7**, 1046 (1974).

[102] V. N. Popov, *Functional Integrals in Quantum Field Theory and Statistical Physics* (Reidel, Dordrecht, 1983).

[103] T. Yefsah, R. Desbuquois, L. Chomaz, K. J. Günter, and J. Dalibard, Physical Review Letters **107**, 130401 (2011).

[104] Y. Kagan, B. Svistunov, and G. V. Shlyapnikov, Journal of Theoretical and Experimental Physics **66**, 314 (1987).

[105] Y. Kagan, V. A. Kashurnikov, A. V. Krasavin, N. Prokof'ev, and B. Svistunov, Physical Review A **61**, 043608 (2000).

[106] I. Boettcher et al., Physical Review Letters **116**, 045303 (2016).

[107] L. Salasnich and F. Toigo, Physical Review A **91**, 011604 (2015).

[108] E. R. Anderson and J. E. Drut, Physical Review Letters **115**, 115301 (2015).

[109] L. He, H. Lü, G. Cao, H. Hu, and X.-J. Liu, Physical Review A **92**, 023620 (2015).

[110] B. C. Mulkerin, K. Fenech, P. Dyke, C. J. Vale, X.-J. Liu, and H. Hu, Physical Review A **92**, 063636 (2015).

[111] G. Bighin and L. Salasnich, Physical Review B - Condensed Matter and Materials Physics **93**, 014519 (2016).

[112] A. Cappellaro, F. Toigo, and L. Salasnich, Physical Review A **98**, 043605 (2018).

[113] F. Larcher, *Dynamical excitations in low-dimensional condensates: sound, vortices and quenched dynamics*, PhD thesis, 2018.

[114] F. Zambelli and S. Stringari, Physical Review A **63**, 033602 (2001).

[115] E. Arahata and T. Nikuni, Physical Review A **80**, 043613 (2009).

[116] M.-C. Chung and A. B. Bhattacherjee, New Journal of Physics **11**, 123012 (2009).

[117] R. H. Petrucci, W. S. Harwood, and G. E. Herring, *General Chemistry Principles & Moden Applications*, 9 ed. (Pearson, Toronto, 2007).

[118] G. Baym and C. J. Pethick, in *The Physics of Liquid and Solid Helium*, edited by K. H. Bennemann and J. Ketterson Vol. 2, pp. 123–175, Wiley, New York, 1978.

[119] S. B. Papp, J. M. Pino, and C. E. Wieman, Physical Review Letters **101**, 040402 (2008).

[120] D. J. Mccarron, H. W. Cho, D. L. Jenkin, M. P. Köppinger, and S. L. Cornish, Physical Review A **84**, 11603 (2011).

[121] S. Tojo, Y. Taguchi, Y. Masuyama, T. Hayashi, H. Saito, and T. Hirano, Physical Review A **82**, 033609 (2010).

[122] E. Nicklas, H. Strobel, T. Zibold, C. Gross, B. A. Malomed, P. G. Kevrekidis, and M. K. Oberthaler, Physical Review Letters **107**, 193001 (2011).

[123] T.-L. Ho and V. B. Shenoy, Physical Review Letters **77**, 3276 (1996).

[124] H. Pu and N. P. Bigelow, Physical Review Letters **80**, 1130 (1998).

[125] P. Ao and S. T. Chui, Physical Review A **58**, 4836 (1998).

[126] M. Trippenbach, K. Góral, K. Rzazewski, B. Malomed, and Y. B. Band, Journal of Physics B **33**, 4017 (2000).

[127] P. Öhberg and S. Stenholm, Physical Review A **57**, 1272 (1998).

[128] C.-C. Chien, F. Cooper, and E. Timmermans, Physical Review A **86**, 023634 (2012).

[129] A. Roy and D. Angom, Physical Review A **92**, 011601 (2015).

[130] J. Armaitis, H. Stoof, and R. A. Duine, Physical Review A **91**, 043641 (2015).

[131] K. L. Lee, N. B. Jørgensen, I.-K. Liu, L. Wacker, J. J. Arlt, and N. P. Proukakis, Physical Review A **94**, 013602 (2016).

[132] A. Boudjemâa, Physical Review A **97**, 033627 (2018).

[133] H. Shi, W.-M. Zheng, and S.-T. Chui, Physical Review A **61**, 063613 (2000).

[134] B. Van Schaeybroeck, Physica A **392**, 3806 (2013).

[135] A. Griffin, Physical Review B **53**, 9341 (1996).

[136] T. Bienaimé et al., Physical Review A **94**, 063652 (2016).

[137] E. Fava, T. Bienaimé, C. Mordini, G. Colzi, C. Qu, S. Stringari, G. Lamporesi, and G. Ferrari, Physical Review Letters **120**, 170401 (2018).

[138] L. Viverit, C. J. Pethick, and H. Smith, Physical Review A **61**, 053605 (2000).

[139] D. S. Petrov, Physical Review Letters **115**, 155302 (2015).

[140] T.-L. Ho and Q. Zhou, Nature Physics **6**, 131 (2009).

[141] I. M. Khalatnikov, Journal of Experimental and Theoretical Physics Letters **17**, 386 (1973).

[142] Y.-J. Lin, K. Jiménez-García, and I. B. Spielman, Nature **471**, 83 (2011).

[143] H. Zhai, Reports on Progress in Physics **78**, 026001 (2015).

[144] I. Ferrier-Barbut, H. Kadau, M. Schmitt, M. Wenzel, and T. Pfau, Physical Review Letters **116**, 215301 (2016).

[145] Y. Li, L. P. Pitaevskii, and S. Stringari, Physical Review Letters **108**, 225301 (2012).

[146] S.-C. Ji et al., Nature Physics **10**, 314 (2014).

[147] L. Tanzi et al., Nature **574**, 382 (2019).

[148] Z.-Q. Yu, Physical Review A **90**, 053608 (2014).

[149] A. Boudjemâa, Physical Review A **98**, 033612 (2018).

[150] B. Mukherjee, Z. Yan, P. B. Patel, Z. Hadzibabic, T. Yefsah, J. Struck, and M. W. Zwierlein, Physical Review Letters **118**, 123401 (2017).

[151] B. Capogrosso-Sansone, S. Giorgini, S. Pilati, L. Pollet, N. Prokof'ev, B. Svistunov, and M. Troyer, New Journal of Physics **12**, 043010 (2010).

[152] P. O. Fedichev and G. V. Shlyapnikov, Physical Review A **58**, 3146 (1998).

[153] J. Goldstone, A. Salam, and S. Weinberg, Physical Review **127**, 965 (1962).

[154] N. M. Hugenholtz and D. Pines, Physical Review **116**, 489 (1959).

[155] F. J. Poveda-Cuevas, P. C. M. Castilho, E. D. Mercado-Gutierrez, A. R. Fritsch, S. R. Muniz, E. Lucioni, G. Roati, and V. S. Bagnato, Physical Review A **92**, 013638 (2015).

[156] D. M. Larsen, Annals of Physics **24**, 89 (1963).

[157] B. Oleś and K. Sacha, Journal of Physics A **41**, 145005 (2008).

[158] D. S. Petrov and G. V. Shlyapnikov, Physical Review A **64**, 012706 (2001).

[159] C. Gaul and C. A. Müller, Physical Review A **83**, 063629 (2011).

[160] J. O. Andersen, U. Al Khawaja, and H. Stoof, Physical Review Letters **88**, 070407 (2002).

[161] U. Al Khawaja, J. O. Andersen, N. P. Proukakis, and H. Stoof, Physical Review A **66**, 013615 (2002).